Investigating the role of cohesin in stage-specific transcription of the human malaria parasite

Catarina Maria da Silva Rosa

Thèse de doctorat en parasitologie moléculaire de

Sorbonne Université / Universite Paris Cité

Ecole Doctorale Complexité du Vivant (ED515)

Unité de Biologie des Interactions Hôte-Parasite

présentée par

Catarina Maria da Silva Rosa

pour obtenir le grade de Docteur de Sorbonne Université sur le sujet:

Investigating the role of cohesin in stage-specific transcription of the human malaria parasite

Membres du jury

Dr. Olivier Silvie	Président du jury
Dr. Jonathan Weitzman	Rapporteur
Dr. Jérôme Govin	Rapporteur
Dr. Lucy Glover	Examinateur
Dr. Mélanie Hamon	Examinateur
Dr. Jessica Bryant	Co-encadrant
Pr. Artur Scherf	Directeur de thèse

Présentée et soutenue publiquement à Paris, le 8 Décembre 2022

Abstract

The most virulent human malaria parasite, *Plasmodium falciparum*, has a complex life cycle between its human host and mosquito vector. Each stage is driven by a specific transcriptional program, but with a relatively high ratio of genes to specific transcription factors, it is unclear how genes are activated or silenced at specific times. The *P. falciparum* genome is relatively euchromatic compared to the mammalian genome, except for specific genes that are uniquely heterochromatinized via HP1. There seems to be an association between gene activity and spatial organization; however, the molecular mechanisms behind genome organization are unclear. While *P. falciparum* lacks key genome-organizing proteins found in metazoans, it does have all core components of the cohesin complex. In other eukaryotes, cohesin is involved in sister chromatid cohesion, transcription, and genome organization. To investigate the role of cohesin in *P. falciparum*, we combined genome editing, mass spectrometry, chromatin immunoprecipitation and sequencing (ChIP-seq), and RNA sequencing to functionally characterize the cohesin subunit Structural Maintenance of Chromosomes protein 3 (SMC3). SMC3 knockdown in early stages of the intraerythrocytic developmental cycle (IDC) resulted in significant upregulation of a subset of genes involved in erythrocyte egress and invasion, which are normally expressed at later stages. ChIP-seq of SMC3 revealed that over the IDC, enrichment at the promoter regions of these genes inversely correlates with their expression and chromatin accessibility levels. These data suggest that SMC3 binding helps to repress specific genes until their appropriate time of expression, revealing a new mode of stage-specific, HP1-independent gene repression in *P. falciparum*.

Résumé

Le parasite du paludisme humain le plus virulent, *Plasmodium falciparum*, a un cycle de vie complexe entre son hôte humain et le moustique vecteur. Chaque étape est pilotée par un programme de transcription spécifique, mais avec un rapport relativement élevé de gènes à des facteurs de transcription spécifiques, on ne sait pas comment les gènes sont activés ou réduits au silence à des moments spécifiques. Le génome de *P. falciparum* est relativement euchromatique par rapport au génome des mammifères, à l'exception de gènes spécifiques qui sont uniquement hétérochromatinisés via HP1. Il semble y avoir une association entre l'activité des gènes et l'organisation spatiale ; cependant, les mécanismes moléculaires derrière l'organisation du génome ne sont pas clairs. Alors que *P. falciparum* manque de protéines organisatrices du génome clés trouvées dans les métazoaires, il possède tous les composants essentiels du complexe cohésine. Chez d'autres eucaryotes, la cohésine est impliquée dans la cohésion, la transcription et l'organisation du génome des chromatides soeurs. Pour étudier le rôle de la cohésine dans *P. falciparum*, nous avons combiné l'édition du génome, la spectrométrie de masse, l'immunoprécipitation et le séquençage de la chromatine (ChIP-seq) et le séquençage de l'ARN pour caractériser fonctionnellement la sous-unité cohésine Structural Maintenance of Chromosomes protein 3 (SMC3). L'inactivation de SMC3 aux premiers stades du cycle de développement intraérythrocytaire (IDC) a entraîné une régulation positive significative d'un sous-ensemble de gènes impliqués dans la sortie et l'invasion des érythrocytes, qui sont normalement exprimés à des stades ultérieurs. ChIP-seq de SMC3 a révélé que sur l'IDC, l'enrichissement au niveau des régions promotrices de ces gènes est inversement corrélé à leurs niveaux d'expression et d'accessibilité à la chromatine. Ces données suggèrent que la liaison de SMC3 aide à réprimer des gènes spécifiques jusqu'à leur moment d'expression

approprié, révélant un nouveau mode de répression génique spécifique au stade et indépendant de HP1 chez *P. falciparum*.

Acknowledgments

This thesis would not have been possible without the help, support, and guidance of several people that I was fortunate to meet over the last 3 years of this, undoubtedly, life-changing experience.

I would like to thank my thesis supervisor, Prof. Artur Scherf, for giving me the opportunity to carry this project in the remarkable research environment that is BIHP! His guidance, invaluable advice, and encouragement during crucial moments of the project were indispensable for its success.

I am deeply grateful to Dr. Jessica Bryant, without whom this thesis would not have been possible! Her continuous guidance, support and encouragement were key to my growth as a scientist. I am very grateful that I had to opportunity to learn with scientific rigor and exemplary attention to the detail. At a personal level, Dr. Jessica Bryant has showed me that is possible to be a successful female scientist without sacrificing other spheres of your life, inspiring me to continue the pursue of a scientific career.

I am thankful to Dr. Sebastian Baumgarten, his expertise on the *Plasmodium* biology and bioinformatics aspect of the project was absolutely essential. Further, constant exchange of ideas has, undoubtedly, contributed majorly to this work! My most sincere thanks to Parul Singh, a recent post-doc in our group, whose arrival had a major impact, both in the project and my personal development as a scientist. Her refreshing scientific insights were of utmost importance to the development of my conceptual thinking regarding different biological phenomena. To Ameya Sinha, I am very grateful for his substantial contribution to this project and for coming to Paris and providing us with, what I have coined the "Ameya effect", i.e. a handful of happiness! I would also like to acknowledge Prof. Peter Preiser and Prof. Peter Dedon for their scientific insights in the project. I am thankful to my thesis committee: Romain Koszul, Benoit Gamain and Heloise

Muller, for their critique and feedback on the project. I would like to thank Liliana Mâncio-Silva for her scientific input and help in the planning of future experiments! I am thankful to Patty Chen for motivating me along this PhD journey. Her scientific input, kind words and positive thinking were remarkably important for carrying out this project! I am thankful to Gretchen Diffendall, who has shared this PhD journey with me! Our exchanges about each other's projects and our moments outside the scientific sphere were incredibly important and I am grateful that I could share this PhD with someone as kind, trustworthy and bright as her. I am thankful to Aurelie Claes for always taking the time to help me with the project and for her care! I am grateful to Flore Nardella and Irina Dobrescu, their selfless help was incredibly important in particularly difficult moments of this PhD! I would like to thank Alexis Dziedziech for her scientific advice and for encouraging me to attend social events, which are undoubtedly important to the work-life balance! I would like to give a very special thanks to Anne Cozanet, whose incredible professionalism and humanism are absolutely exemplary! Her genuine care and availability have been a constant across this PhD journey. Finally, I would like to thank all the other past and present members of the lab that have been part of this incredible journey!

More than academic support, the puzzle of this PhD journey could not be completed without the encouragement of friends and family! Coming to Paris has given me the opportunity to meet a lot of people, which has opened my mind to different ideas, perspectives and likely had an impact in my academic research. I am grateful for the people that entered my life during my stay at Cité Universitaire! Vincent and Julia, that exposed me, for the first time, to the culture life in Paris, from jazz in La gare to art exhibitions in a boat in the Seine! To Joel, Jesus and Cris I am especially grateful, has they have been my family away from home. Our weekend meals, our tea parties, our travels, all of it, and much more, was essential for me to be able to carry this PhD. I am thankful to my friends in

Portugal, Ana and Joana, for all their support, for always reaching to me. Especially, I am thankful to Ana, who took the time to visit me more than once, without her I would have not taken the time to do the touristic tours!

I am eternally grateful to my family. My mom and dad have always encouraged me to follow my dreams and, along these years, they have always supported me in my academic endeavours I learned with their example, sometimes it is needed to go out of your comfort zone to progress. They always prioritized their children education and it was because of their sacrifices that I am able to progress and always aim for higher in my academic journey. To my brother, who is always there for me, I am fortunate to have grown up with him, his curiosity and brightness has pushed me for more, and if now I am in this final phase of my academic parcours, is also thanks to him! To my brother and Bia I am also deeply grateful that they chose, has their first travel outside Portugal, a travel to Paris to visit me! To all my family, my grandparents, my uncles and aunts, my cousins, I am thankful, all of them, have had an impact in my upbringing and in the decisions that culminated with coming to Paris, working on what I love the most, research. I would also like to dedicate this thesis to my grandpas. My grandpa Fernando, who worked here in France for several years, it is because of him that since a very young age I had such an impulse to come here. To my grandpa Joaquim, who was very happy to have a future doctor in the family, this thesis is also for him.

Last, but not least, I am immensely grateful to David, for his constant support, for always being there, in the good and less good moments, and for being my pillar throughout the PhD journey. His constant critique on my work has been crucial to think more outside the box which prepared me to answer questions to a broader audience. I am thankful that he also brought me outside the box of research, for pushing me to travel and experience novel adventures!

Table of Contents

List of Figures

List of Tables

Abbreviations

ApiAP2	Apicomplexan Apetala 2
AT	Adenine-Thymine
ATAC-seq	Assay for Transposase-Accessible Chromatin by sequencing
ChIP-seq	Chromatin Immunoprecipitation sequencing
CTCF	CCCTC-binding Factor
FISH	Fluorescence *in situ* hybridization
FPKM	Fragments per kilobase of transcript per million fragments mapped
GAP45	Glideosome-associated protein 45
GC	Guanine-Cytosine
PTMs	Post-translational modifications
HP1	Heterochromatin protein 1
hpi	Hours post invasion
HMGB1	high-mobility-group-box protein 1
IDC	Intraerythrocytic developmental cycle
IP LC-MS/MS	Immunoprecipitation followed by liquid chromatography-mass spectrometry
iRBC	Infected red blood cell
kb	Kilobase
Mb	megabase
kDa	kDalton
mRNA	messenger RNA
*Pf*EMP1	P. *falciparum* erythrocyte membrane protein 1
Pol	Polymerase
PCR	Polymerase chain reaction
RAP2	Rhoptry-associated protein 2
rDNA	ribosomal DNA
RNA-seq	RNA sequencing
SMC	Structural mantainance of chromosomes
TAD	Topologically associating domain
TES	Transcription end site
TF	Transcription factor
TSS	Transcription start site
UTR	Unstranslated region
VSA	Variant surface antigen
WHO	World Health Organization
WT	wild type

PART ONE

INTRODUCTION

1.1 Introduction to malaria

Malaria, one of the most important infectious diseases worldwide, is caused by protozoan hemoparasites from the genus *Plasmodium* (phylum *Apicomplexa*, order *Piroplasmida*). The parasites are transmitted to the host during a blood meal of the vector - female mosquitoes from the genus *Anopheles* – infecting mammals, reptiles, and birds. Malaria is an ancient disease with the oldest evidence being the presence of *Plasmodium* stages in a mosquito vector fossil dated to 30 million years ago (Poinar, 2005). There are at least five *Plasmodium* species that regularly infect humans: *P. falciparum*, *P. vivax*, *P. malariae*, *P. ovale curtsi* and *P. ovale wallikeri* (Kantele & Jokiranta, 2011; Sutherland et al., 2010). Others, such has *P. knowlesi*, *P. simium*, and perhaps even *P. brasilianum*, represent ongoing and emerging zoonotic agents (Voinson et al., 2021).

While the origins of human-infective *Plasmodium* species have been a subject of much discussion (Loy et al., 2017), inarguably human malaria has existed for thousands of years. *Plasmodium* has possibly been the pathogen with more selective pressure on human evolution, even selecting for certain genetic polymorphisms, such as the sickle cell trait, that confer a degree of protection against malaria (Weatherall et al., 2002).

Attesting to the importance of malaria infection, the first reports of its symptoms appear in the Chinese Canon of Medicine dating back to 2700 BC. Other descriptions of the disease have also been found in clay tablets from Mesopotamia (2000 BC) and Egyptian papyri (1500 BC) (Cox, 2010). However, understanding the malaria parasite only started in 1880 when Alphonse Laveran, after examining numerous blood smears of infected patients, identified the protozoan parasite causing the disease (Laveran, 1907). In 1897,

Ronald Ross discovered that culicine mosquitoes were vectors for the avian malaria parasites, suggesting that human malaria could be transmitted in a similar manner (Ross, 1902). Over the following two years, a group of Italian malariologists demonstrated that malaria was transmitted by female *Anopheles* mosquitos (Cox, 2010).

1.1.1 Malaria epidemiology

In 2020, almost half of the world population was living in areas at risk of contracting malaria, with transmission occurring in 85 countries (Fig. 1.1). However, despite this broad geographical distribution, the malaria burden is not evenly distributed. Most cases and deaths occur in countries of sub-Saharan Africa and more than half of malaria cases reported globally in 2020 happened in only six countries – Angola, Burkina Faso, Uganda, Nigeria, the Democratic Republic of the Congo, and Mozambique. The three latter and the United Republic of Tanzania accounted for just over half of all malaria deaths globally (World Health Organization, 2021).

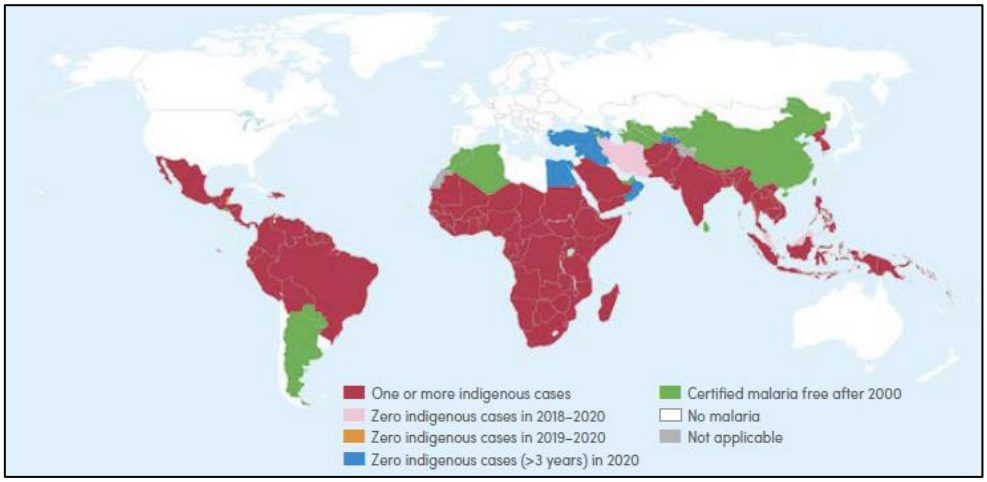

Figure 1.1. Countries with indigenous cases in 2000 and their status by 2020. Countries with zero indigenous cases for at least three consecutive years are considered to have eliminated malaria. China and El Salvador were certified malaria-free in 2021, following four years with zero malaria cases (World Health Organization, 2021). Image taken from (World Health Organization, 2021).

P. falciparum is the most prevalent and the deadliest malaria parasite globally, carrying a particularly high burden for communities of African countries where it was

responsible for 95% of the estimated malaria cases in 2020 (World Health Organization, 2021). In 2020, *P. falciparum* accounted for the majority of the ~241 million malaria cases and 627 000 malaria-related deaths registered globally. Particularly, children aged under five years are relentlessly affected, representing 77% of the reported malaria deaths (World Health Organization, 2021).

In 2015, the World Health Organization (WHO) adopted the global technical strategy (GTS) for malaria 2016-2030. It consisted of a framework to guide malaria control and elimination efforts, setting milestones for measuring the progress in 2020 and 2025 towards the global targets of 2030 (World Health Organization, 2015) (Table 1.1). The 2020 GTS milestones for morbidity and mortality have not been achieved. Globally, the GTS target is ~ 40% lower than the current case and mortality incidence (i.e. cases per 1000 and 100 000 population at risk, respectively). If urgent actions are not taken, by 2030, the GTS will be off track by ~ 90% (World Health Organization, 2021).

Goals	**Milestones**		**Targets**
	2020	2025	2030
1. Reduce malaria mortality rates globally compared with 2015	At least 40%	At least 75%	At least 90%
2. Reduce malaria case incidence globally compared with 2015	At least 40%	At least 75%	At least 90%
3. Eliminate malaria from countries in which malaria was transmitted in 2015	At least 10 countries	At least 20 countries	At least 35 countries
4. Prevent re-establishment of malaria in all countries that are malaria-free	Re-establishment prevented	Re-establishment prevented	Re-establishment prevented

Table 1.1. Goals, milestones, and targets towards a malaria-free world. Table adapted from (World Health Organization, 2015)**.**

According to the World Malaria Report 2021, malaria case incidence (cases per 1000 population at risk) has declined from 81 in 2000, to 59 in 2015, and 56 in 2019. In a similar trend, malaria deaths have reduced from 896 000 in 2000, to 562 000 in 2015, and 558 000 in 2019. In 2020, due to service disruptions caused by the COVID-19 pandemic,

malaria case incidence increased to 59 – a 5% increase – and malaria deaths rose to an estimated 627 000 – a 12 % increase (World Health Organization, 2021). However, even before the emergence of COVID-19, the progress towards achieving the GTS milestones was stalling and, while disease burden has remained controlled, the number of malaria cases and deaths remains unacceptably high (Noor & Alonso, 2022).

1.1.1.1 Current drugs and control strategies for malaria

The fight against malaria relies on a multidimensional approach that comprises vector-control strategies, use of drugs for treatment and chemoprophylaxis and, more recently, a vaccine. Interventions to prevent malaria include the use of insecticide-treated bed nets (ITNs) and indoor residual spraying of insecticides (IRS) for vector control, intermittent preventive treatment of malaria during pregnancy and in infants, and seasonal malaria chemoprophylaxis in children. Even though these measures have considerably contributed to a reduction in the global malaria burden, insecticide resistance in malaria vectors and drug resistance in the malaria parasites represent an important threat for malaria control and elimination efforts (World Health Organization, 2021).

The first antimalarial drug was quinine, an alkaloid from the bark of the cinchona tree, used to treat malaria from as early as the 1600s (Greenwood, 1992), with resistance being detected for the first time in Brazil in 1907 (Neiva, 1910). For quinine, resistance only appears to have emerged almost three centuries after its introduction; however, for other anti-malarial drugs, resistance has appeared at a much faster pace (Calderón et al., 2013) (Fig. 1.2). One well-studied example is *P. falciparum* resistance to chloroquine, a safe and cost-effective synthetic drug first introduced in the 1940s. However, after only a decade of use of this drug as a first-line antimalarial, resistance emerged, spreading rapidly across malaria-endemic regions (Trape et al., 2002; Wellems et al., 2009).

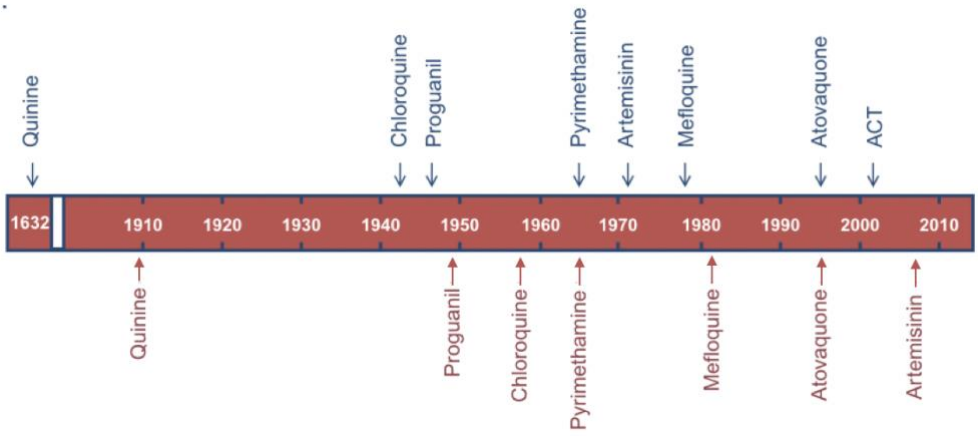

Figure 1.2. Timeline of antimalarial drug resistance. The top panel indicates the year of the introduction of each drug (blue), and the lower panel indicates the year of appearance of resistance (red). Modified from (Calderón et al., 2013)**.**

Currently, first-line treatment for *P. falciparum* involves the use of artemisinin-based combination therapies (ACTs) (World Health Organization, 2021). Artemisinin was isolated from *Artemisia annua* (herb Qinghao) - used in traditional Chinese medicine to treat fever – by Tu Youyou, in 1972 (Tu Youyou, 2015). Since this discovery, progress has been made, with the development of artemisinin derivatives (Miller & Su, 2011; Tu, 2011) and the production of semi-synthetic artemisinin (Paddon & Keasling, 2014).

ACTs are based on the combination of artemisinin or derivative with a partner drug, a multi-target strategy which should have hampered the emergence of resistance. However, resistance to artemisinin, since it was first reported in Cambodia (Dondorp et al., 2009), has spread quickly throughout Southeast Asia (Ashley et al., 2014). In turn, resistance to the partner drugs also started to emerge in Cambodia (Amaratunga et al., 2016; Mairet-Khedim et al., 2021) and Vietnam (Thanh et al., 2017), raising concerns about the spread of these *P. falciparum*-resistant strains to high-burden malaria countries (Fig. 1.3)

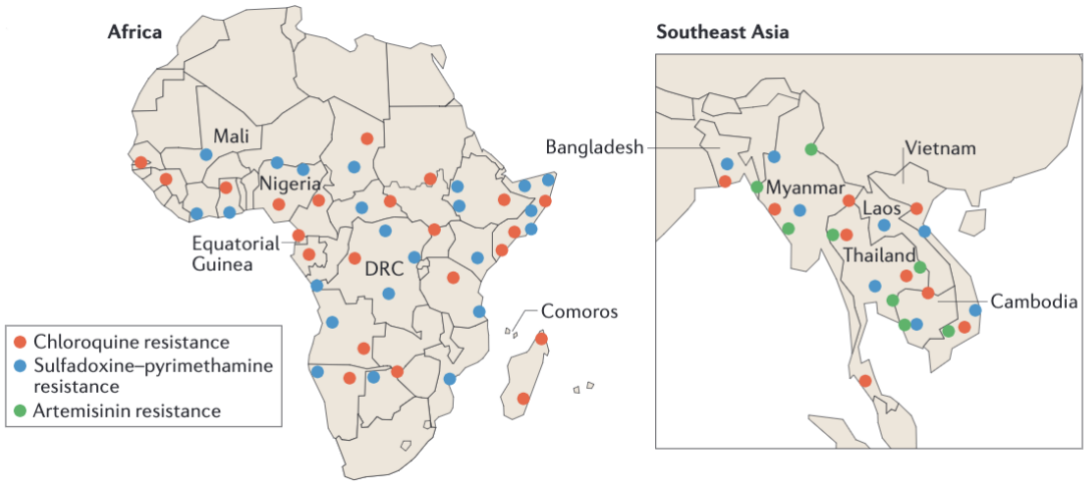

Figure 1.3. Epidemiology of antimalarial drug resistance. Detailed maps showing the distribution of *P. falciparum* resistance to chloroquine, sulfadoxine–pyrimethamine, and artemisinin in Africa and southeast Asia. Image taken from (Haldar et al., 2018).

The identification of molecular markers associated with drug resistance is therefore of utmost importance to track and monitor resistant parasites, guiding interventions to control or eliminate them (WHO, 2020). Artemisinin resistance is associated with single point mutations in the *P. falciparum* gene Kelch13 (PfK13) (Ariey et al., 2014; Straimer et al., 2015). Of concern, *Pf*kelch13-mediated artemisinin resistance has emerged in Africa (Asua et al., 2021; Uwimana et al., 2020). Even though ACTs are still considered efficacious, a WHO immediate priority is to ameliorate therapeutic efficacy by increasing genotypic surveillance to map the extent of resistance (World Health Organization, 2021).

Given the numerous threats to malaria eradication, such as the emergence of resistance to the most widely used artemisinin-based treatments, the development of an effective vaccine would be a crucial step towards malaria eradication. The RTS, S/AS01 vaccine consists of a recombinant protein comprising epitopes from *P. falciparum* circumsporozoite protein (CSP), a viral envelope from hepatitis B virus (HBsAg), and a chemical adjuvant (AS01). Since October 2021, the WHO has recommended the RTS,S malaria vaccine usage for prevention against *P. falciparum* in children living in endemic regions with high malarial transmission (WHO, 2021). However, there are limitations to

this vaccine, including a schedule of four doses and a modest protection - 30% reduction in clinical malaria - that decreases over time (RTSS SAGE/MPAG Working Group, 2021).

Therefore, the development of novel prevention and treatment strategies together with epidemiological surveillance are crucial more than ever to oppose biological threats. Exploring and understanding important features of *P. falciparum* biology is an important step towards the discovery of novel therapeutic targets that may finally tilt the balance from malaria control to elimination.

1.1.2 *Plasmodium* biology

The phylum *Apicomplexa* includes a large array of single-celled obligate intracellular parasites such as *Plasmodium*, *Toxoplasma*, *Theileria,* and *Babesia* parasites, which are responsible for diseases of medical and veterinary importance. Apicomplexans have a remarkable evolutionary history, as witnessed by the appearance of an apicoplast - a non-photosynthetic organelle - that evolved from a red algal endosymbiont and is essential for their survival (van Dooren & Striepen, 2013; White & Suvorova, 2018).

Apicomplexan parasites have an especially complex life cycle, whereby they undergo multiple developmental stages in a wide range of host cell niches and undergo both asexual and sexual replication (Francia & Striepen, 2014).

1.1.2.1 *P. falciparum* life cycle

P. falciparum has a complex life cycle maintained between the human host and the female *Anopheles* mosquito vector, including differentiation through morphologically distinct forms and both asexual and sexual replication (Josling & Llinás, 2015; Venugopal et al., 2020). Malaria infection initiates with the injection of sporozoites into the dermis of the human host during the ingestion of a blood meal by the female *Anopheles* mosquito. Once the sporozoites enter the vasculature, they are transported to the liver where they

invade hepatocytes, undergoing extensive rounds of asexual replication. The tens of thousands of merozoites that result are released into the bloodstream and infect the red blood cells (RBCs) (Fig. 1.4 A-B**)**. In the RBC, asexual replication is accomplished as the merozoite undergoes development through three consecutive and distinct morphological forms: ring, trophozoite, and schizont. At the end of each intraerythrocytic developmental cycle (IDC), which takes approximately 48 hours, the multinucleated schizont releases up to 32 merozoites that will egress out of the host RBC and invade new RBCs (Fig. 1.4 C) (Josling & Llinás, 2015; Venugopal et al., 2020)

During the IDC, the parasite avoids clearance of infected RBCs by the spleen by expressing variant surface antigens (VSAs) on the surface of the RBCs. These VSAs allow infected RBCs to sequester in the microvasculature of the host, which can lead to pathogenesis. In a process called antigenic variation, the parasite switches the repertoire of expressed VSAs in order to evade the host's eventual immune response to these molecules. Thus, the parasite is able to maintain a chronic infection with characteristic waves of parasitemia. In contrast to the asymptomatic infection of liver cells, the ongoing blood-stage cycle is responsible for the clinical manifestations of the disease, such as fever, shivering, cough, headache, and vomiting, which occur at regular intervals (Scherf et al., 2008).

During blood stage proliferation, the parasite also needs to ensure a balance between virulence and transmission, and as such, a proportion of the asexually reproducing parasites will commit to gametogenesis, or the process by which a parasite differentiates into male or female sexual stages. The resultant gametocytes are sequestered into the bone marrow where they progress through five developmentally distinct morphological forms. Finally, the mature gametocytes are released to the blood stream where they then be taken along with the blood meal by a female *Anopheles* mosquito and emerge as extracellular male and

female gametes in the midgut. Here the gametes fuse and form a diploid zygote, which undergoes DNA replication and meiosis. The resultant ookinete traverses the midgut epithelium and develops into an oocyst, where asexual sporogonic replication occurs. When the oocyst ruptures, the motile sporozoites migrate to the salivary glands where they undergo a maturation process that allows them to be transmitted to the next human host (Fig. 1.4 D) (Josling & Llinás, 2015; Venugopal et al., 2020).

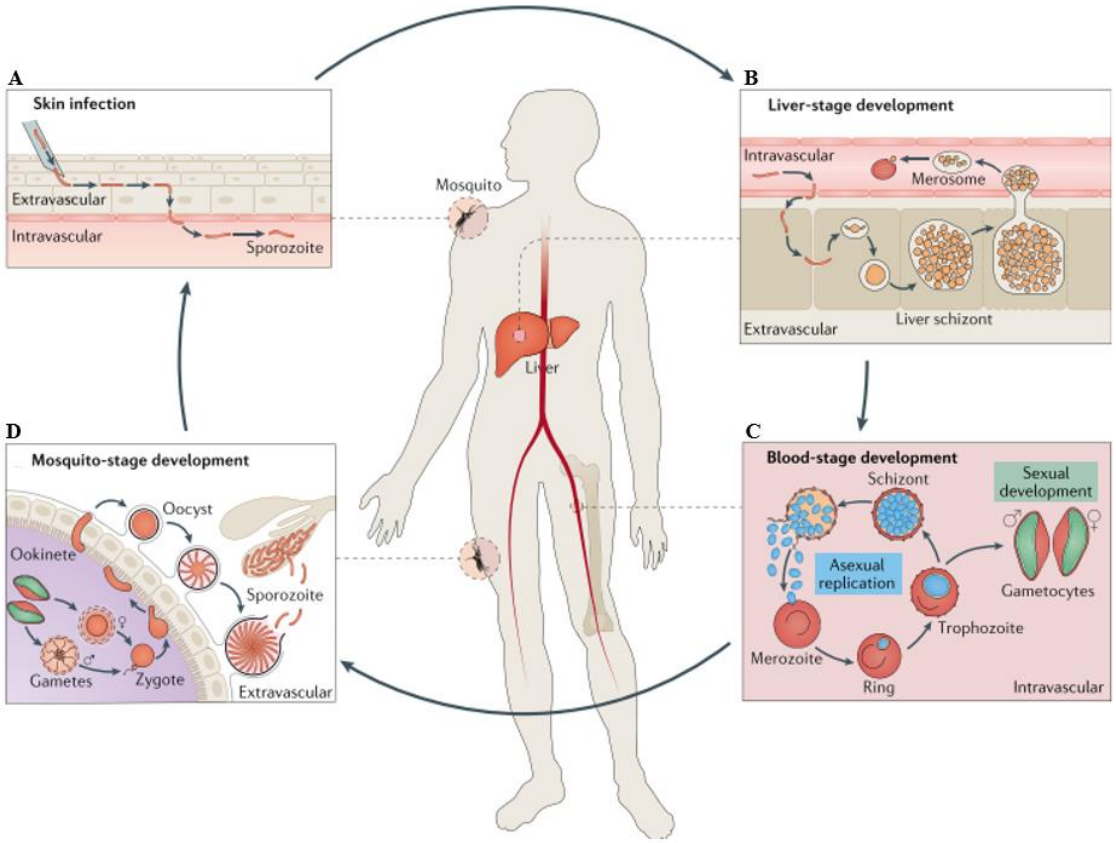

Figure 1.4. Schematic of the *P. falciparum* life cycle. A. During a blood meal, the female *Anopheles* mosquito transmits sporozoites via the skin of the human host. **B.** Sporozoites travel to the liver, invade hepatocytes, and generate thousands of merozoites that enter the bloodstream and invade erythrocytes. **C**. The ~ 48 h asexual blood stage begins with erythrocyte invasion by a merozoite followed by development through ring, trophozoite, and schizont stages, which generates up to 32 daughter merozoites that will egress from the erythrocyte and infect new erythrocytes. A small fraction (< 5%) of these intraerythrocytic parasites will develop into male or female sexual stages - gametocytes - which will be taken up by a mosquito during a blood meal. **D.** In the mosquito midgut, gametes fuse to form zygotes, which undergo meiosis to form ookinetes. The motile ookinete crosses the epithelium and differentiates into an oocyst. These oocysts will

release thousands of sporozoites into the mosquito body cavity that will travel to the salivary glands, set to be transmitted to the next human host. Image taken from (Venugopal et al., 2020).

1.1.2.2 The intraerythrocytic developmental cycle

The ~ 48 h *P. falciparum* IDC begins with the release of thousands of merozoites into the bloodstream. In a highly coordinated and sophisticated process, a merozoite attaches to and invades an RBC. Shortly after, the intracellular parasite begins to export proteins that remodel the host erythrocyte, allowing the parasite to obtain nutrients for development and hide from the host immune system. A single haploid parasite (1N) develops through three morphologically distinct stages: ring [~ 0 – 24 hours post invasion (hpi)], trophozoite (~ 24 – 36 hpi), and schizont (~ 36 – 48 hpi) (Maier et al., 2009). In late stages of the IDC, consecutive rounds of DNA replication and mitosis, followed by nuclear membrane division and cytoplasm segmentation (i.e. schizogony) result in the formation of up to 16-32 daughter merozoites (Arnot et al., 2011) (Fig. 1.5). The incredible ability of the parasite to both invade and remodel the host erythrocytes leads to the exponential growth but requires key virulence factors that lead to malaria pathology and morbidity.

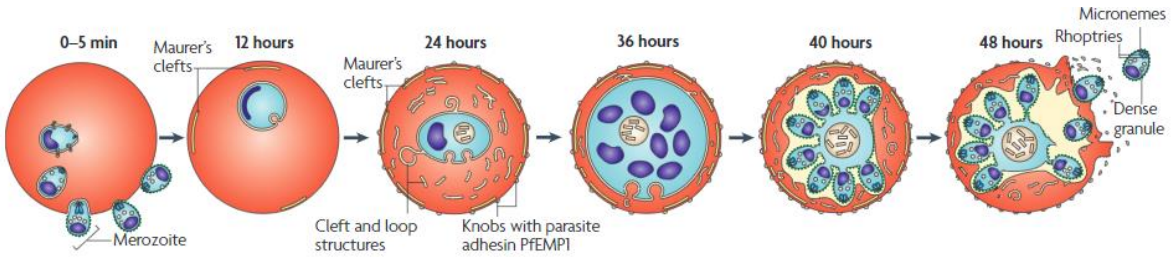

Figure 1.5. Intraerythrocytic developmental cycle of *P. falciparum*. The merozoite stage attaches to and invades mature erythrocytes, developing in a parasitophorous vacuole (PV) through ring (~ 0–24 hpi), trophozoite (~ 24–36 hpi) and schizont (~36–48 hpi) stages. During the trophozoite stage, remodelling of the infected erythrocyte occurs, with formation of membrane-bound structures in the cytoplasm (cleft and loop structures and Maurer's clefts) and knobs at the surface of the erythrocyte displaying the exported parasite antigen *Pf*EMP1 (*P. falciparum* erythrocyte membrane protein 1). At approximately 48 hpi, 16 to 32 daughter merozoites, whose structures (micronemes, rhoptries and dense granules) are designed to invade more erythrocytes, are released into the bloodstream. Image taken from (Maier et al., 2009).

1.1.2.2.1 Erythrocyte invasion and egress

The blood-stage merozoite is an extracellular form of the parasite that is specialized for invading host erythrocytes. The apical complex structure - distinctive of the extracellular invasive stages – forms the basis of the phylum name *Apicomplexa*. The invasive stages, the *zoites* (merozoites and sporozoites in *Plasmodium*) are polarized and elongated, with the apical end containing organelles and structures – micronemes and rhoptries – that facilitate invasion of the host cell (Fig. 1.6) (Cowman & Crabb, 2006). Erythrocyte invasion is a highly efficient and complex process, and the compartmentalization of these distinct organelles are key for the temporal release of the specific ligands that drive each step (Cowman et al., 2017; Weiss et al., 2016).

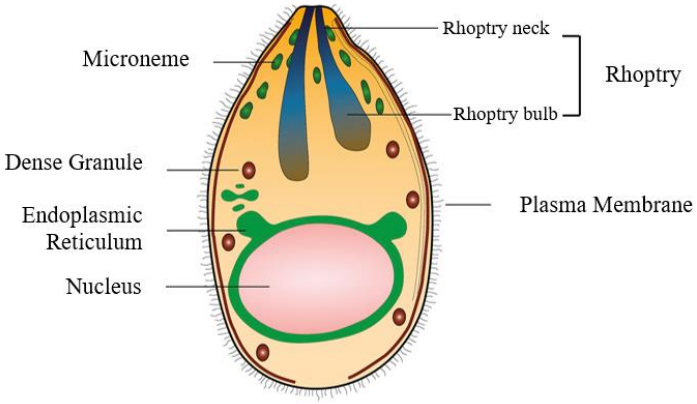

Figure 1.6. Merozoite structure. Subcellular structure of a *P. falciparum* merozoite depicting key invasion-related structures: the microneme and rhoptry (rhoptry neck and bulb) organelles at the apical end and the dense granules. Image adapted from (Cowman et al., 2017).

P. falciparum merozoites released into the bloodstream recognize a target erythrocyte in less than one minute, and the invasion process lasts less than 30 seconds after the initial contact (Gilson & Crabb, 2009). In the first step, the merozoite attaches reversibly and with low affinity to the erythrocyte membrane (Bannister & Dluzewski, 1990). Attachment is followed by membrane deformation, apical re-orientation towards the erythrocyte, and wrapping of the erythrocyte membrane around the merozoite (Gilson &

Crabb, 2009). Next, the formation of an irreversible tight junction acts as a nexus in which the release of proteins and lipids from the rhoptry bulb creates a parasitophorous vacuole (Riglar et al., 2011). The merozoite uses its actinomyosin motor to propel itself into this space (Keeley & Soldati, 2004), a unique niche for nutrient acquisition and the export of virulence factors (Matz et al., 2020). Finally, the infected erythrocyte undergoes a process of echinocytosis (rapid shrinkage of the erythrocyte with evenly spaced projections) and recovery (Gilson & Crabb, 2009) (Fig. 1.7).

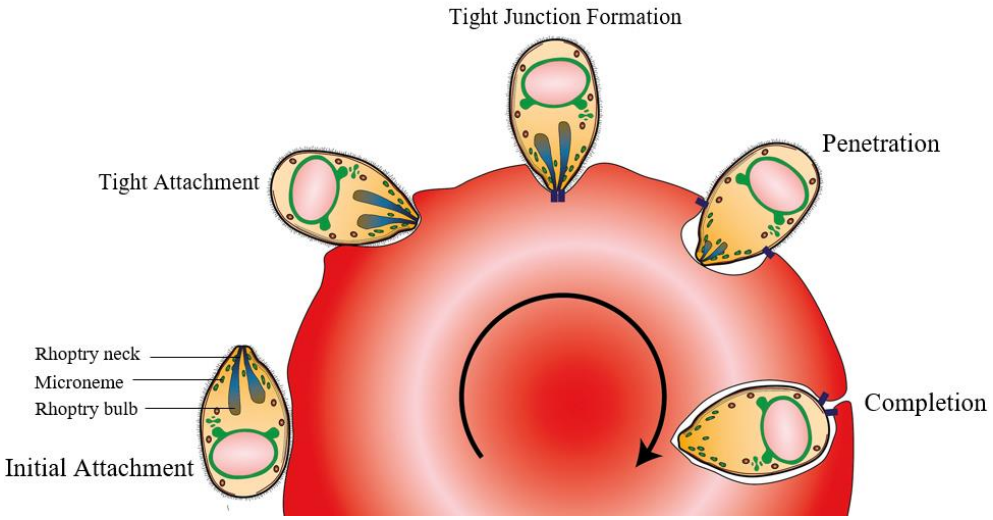

Figure 1.7. Merozoite invasion of erythrocytes. The initial interaction with the erythrocyte may be mediated by merozoite surface proteins (MSPs). The tight interaction with the erythrocyte is likely mediated by two major families of adhesins - the Duffy binding-like (DBL) or erythrocyte-binding-like (EBL) protein and the reticulocyte-binding-like protein homolog (Rh or RBL), released from the micronemes and the rhoptry neck, respectively. After, *Pf*Rh5 forms a complex with *P. falciparum* Rh5 interacting protein (*Pf*Ripr) and cysteine-rich protective antigen (CyRPA) that, directly or indirectly, will lead to the formation of a pore and subsequently a tight junction in the merozoite-erythrocyte interface. The formation of a tight junction is marked by the presence of RON4 and AMA1 and provides a nexus for the release of proteins and lipids from the rhoptry bulb, which creates the parasitophorous vacuole. The merozoite actinomyosin motor (the glideosome) propels the parasite into the vacuole. Finally, the erythrocyte sealing at the posterior of the invading merozoite is followed of a brief echinocytosis, with the erythrocyte returning to a normal morphology within 10 minutes. Image adapted from (Cowman et al., 2017).

Like the invasion process, egress from the erythrocyte is driven by multiple factors. Before the initiation of egress, the malarial cGMP-dependent protein kinase G (PKG) is activated, regulating the release of a parasite serine protease - subtilisin 1 (SUB1) (Collins

et al., 2013). It is secreted from the exonemes into the parasitophorous vacuole where it proteolytically cleaves several proteins that will enable parasite egress (Yeoh et al., 2007). SUB1 substrates include SERAs and MSP1/6/7 (de Monerri et al., 2011); however, the downstream events that lead to the parasite egress are less understood. Effector proteins involved in the disruption of the erythrocyte membrane, such as the perforin-like protein (PLP1), have been implicated in the egress process (Garg et al., 2013).

1.1.2.2.2 Schizogony

The standard eukaryotic cell cycle follows well-defined stages during which the cell grows (interphase), replicates its DNA (S phase, which is frequently flanked by two gap phases, G1 and G2), and divides (M phase). In *P. falciparum*, similarly to other *Apicomplexans,* it is challenging to assign this classical cell cycle stages. The first 24 hours post-invasion of the RBC can be considered interphase, during which the parasites possess a single haploid nucleus. The assembly and duplication of the centriolar plaque – functionally equivalent to the centrosome of other eukaryotes – begins ~ 20-24 hpi, with the onset of DNA replication not occurring before this time point (Arnot et al., 2011; Ganter et al., 2017). However, a central difference is that unlike in most model systems where one replicative cycle duplicates the cell number, one *P. falciparum* cell can produce up to 36 new daughter cells (H. Matthews et al., 2018) (Fig. 1.7).

Apicomplexa replicate within the host cells and can generate up to thousands of progenies, making it difficult to compare to the principles that govern classical cell division in the model eukaryotic cell (Francia & Striepen, 2014). In the IDC of *P. falciparum*, asexual replication is accomplished through endocyclic schizogony, during which asynchronous rounds of DNA replication and mitosis lead to multinucleated cells, all in the absence of chromosome condensation. Schizogony culminates with a final round of nuclear division before cytokinesis (Klaus et al., 2022; Rudlaff et al., 2020) (Fig. 1.8). While much

recent progress has been made in elucidating the mechanisms behind this unique cell division, many questions remain.

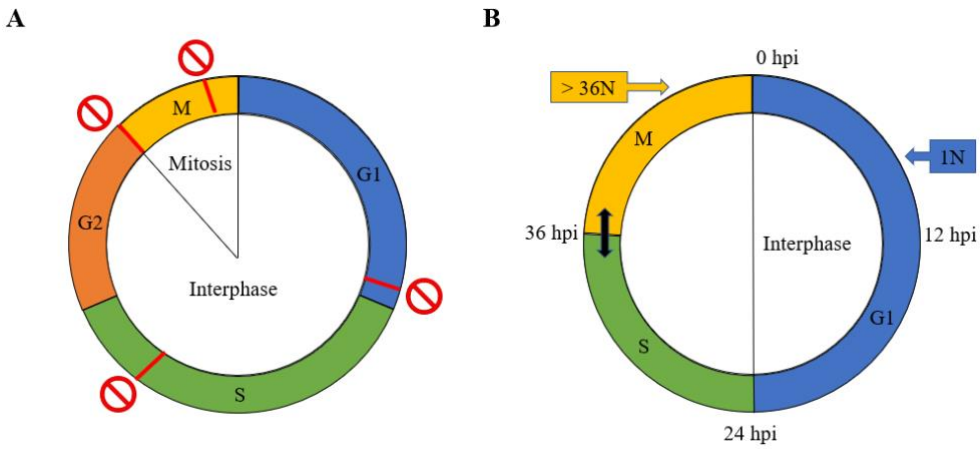

Figure 1.8. Schematics of a eukaryotic conventional cell cycle (A) and *P. falciparum* intraerythrocytic developmental (IDC) cell cycle (B). Known cell cycle checkpoints are highlighted and cell cycle progression along the IDC is shown in hours post invasion (hpi). Image adapted from (H. Matthews et al., 2018).

1.1.3 *P. falciparum* malaria persistence and pathogenesis

P. falciparum infection can be asymptomatic or cause a diverse array of clinical symptoms that can ultimately lead to death. First symptoms of malaria can be quite unspecific and include fever, chills, body aches, headache, cough, and diarrhea (Bartoloni & Zammarchi, 2012). A distinctive feature of malaria infection can be periodic waves of fever caused by the cyclical release of merozoites during schizont rupture after exponential growth of the parasite during each ~ 48 h IDC (Oakley et al., 2011). The risk of developing severe disease is considerably higher in children, pregnant women, immunocompromised people, or individuals travelling to regions of high malaria transmission (World Health Organization, 2021). Severe malaria is multi-syndromic, with associated complications including severe anemia, respiratory failure, acute renal failure, and cerebral malaria, which can evolve to a coma and death (Bartoloni & Zammarchi, 2012). These disease manifestations are associated with the ability of the infected RBC to sequester in diverse

tissues and organs via adhesion by VSAs expressed on the surface of the infected RBC (iRBC).

1.1.3.1 Antigenic variation

Multiple pathogens undergo antigenic variation as an immune evasion mechanism. Antigenic variation is the random switching of the repertoire of VSAs that are exposed to the immune system, allowing the parasite to avoid immune clearance, and leading to chronic infection. The genomes of several protozoan pathogens encode for multigene families whose products are involved in antigenic variation. Examples include *Trypanosoma brucei (*~1000 *vsg* genes that encode a variant surface glycoprotein), *Babesia bovis* (~130-160 *ves*α and *ves*β that encode for a variant surface antigen), and *Plasmodium falciparum* [~60 *var* genes encoding for Erythrocyte membrane protein 1 (*Pf*EMP1)] (Deitsch et al., 2009).

A key feature of antigenic variation is mutually exclusive expression whereby, at a given time, only one member of a multigene family is expressed while all the remaining members are maintained in a repressed state. In *P. falciparum*, the most important VSA, *Pf*EMP1, is encoded by the 60-member *var* gene family and expressed in a mutually exclusive manner. Even though *var* genes have a wide genomic distribution, across subtelomeric and central chromosomal clusters on 13 out of 14 chromosomes, transcription is tightly coordinated so that all but one *var* gene is transcribed in a ring stage parasite while all the others remain silenced. This mutually exclusive transcription and occasional switching ensures evasion of the host immune response and the establishment of chronic infections (Guizetti & Scherf, 2013; Scherf et al., 2008) (Fig. 1.9).

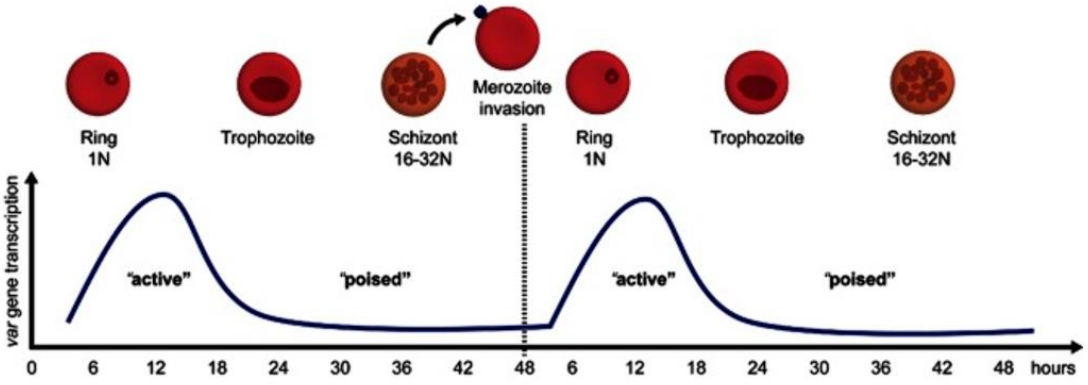

Figure 1.9. *var* gene activation and silencing throughout P. falciparum intraerythrocytic developmental cycle (IDC). The single *var* gene is transcribed at the beginning of the IDC (ring), soon after merozoite invasion. Shortly before the onset of DNA replication, *var* gene transcription ceases, remaining in a poised state (trophozoite and schizont) ready to be activated at the next IDC. Image taken from (Guizetti & Scherf, 2013).

Indeed, the switching between *var* family members serves a dual purpose as (1) it hampers the host immune response to the population of iRBC and (2) leads to the expression of different *Pf*EMP1 variants with different binding phenotypes corresponding to varying levels of disease severity (Smith et al., 2013). The most common adhesion phenotype is the binding of *Pf*EMP1 to the platelet glycoprotein 4 (CD36) cell receptor that, by sequestering the iRBCs to sites like adipose tissue or skeletal muscle rather than the brain, is associated with uncomplicated malaria (F. L. Hsieh et al., 2016; Smith et al., 2013). In contrast, *Pf*EMP1binding to the EPCR and intercellular adhesion molecule 1 (ICAM1) has been implicated in sequestration of iRBCs to the brain capillaries, causing cerebral malaria that can lead to coma and death (Turner et al., 2013). In pregnant women, the *Pf*EMP1 variant VAR2CSA binds specifically to the chondroitin sulphate A (CSA) present in placental syncytiotrophoblasts, which is associated with severe outcomes for both the mother and baby (Viebig et al., 2005) (Fig. 1.10). Therefore, antigenic variation resulting in the expression *Pf*EMP1 variants is a crucial factor in both chronic infection and pathogenesis.

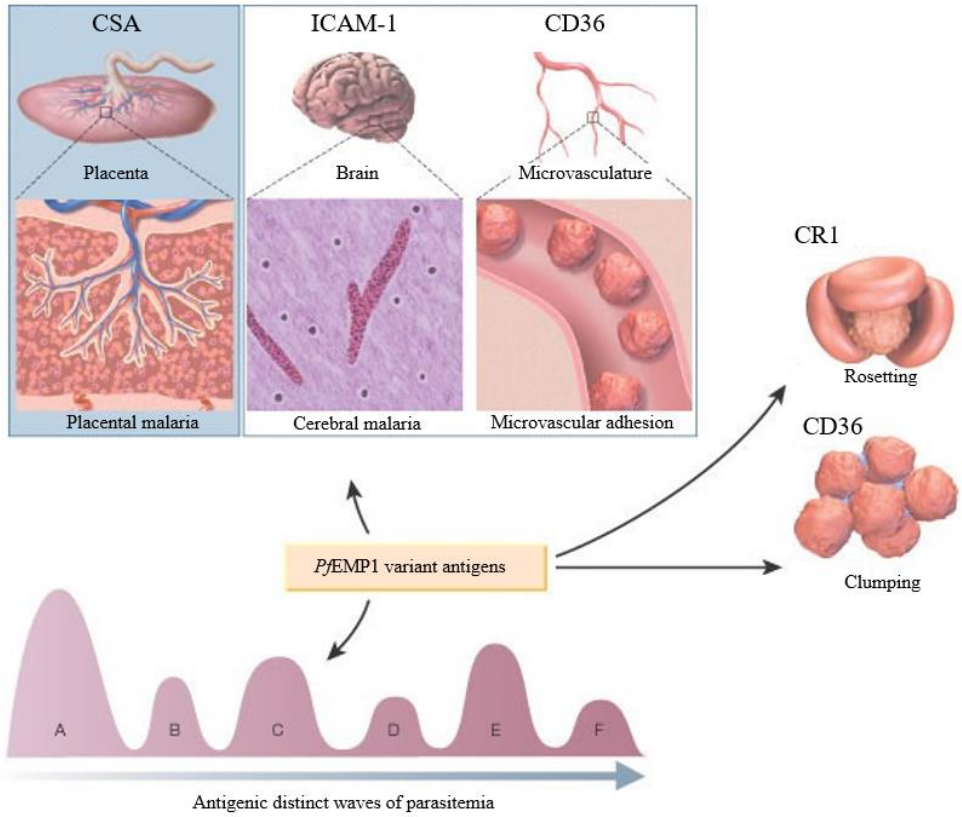

Figure 1.10. *Pf*EMP1 variant surface antigen family is key to immune evasion and pathogenesis. *Pf*EMP1variants expressed on the surface of RBCs infected with *P. falciparum* are involved in antigenic variation and can bind to distinct host receptors. Placental malaria is associated with binding of the *Pf*EMP1 variant VAR2CSA to CSA present in placental syncytiotrophoblasts. Cerebral malaria is associated with binding to ICAM1, which causes sequestration of the iRBC in the brain capillaries. *Pf*EMP1 binding to CD36 is the most common adhesion phenotype. The right panel shows that CD36 is also involved in platelet-mediated clumping of iRBCs and that binding to the complement receptor 1 (CR1) of uninfected RBCs is involved in the formation of rosettes. Both are key for malaria pathogenesis, as these formations obstruct the blood flow in the thin capillaries of critical organs, resulting in symptoms of severe disease. In parallel, switching between distinct *Pf*EMP1 variants enables the parasite to avoid the immune system, resulting in waves of parasitaemia. Image adapted from (H. Miller et al., 2002).

1.2. *P. falciparum* transcription and epigenetics

In eukaryotic cells, gene expression involves multiple layers of regulation in the nucleus. The most basic layer of control lies in the linear DNA sequence of regulatory elements such as promoters and enhancers, which are specifically bound by transcription factors and RNA polymerases (Fig. 1.11). An intermediate layer is the composition of chromatin, regulated by several epigenetic determinants such as histone post-translational modifications (PTMs) and the activity of chromatin remodelling complexes. A final layer lies in the spatial organization of factors and sequences within the nucleus into functional compartments, with the chromosomes themselves occupying discrete territories. This higher order chromosome organization plays an important role in gene regulation, for example by bringing together promoters and DNA regulatory elements such as enhancers (Branco & Pombo, 2007; Pombo & Dillon, 2015).

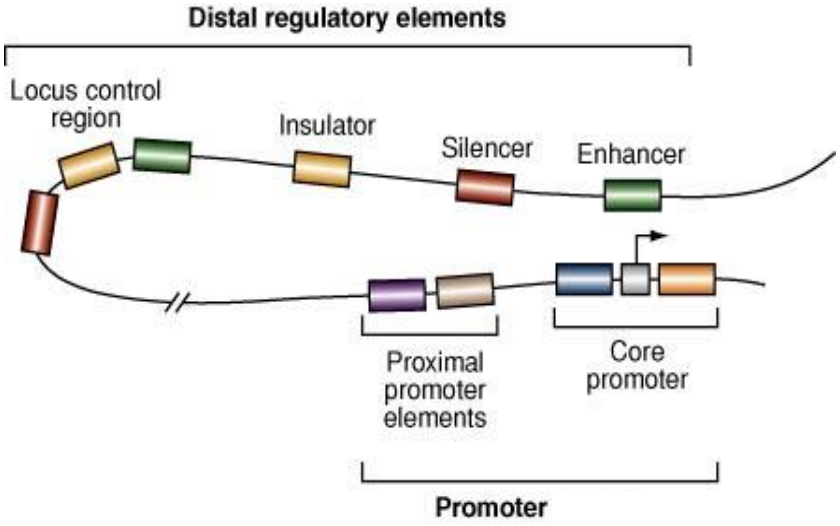

Figure 1.11. Representative eukaryotic gene regulatory region. A typical eukaryotic gene contains a promoter region that includes a core promoter and *cis*-acting proximal regulatory elements (i.e. recognition sites for transcription factors). Distal regulatory elements include enhancers, silencers, insulators, and other control regions that contact the promoter region via DNA looping. Image taken from (Maston et al., 2006).

1.2.1 *P. falciparum* genome

The most commonly used *P. falciparum* laboratory strain, 3D7, has a 22.8 megabase (Mb) nuclear genome and two extrachromosomal genomes: a 6 kilobase (kb) mitochondrial genome and a 35 kb apicoplast circular genome. The haploid nuclear genome is organized in 14 linear chromosomes that range between 0.643 to 3.29 Mb in size (Gardner et al., 2002). More than half of the nuclear genome corresponds to coding sequences for approximately 5300 proteins, and almost 80% of the genome is transcribed across the IDC, with 24% of genes having antisense transcription (Siegel et al., 2014).

P. falciparum chromosome contents are organized similarly to those of other eukaryotes, with housekeeping genes involved in replication and progression through the cell cycle located at the internal regions and mostly silenced clonally variant gene families mainly located in arrays within subtelomeric domains (Fig 1.12). However, a remarkable difference lies on *P. falciparum* unique base composition, with an overall AT-content of 80.6%, which rises to ~90% in intronic and intergenic regions (Gardner et al., 2002).

Between the telomere and the variant genes are conserved telomere-associated repeat elements (TARE 1-6), which are always displayed in the same order, but with lengths varying from 10 to 30 kb. Telomeres are composed of degenerate G-rich heptamer repeats (mainly 5'-GGGTT(T/C)A-3') and display a higher-order organization (Figueiredo et al., 2002). *P. falciparum* chromosome ends were found to form clusters of four to seven telomeres at the nuclear periphery, which facilitates recombination events between the subtelomeric virulence genes (Freitas-Junior et al., 2000). Indeed, the dynamic nature of subtelomeric regions is mirrored in the observation that the majority of pseudogenes belongs to the *rif*, *stevor*, and *var* clonally variant gene families, most of which are located in those regions (Mok et al., 2008). The cluster formation observed in the chromosome ends was found to involve a unique 21 bp repeat (Rep20) present in one of the TAREs;

however, the factors driving the specific perinuclear positioning are still unknown (Figueiredo et al., 2002; O'Donnell et al., 2002) (Fig. 1.12).

P. falciparum centromeres have been identified in all the 14 chromosomes as unique tandem repeat sequences with an extremely high AT content (~97%) (Kelly et al., 2006). Centromeres and associated proteins have an essential role in the segregation of chromosomes during cell division (Mahajan et al., 2008). Interestingly, while centromeric regions are encompassed in heterochromatin in most model eukaryotes (Bloom, 2014), this characteristic appears to be absent in *P. falciparum* (Hoeijmakers et al., 2012).

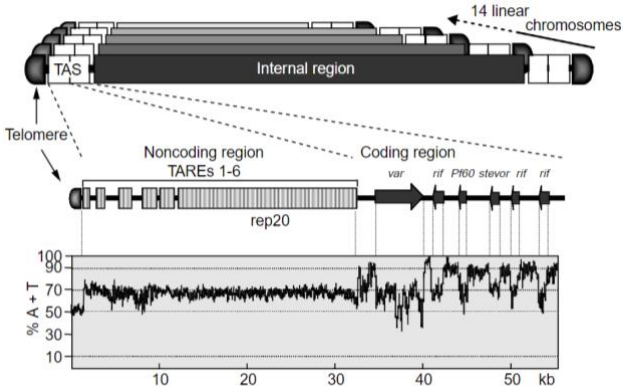

Figure 1.12. A model of the *P. falciparum* genome and features. Top panel: The *P. falciparum* haploid genome is organized into 14 chromosomes. Each chromosome comprises an internal region (containing housekeeping genes) and telomere-associated sequences (TAS) at the chromosome ends. Middle Panel: A schematic of the end of chromosome 3 exemplifies the contents of this region, which include the telomere and the TAS. The TAS is comprised of a non-coding region (TAREs 1-6) and a coding region with gene families associated with virulence (*var*, *rif* and *stevor*). Lower panel: AT content across the TAS. Image taken from (Scherf et al., 2001).

1.2.2 *P. falciparum* transcription and epigenetics

The *P. falciparum* IDC is driven by the dynamic transcription of more than 80% of the genome (Bozdech et al., 2003; Painter et al., 2018). Earlier studies described that gene expression was highly periodic and followed a transcriptional cascade, in which a "just-in-time" transcription of any gene would occur only at the time where the protein function would be needed (Bozdech et al., 2003; Llinás et al., 2006) (Fig. 1.13). At any moment

during the life cycle, only a subset of the ~5300 genes are expressed in a monocistronic manner, similarly to other eukaryotes (Lanzer et al., 1992). Since the major limiting step for gene expression is transcription initiation (Caro et al., 2014), one possibility is that expression patterns result from a precisely timed production and/or binding of sequence-specific transcription factors (TFs). While recent chromatin accessibility studies show evidence for dynamic exposure of potential TF binding sites upstream of genes (Toenhake et al., 2018), the *P. falciparum* genome encodes few sequence-specific TFs compared to other eukaryotes, accounting for less than 1% of the protein-coding genes (Balaji et al., 2005; Campbell et al., 2010). Thus, other regulatory mechanisms are likely responsible for the strictly-timed transcriptional programs observed during each developmental stage of the parasite.

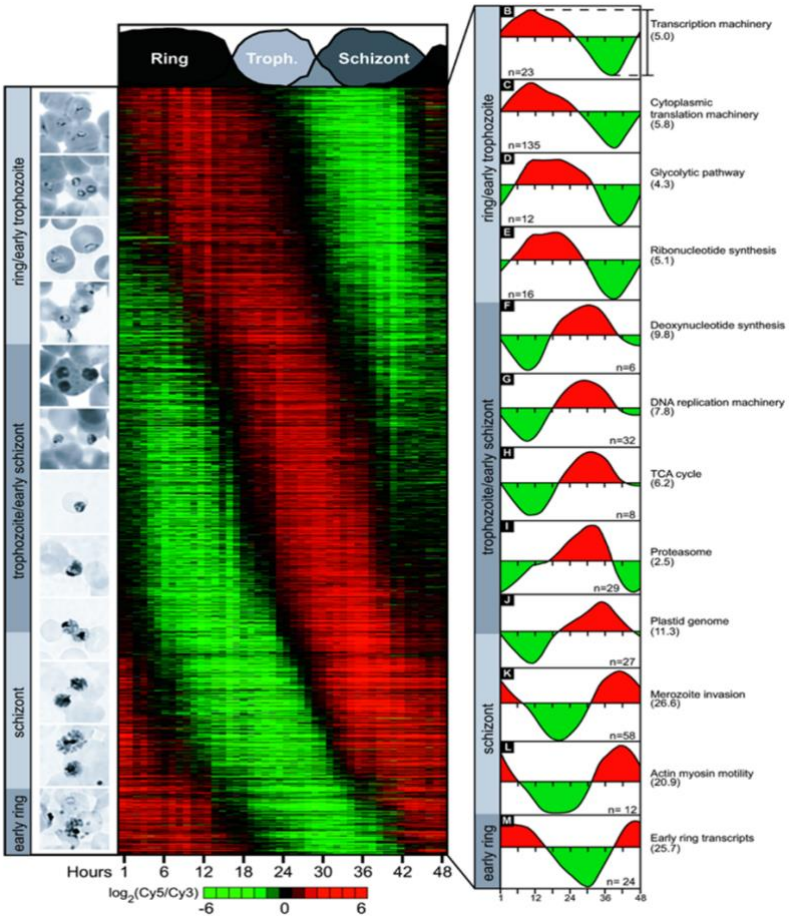

Figure 1.13. Overview of the *P. falciparum* transcriptome across the intraerythrocytic developmental cycle. A. Transcriptional profile of 2,712 genes ordered by phase expression (y-axis) across the ~48h IDC

(x-axis). On the left, representative pictures of the parasite stages are shown aligned with the correspondent phase of peak expression. B-M. Graphs with the average expression profile of genes grouped by their biochemical processes and functions (y-axis) across the ~48h IDC (x-axis). Image taken from (Bozdech et al., 2003).

1.2.2.1 Transcriptional machinery

Overall, *P. falciparum* has similar transcriptional mechanisms to those of other eukaryotes, with a basal canonical transcriptional machinery and transcription initiation via coordinated molecular events over a bipartite promoter. The core promoter drives basal transcription through assembly of the RNA polymerase II complex (RNA pol II) with the pre-initiation complex (PIC). The latter includes general transcription factors that will ensure RNA pol II binding and orientation over the core promoter. A second regulatory upstream region has binding sites for specific TFs, which can result in more or less RNA pol II transcriptional activity (Horrocks et al., 2009). The broadest scan for TFs in *P. falciparum* has revelated a total of 202 proteins, comprising those associated with the general transcriptional machinery, chromatin-associated factors, and 73 specific TFs (Bischoff & Vaquero, 2010). The sequence-specific TFs account for ~1% of the protein-coding genes (Bischoff & Vaquero, 2010; Campbell et al., 2010), which is a lower percentage than that observed in other eukaryotes such as *Saccharomyces cerevisiae* (2.8%) (Hahn & Young, 2011), *Drosophila melanogaster* (5%) (Shokri et al., 2019), and *Homo sapiens* (6%) (Vaquerizas et al., 2009).

Among the sequence-specific TFs, the 27-member Apicomplexan Apetala 2 (ApiAP2) family is believed to comprise the major transcriptional regulators identified in *P. falciparum.* Each member of the ApiAP2 family contains a conserved version the AP2 - integrase DNA binding domain also found in TFs of plants such as *Arabidopsis thaliana*, in which the AP2 family comprises the second largest class of regulators (Balaji et al., 2005; de Silva et al., 2008). Despite a conserved core secondary structure, the AP2 domain

of each ApiAP2 factor generally recognizes distinct DNA motifs. Moreover, the ApiAP2 proteins have different expression patterns across the *P. falciparum* life cycle, suggesting distinct functional properties (Balaji et al., 2005; Campbell et al., 2010; Painter et al., 2011). In *P. berghei*, the ApiAP2 family members have transcription regulation roles across all developmental stages (Modrzynska et al., 2017), implying a similar importance in *P. falciparum* transcriptional coordination.

In *P. falciparum*, several ApiAP2 factors have been characterized along the IDC. *P. falciparum* SPE2-interacting protein (*Pf*SIP2) binds to TAREs and has been suggested to have a role in heterochromatin formation (Flueck et al., 2010). *Pf*AP2Tel, which harbors a non-canonical DNA-binding AP2 domain, binds to telomeric regions of all 14 chromosomes (Sierra-Miranda et al., 2017). Another AP2 member binds to a motif in the *var* gene intron and may function in the subnuclear positioning of *var* genes (Q. Zhang et al., 2011). *Pf*AP2-I plays a role in the transcription of RBC invasion genes, possibly via recruitment of the chromatin-associated bromodomain protein *Pf*BDP1 (Santos et al., 2017). *Pf*AP2-G has been established as a master of sexual commitment, binding to and activating genes involved in gametocytogenesis (Brancucci et al., 2014).

Recently, *Pf*AP2-HS was found to play a role in the regulation of *P. falciparum* protective heat-shock response via binding to a G-box DNA motif in the promoter region of the *heath shock protein 70-1* (*hsp70-1*). Under elevated temperatures (mimicking the human host fever), both *hsp70-1* and *hsp90* were found to be upregulated. These findings are the first proof of the parasite's ability to respond to temperature changes in its environmental conditions (Tintó-Font et al., 2021). Other DNA binding proteins that have been experimentally validated in *P. falciparum* are described in Table 1.2.

Importantly, a recent study that sequenced accessible chromatin regions of the genome identified more than 4,000 regulatory regions across the IDC (Toenhake et al.,

2018). While it found sequences that correlated with stage-specific gene expression and that were bound by ApiAP2 factors, the sequences predicted to be bound by other DNA-binding factors such as Myb-type or HMGB domain-containing proteins were not detected. Therefore, it is still quite puzzling how stage-specific transcription is driven in the presence of such a small number of specific TFs.

DNA binding protein	Gene ID	Class / Subclass	Biological process	Reference
***Pf*Myb1**	PF3D7_1315800	Specific TF / Helix-turn-helix	Transcriptional control of genes involved in cell cycle regulation and progression	(Boschet et al., 2004; Gissot et al., 2005)
***Pf*TRZ**	PF3D7_1209300	Specific TF / Zinc finger	Binding to telomeric TT(T/C)AGGG repeats and regulates expression of 5S rDNA loci	(Bertschi et al., 2017)
***Pf*PREP**	PF3D7_1011800	Specific TF / K homology	Transcriptional regulation of IDC stages	(Komaki-Yasuda et al., 2013)
***Pf*Albas**	PF3D7_0814200 PF3D7_1346300 PF3D7_1006200 PF3D7_1347500	Alba	Non-specific DNA binding enriched in subtelomeric regions	(Chêne et al., 2011; Goyal et al., 2012)
***Pf*HMGBs**	PF3D7_1202900 PF3D7_0817900	Chromatin remodeling factor / high mobility group box proteins	Non-specific DNA binding; HMGB1 is enriched in centromeric regions (detailed in Chapter 3.1.2)	(Briquet et al., 2006; Kumar et al., 2008; Lu et al., 2021)

Table 1.2. DNA binding proteins regulating transcription or chromatin remodeling in P. falciparum. Adapted from (Toenhake & Bártfai, 2019)**.**

1.2.2.2 Epigenetic machinery

The term “epigenetics” - derived from the Greek word “epi”, meaning “over” or “above” the genes – was originally conceived by Conrad Waddington in an attempt to comprehend cellular phenomena that could not be explained by traditional genetic principles (Figure 1.14) (Waddington, 1957). Epigenetic regulation mechanisms are classically defined as mitotically and/or meiotically heritable changes in gene expression that do not involve changes in DNA sequence (Berger et al., 2009). Chromatin, or DNA

and its closely associated proteins, is the platform for the epigenetic machinery to work. The basic building block of chromatin is the nucleosome, which consists of an octamer of two copies of each of the canonical histones (H2A, H2B, H3, and H4) with approximately 147bp of DNA wrapped ~1.7 times around it. The functional chromatin landscape is further characterized by 1) the presence of histone variants that alter the biophysical properties of a nucleosome, 2) the presence or absence of histone post-translational modifications (e.g. methylation, acetylation) and 3) the spacing between nucleosomes (nucleosome occupancy). Indeed, a more "relaxed" use of the term "epigenetics" includes all the chromatin-based processes that influence transcription, independently of transmission through cell division or generations.

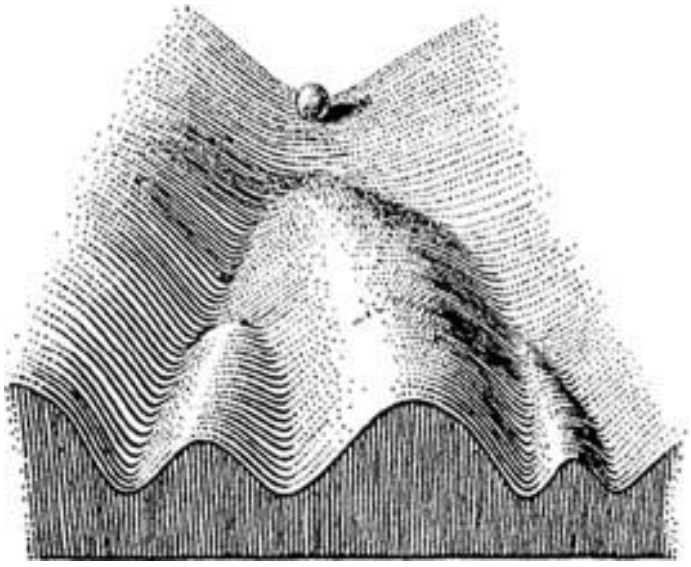

Figure 1.14. Waddington's epigenetic landscape. Conrad Waddington used the concept of the epigenetic landscape to describe the process whereby a cell, pictured here as a ball, may follow many different paths of differentiation during development (Waddington, 1957).

1.2.2.2.1 Nucleosome composition and occupancy

P. falciparum nucleosomes are composed of the four core histones H2A, H2B, H3, and H4, as well as four histone variants: H2A.Z, H2Bv (or H2B.Z), H3.3 and centromeric H3 (CenH3) (Miao et al., 2006). The basic N-terminal tail domain of histones can be modified with an array of PTMs, which can directly alter the interactions between the

nucleosome and the DNA or serve as binding platforms for chromatin-associated proteins involved in processes from transcription to DNA repair (Cosgrove et al., 2004). In most eukaryotes, the linker histone H1 completes the nucleosome by binding to the entry/exit sites of DNA, enabling higher order chromatin structure (Bednar et al., 1998); however, this element has not yet been identified in *Plasmodium* or other Apicomplexans (Sullivan et al., 2006).

The level of chromatin compaction can affect accessibility of factors to the underlying DNA regulatory regions, therefore impacting transcription, DNA repair, and mitosis. Indeed, chromatin is traditionally classified into two distinct states: euchromatin - uncondensed and accessible to the transcriptional machinery – and heterochromatin – condensed, inaccessible, and transcriptionally inactive. The heterochromatic state can be further divided into facultative and constitutive heterochromatin. While facultative chromatin can be reversed to a state of euchromatin - as occurs in the context of mutually exclusive expression of *var* genes (see chapter 2.2.2.4) – constitutive heterochromatin is a relatively permanent state of compaction, comprising sequences such as telomeres.

In the context of eukaryotes, lower nucleosome occupancy is usually found upstream of transcriptionally active genes while higher occupancy is usually found in the regulatory regions of repressed genes. The AT-rich genome of *P. falciparum* poses a technical challenge to the efforts to obtain accurate mapping of the nucleosome landscape. Therefore, earlier findings reporting lower nucleosome occupancy in intergenic regions (Bunnik et al., 2014; Ponts et al., 2010; Westenberger et al., 2009), could have been a result of technical biases towards against AT-rich regions. An optimized micrococcal nuclease (MNase) protocol, based on the preferential digestion of this endo- and exo-nuclease towards naked DNA between nucleosomes, followed by sequencing of the nucleosome-associated (i.e. protected) DNA, resulted in a plausibly more accurate nucleosome

landscape (Kensche et al., 2016). It revealed nucleosome positioning in regulatory regions and near transcriptional landmark sites (e.g. TSS, ATG, splice donor and acceptor sites, STOP, TTS). Interestingly, dynamic local nucleosome depletion over the TSS, across the IDC, correlated with temporal gene expression (Kensche et al., 2016).

Subsequent studies used an Assay for Transposase-Accessible Chromatin by sequencing (ATAC-seq) to obtain a more refined map of both nucleosomes and DNA-binding protein-protected sites. This technique relies on a Tn5 transposase to insert sequencing adaptors into accessible regions of the genome, such as linker DNA between nucleosomes or nucleosome-free regions in the promoter of a gene (Ruiz et al., 2018; Toenhake et al., 2018). These studies corroborated the previous observations, revealing a strong correlation between chromatin-accessibility changes and expression of stage-specific genes. In general, switching from a "closed" to a "open" chromatin state was associated with gene expression. It suggested an important role of activating rather than repressive factors, with the limitation that the technique may preferentially detect activator-bound chromatin regions (Ruiz et al., 2018; Toenhake et al., 2018). Binding motifs for ApiAP2 TFs were detected in *cis*-regulatory sites related to stage specific expression (Ruiz et al., 2018). Indeed, ApiAP2 family members were the only TFs enriched in regulatory regions, closely associated with epigenetic factors such as chromatin remodellers or acetylated histone binding proteins, suggesting regulation of gene activation through association with epigenetic complexes (Toenhake et al., 2018).

1.2.2.2.2 Chromatin remodelling enzymes

Nucleosome positioning and composition is coordinated by ATP-dependent chromatin remodelling complexes that have roles in (1) nucleosome assembly by participating in the deposition of histones and nucleosome maturation and spacing; (2) chromatin accessibility by catalysing the translational movement of a nucleosome (sliding)

and eviction of the nucleosome or of histone dimers; and (3) nucleosome editing, with exchange of canonical and variant histones. Based on the ATPase catalytic domain, chromatin remodellers can be grouped into four subfamilies: imitation switch (ISWI), chromodomain helicase DNA-binding (CHD), switch/sucrose non-fermentable (SWI/SNF), and INO80 (Clapier et al., 2017).

In *P. falciparum*, most of the understanding about chromatin remodelling enzymes originated from computational searches and, despite their role in regulating the dynamic nucleosome landscaped observed during the IDC, few functional studies have been performed. Analysis of the genome led to the identification of 11 SWI2/SNF2 ATPases (Templeton et al., 2004), seven of which correspond to putative chromatin modifying enzymes. These include homologues of ISWI (SNF2 helicase), CHD1, four SWI/SNF (1 DEAD/DEAH box helicase and 3 DNA helicases), and SNF2L (Bischoff & Vaquero, 2010). Similarly, three putative RuvB (part of the INO80 complex) homologues have been identified in the parasite genome (Ahmad & Tuteja, 2012). In eukaryotes, SWIB/MDM2 domains have been identified in proteins from the chromatin remodelling SWI/SNF complex, and *P. falciparum* encodes two putative SWIB/MDM2 domain-containing proteins: *Pf*MDM2 and *Pf*SWIB (Vieira & Coetzer, 2016).

Comparisons of the Apicomplexan SWI2/SNF2 ATPases with those from other eukaryotes revealed unique domain architectures in some of these chromatin remodellers including *Pf*ISWI, which has five Plant HomeoDomain (PHD) fingers around the core helicase domains (Templeton et al., 2004). In particular, *Pf*ISWI was found to bind to the promoters of transcriptionally active genes and chromatin-accessible intergenic regions. *Pf*ISWI functional characterization revealed a role in enabling transcriptional activation, possibly via chromatin remodelling at the *Pf*ISWI-bound promoter regions (Bryant et al., 2020). It is clear that, given the potential roles of chromatin remodellers in gene regulation,

further studies to address their functions in the malaria parasite epigenetic landscape are essential.

1.2.2.2.3 Histones variants

Canonical histones are mainly synthetized and assembled in a replication-coupled manner whereas their non-allelic isoforms - histone variants – are locally incorporated into chromatin independent of replication. Through the coordinated action of chromatin remodellers and chaperones, integration of histone variants can alter the nucleosome and local chromatin structure and/or erase PTMs of the previous histone. Accordingly, histone variants have been found to have roles in many diverse processes such as transcription, DNA repair, and chromosome segregation (Sarma & Reinberg, 2005) (Table 1.3).

In *P. falciparum*, across the IDC, expression of canonical histones peaks in the schizont stage, consistent with the required histone deposition during DNA replication, with histone variants showing an overall lower expression in comparison with their canonical counterparts (Coetzee et al., 2017).

Examples of histone variants include *Pf*H3.3, found in euchromatic GC-rich coding regions and subtelomeric repetitive sequences of the genome (S. A. K. Fraschka et al., 2016). The H2A.Z and H2Bv double-variant nucleosome is enriched in AT-rich promoters and correlates with promoter strength, but not temporal activity (Bártfai et al., 2010; Hoeijmakers et al., 2013). Finally, CenH3 is present in centromeric regions, which are also enriched in H2A.Z; however, pericentric heterochromatin in *P. falciparum* is not enriched in trimethylation of histone H3, lysine 9 (H3K9me3), as it is in certain model eukaryotes (Hoeijmakers et al., 2012; Lopez-Rubio et al., 2009; Maison et al., 2002).

Noteworthy, the N-terminal region of the canonical histone H3 – modified with PTMs associated with transcriptional activation - can be clipped by a nuclear protease during the IDC. In several eukaryotes, histone clipping is involved in transcriptional

regulation via removal of associated PTMs, with this being the first report of such a remarkable epigenetic mechanism in protozoan pathogens (Herrera-Solorio et al., 2019).

Variant	Chromatin effect	Function
H2A.Z	Open/closed chromatin	Transcription activation/repression, chromosome segregation
CenH3	-	Kinetochore formation/function
H3.3	Open chromatin	Transcription

Table 1.3. Functions of ubiquitous histone variants. Table modified from (Kamakaka & Biggins, 2005)**.**

1.2.2.2.4 Histone post-translational modifications

Histones PTMs have a fundamental role in the epigenetic regulation of genes by either altering DNA-nucleosome and nucleosome-nucleosome interactions or by providing specific binding sites for enzymes and protein complexes. Altogether, these can affect several processes, including transcription, replication, chromatin condensation, and DNA repair (Table 1.4) (Rothbart & Strahl, 2014).

Modification type (abbreviation)	Residues modified	Function
Acetylation (ac)	K-ac	Transcription, chromatin structure
Methylation (me)	K-me1/2/3	Transcription, DNA repair, DNA replication, heterochromatin
	R-me1/2/3	Transcription
Phosphorylation (ph)	S-ph	Transcription, DNA repair, mitosis
	T-ph	Mitosis
Ubiquitination (ub)	K-ub	Transcription, DNA repair, heterochromatin
SUMOylation (su)	K-su	Transcription
ADP ribosylation (ar)	K-ar	Transcription, DNA repair, heterochromatin

Table 1.4. Selection of histone-post translational modification (PTMs) and their functions. Functions of PTMS in lysine (K), arginine (R), serine (S), and threonine (T) residues are shown. Table adapted from (Rothbart & Strahl, 2014).

In *P. falciparum*, a wide array of PTMs has been identified on core histones and histone variants (Table 1.5) (Coetzee et al., 2017; Saraf et al., 2016; Trelle et al., 2009). In contrast to multicellular eukaryotes, the *P. falciparum* genome during the IDC has a predominantly transcriptionally permissive, euchromatic epigenome (Lopez-Rubio et al.,

2009; Salcedo-Amaya et al., 2009). This was found to correlate with a high abundance of histone H3 acetylation (Coetzee et al., 2017; Saraf et al., 2016; Trelle et al., 2009). Indeed, acetylation of H3K9/14/56 and H4K8/16 in addition to mono-methylation of H4K20me1 had been previously associated with euchromatin formation and linked to transcriptional regulation across the IDC (Gupta et al., 2013). Acetylation of H3K9, H3K1 and H3K27 was found to correlate both with stage-specific transcription and chromatin accessibility across the IDC (Ruiz et al., 2018; Tang et al., 2020).

Histone	Acetylation	Methylation			Phosphorylation
		Mono-	Di-	Tri-	
H2A	N-term, K3, K5				S18
H2A.Z	N-term, K11, K15, K19, K25, K28, K30, K35, K37	K28			S33
H2B					S28, S50, S56
H2Bv (or H2B.Z)	N-term, K3, K8, K13, K14, K18				S1, S32, T84
H3	K4, K9, K14, K18, K23, K27, K36, K56, K79, K122	K4, K9, K14, R17, K18, K23, K27, K36, K56, K79	K4, K9, R17, K27, K36, K56, K79	K4, K9, K27, K36, K56, K79	S10, T11, S22, S28, S32, S57
H3.3	K9, K14, K18, K23, K27, K36, K79	K4, K9, R17, K79	K4, K9, R17, K79	K4, K9, K79	S22, S28, S32, S57, T58
H3Cen	K23, K26				
H4	N-term, K5, K8, K12, K16, K20	R3, K5, K12, K16, R17, K20	R3, K20	K20	

Table 1.5. Histone post-translational modification landscape of *P. falciparum.* PTMs have been detected on lysine (K), arginine (R), serine (S), and threonine (T) histone residues (Coetzee et al., 2017)**.**

Recently, it was shown that during the earlier stages of sexual differentiation, there is an increased abundance of repressive marks such as H3K9me3 and H3K36me3, suggestive of a prominent heterochromatin status in these parasites (Coetzee et al., 2017). Along the IDC, heterochromatin exceptionally encompasses clonally variant genes, enriched in H3K9me3 and H3K36me3 (Flueck et al., 2009; Lopez-Rubio et al., 2009; Paddon et al., 2013; Salcedo-Amaya et al., 2009); while for the remaining genes,

transcriptional silence is generally associated with unacetylated histones (Chaal et al., 2010).

1.2.2.2.5 Chromatin modifying enzymes

The proteins that place ("writers"), remove ("erasers"), or bind to ("readers") histone PTMs play an important role in the dynamic chromatin landscape. In *P. falciparum*, the epigenetic writers identified so far include histone methyltransferases, which attach methyl groups to either lysine (HKMT) or arginine residues (HRMT), and histone acetyltransferases (HATs), which attach acetyl groups to lysine residues. Several epigenetic erasers, which remove methyl (histone demethylases) and acetyl [histone deacetylases (HDACs)] groups, have also been identified (Deitsch & Dzikowski, 2017; Duraisingh & Skillman, 2018; Guizetti & Scherf, 2013; Scherf et al., 2008). Some of these have been functionally characterized and have roles in *var* gene regulation (Table 1.6).

Protein name	Gene ID	Function	Reference
Histone methyltransferases			
***Pf*SET2**	PF3D7_1322100	Role in *var* gene silencing via H3K36me3	(Cui et al., 2008; Jiang et al., 2014; Ukaegbu et al., 2014)
Histone deacetylases			
PfSIR2A	PF3D7_1328800	NAD-dependent histone deacetylases with role in the silencing of different cohorts of *var* genes	(Duraisingh et al., 2005; Freitas et al., 2005; Merrick & Duraisingh, 2007; Tonkin et al., 2009)
PfSIR2B	PF3D7_1451400		
***Pf*Hda2**	PF3D7_1008000	Class II histone deacetylase, linked to *var* gene silencing and sexual differentiation	(Andrews et al., 2012; Coleman et al., 2014)
Histone acetyltransferases			
PfGCN5	PF3D7_0823300	Global regulator of stress responsive genes	(Rawat et al., 2021)

Table 1.6. Experimentally validated epigenetic writers and erasers in *P. falciparum*.

Finally, epigenetic writers and erasers are complemented by the action of the readers, which have domains that are able to bind to specifically modified residues such as acetylated lysine (e.g. bromodomains) or methylated lysine (e.g. chromodomains and PHD fingers) (Cui & Miao, 2010; Doerig et al., 2015).

In *P. falciparum*, the bromodomain-containing protein (*Pf*BDP1) that binds to acetyl modifications (H3K9/14ac) can interact with another bromodomain-containing protein (*Pf*BDP2) and AP2-I to regulate expression of genes involved in RBC invasion (Josling et al., 2015). The chromodomain-containing heterochromatin protein 1 (*Pf*HP1), which binds to H3K9me3, plays a central role in the maintenance of facultative heterochromatin, a remarkable exception of a mostly euchromatic genome landscape.

1.2.2.2.5.1 Heterochromatin protein 1 and transcriptional repression

During the *P. falciparum* IDC, *Pf*HP1/H3K9me3 demarcates large heterochromatic domains encompassing ~ 400 genes across subtelomeric and internal regions of the genome. Almost all *Pf*HP1-silenced genes are part of clonally variant gene families, such as the *var* gene family, involved in antigenic variation (see section 1.1.3.1) (Flueck et al., 2009; Lopez-Rubio et al., 2009), with certain exceptions including *pfap2-g*, which encodes a transcription factor that is the master inducer of gametocytogenesis (sexual differentiation) (Brancucci et al., 2014).

For sexual commitment to occur, *P. falciparum* gametocyte development 1 (GDV1) binds to *Pf*HP1 and displaces it from H3K9me3-enriched *pfap2-g*, which leads to a reversal of heterochromatin and de-repression. However, de-repression via GDV1 was found to be specific for HP1-associated genes involved in sexual stage commitment and development (Filarsky et al., 2018). How GDV1 achieves this specificity despite binding to HP1-enriched regions genome-wide and the mechanism by which HP1 is evicted from the active *var* gene remain challenging questions (Filarsky et al., 2018).

In model eukaryotes, the epigenetic machinery acts in developmental contexts to silence genes that are no longer needed in differentiated cells (Becker et al., 2016). Similarly, in *P. falciparum* IDC, *Pf*HP1-dependent silencing ensures expression of certain gene groups and repression of others in asexually reproducing and sexually differentiating

parasites (Filarsky et al., 2018; S. A. Fraschka et al., 2018). Intriguingly, these *Pf*HP1-dependent genes represent only a fraction of the ~5300 genes expressed along the IDC, with thousands of other genes presenting an identically strict transcriptional control. An outstanding question in the malaria field still remains: how are HP1-independent genes silenced until their appropriate time of expression?

1.3 Genome organization and gene regulation in *P. falciparum*

Chromosome organization of the interphase eukaryotic nucleus – key for genome maintenance and transcription regulation - is achieved in a hierarchical manner via chromatin folding/looping at multiple levels. The smallest scale of chromatin folding occurs at the DNA-histone association level – nucleosomes - with the formation of the chromatin fiber. At a higher level of genome organization, the formation of chromatin loops generates genomic regions – topologically associating domains (TADs) - which present preferential interactions with each other rather than with the rest of the genome. At the chromosomal scale, chromatin is segregated into active "A" and repressed "B" compartments of interactions, which reflects preferential contacts of chromatin regions with the same general epigenetic features. The highest unit of genome organization is the chromosome, and each one occupies a defined space within the 3D nucleus, forming a chromosome territory (Figure 1.15) (Misteli, 2020).

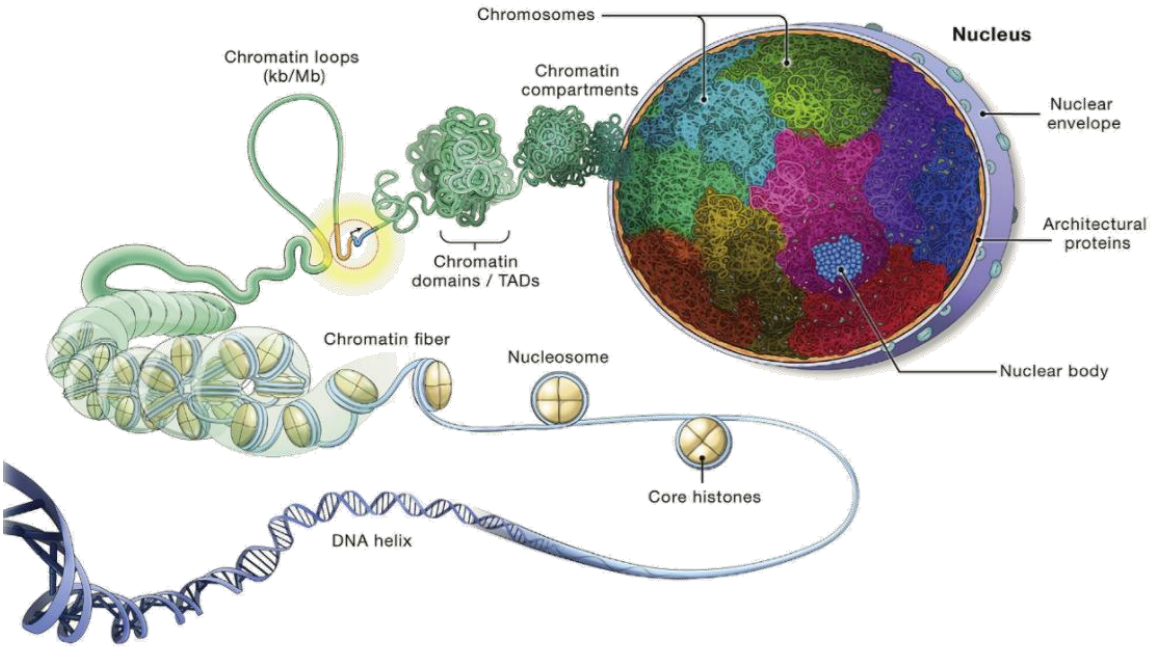

Figure 1.15. Eukaryotic genome organization. The association of DNA and an octamer of core-histones form nucleosomes, which are organized into the chromatin fiber. In turn, folding/looping of this chromatin fiber can bring enhancers (yellow) into close proximity with gene promoter regions (blue) to regulate their

transcription. The fiber then folds into higher-order chromatin regions - topologically associating domains (TADs). At a higher scale, chromatin is segregated into active and repressed compartments of interactions, with the space occupied by each individual chromosome forming chromosome territories (multiple colours) within the cell nucleus. In the DNA-free space, the nucleus also contains RNA and proteinaceous protein aggregates which form nuclear bodies (blue). Image taken from (Misteli, 2020).

Chromatin contacts and their functions are likely to be influenced by the biophysical environment in which chromosomes exist. Subnuclear compartments, such as the nuclear lamina and the nucleolus, can serve as a scaffold for chromatin tethering. Genomic interactions with the nuclear lamina, which lies on the inner side of the nuclear envelope, are often associated with chromatin features typical of heterochromatin and a transcriptionally repressive state (van Steensel & Belmont, 2017). Similarly, genomic regions near the nucleolus appear to be a hub for repressive chromatin (Bersaglieri & Santoro, 2019).

At a lower level and independent from subnuclear compartments, TADs constitute basic functional units of chromosomal organization. It has been observed that these domains often insulate contacts between genes and their regulatory sequences (i.e. enhancers) (Sun et al., 2019; Symmons et al., 2014) and that physical contact between a promoter and an enhancer is associated with enhanced gene activation (Deng et al., 2012). In line with these observations, deletion of a boundary between two TADs causes ectopic contacts between loci that were previously insulated from each other (Nora et al., 2012), which can cause aberrant gene activation (Lupiáñez et al., 2015). Even though the mechanistic link between TAD structure and transcription might be more complex and organism-specific, these domains have been found to be involved in the regulation of cell type- and developmental stage-specific transcriptional programs (Sikorska & Sexton, 2020; Szabo et al., 2019).

In mammalian cells, cohesin and the CCCTC-binding Factor (CTCF) are often found at the boundaries of TADs, and the deletion of CTCF binding sites leads to the loss

of these chromatin domains (Dixon et al., 2012; Nuebler et al., 2018; Rao et al., 2017). While the presence of CTCF at TAD borders appears to be specific to mammals (N. E. Matthews & White, 2019), TAD or TAD-like domains have been described in a large range of organisms. Indeed, contact domains, reminiscent of those seen in mammals, have been found in other eukaryotes including some without known CTCF homologs, such as *P. falciparum, S. pombe, S. cerevisiae, C. elegans, and A. thaliana* (Heger et al., 2012; Rowley et al., 2017; Rowley & Corces, 2016).

1.3.1 Genome organization in *P. falciparum*

As in other eukaryotes, genome organization within the nucleus appears to be crucial for gene regulation in *P. falciparum*. Although many important early observations established the general structure of the *P. falciparum* genome, the advent of chromosome conformation capture techniques has provided insight into the 3D organization of the genome and its effects on transcription by mapping DNA-DNA interactions genome-wide. Since their development by (Dekker et al., 2002), genome-wide 3C-based techniques (i.e. 4C, 5C, Hi-C, and Capture-C), have revealed genome architectural features with increasing levels of detail (Kempfer & Pombo, 2020).

1.3.1.1 Telomeres and Centromeres

Over 20 years ago, the Scherf laboratory used DNA fluorescence *in situ* hybridization (FISH) to probe a highly repetitive subtelomeric element, *rep 20*, and showed that *P. falciparum* chromosome ends formed clusters of four to seven telomeres at the nuclear periphery. This particular nuclear positioning was found to facilitate recombination events between the subtelomeric virulence genes (Freitas-Junior et al., 2000). Moreover, both TAREs and *rep20* were found to be involved in cluster formation (Figueiredo et al., 2002). Indeed, plasmids carrying the *rep 20* sequence co-localized with those telomeric

clusters, indicating that these chromosomal interactions are sequence-dependent (O'Donnell et al., 2002).

In addition to telomeres, centromeres form clusters before and during schizogony, suggesting that this organization is needed during interphase and mitosis (Hoeijmakers et al., 2012). Even though the functional importance of this spatial arrangement remains poorly understood, it has been shown in other eukaryotes that centromeric clustering is a relevant topological constraint that can affect transcription by preventing intrachromosomal arm interactions (Tolhuis et al., 2011).

In 2013, the chromosome conformation capture technique Hi-C was used for the first time to map genome-wide chromosome contacts in the *P. falciparum* ring stage and largely confirmed what had been previously observed. It revealed a structured genome driven mainly by two factors: 1) the spatial clustering of telomeric regions and clonally variant gene families at the nuclear periphery and 2) that centromeres and telomeres cluster at opposite sides of the nucleus (Ay et al., 2014; Lemieux et al., 2013) (Figure 1.16).

1.3.1.2 Ribosomal DNA

Another feature of *P. falciparum* higher order chromosomal organization is the nucleolus, formed by transcription of ribosomal DNA (rDNA) into rRNA by RNA polymerase I (Pol I) (Mancio-Silva et al., 2010). Despite the seven rDNA gene loci being spread across different chromosomes (1, 5, 7, 11, and 13) (Gardner et al., 2002; Langsley et al., 1983), they cluster together to form the nucleolus in the parasite pre-replicative stages (Mancio-Silva et al., 2010). This contrasts with what is observed in budding yeast, in which one single chromosome harbours the ~150 rDNA units that in turn cluster in one single nucleolus that does not disassemble during mitosis (Carmo-Fonseca et al., 2000). In human cells, rDNA loci exist in clusters on five different chromosomes and form multiple nucleoli per nucleus (McStay & Grummt, 2008).

During the *P. falciparum* IDC, the rDNA units on chromosomes 5 and 7 are predominantly transcribed (A-type), whereas during mosquito stage, rDNA units on chromosomes 11 and 13 are predominantly transcribed (S-type) (Fang & McCutchan, 2002). A 3D model for ring stage parasites based on Hi-C data revealed a strong colocalization of A-type rDNA near the nuclear periphery, and a decreased frequency of contacts as the parasite progresses through trophozoites and schizont stages (Ay et al., 2014), hinting that genes with similar expression profiles may associate in a spatiotemporal manner during the IDC.

1.3.1.3 *var* Genes

The most striking proof that nuclear positioning plays a role in *P. falciparum* transcriptional regulation lies in the context of mutually exclusive transcription of the *var* gene family. Even though *var* gene loci are spread across 13 out 14 chromosomes, DNA FISH showed that subtelomeric and central *var* genes form four to seven clusters at the transcriptionally repressive nuclear periphery (Lopez-Rubio et al., 2009; Ralph et al., 2005), with the single active *var* gene spatially separated from those repressive clusters (Mok et al., 2008; Ralph et al., 2005) (Fig. 1.16). DNA and RNA FISH demonstrated that, after switching, the newly active *var* gene relocates to an as-yet undefined transcriptionally competent site at the nuclear periphery (Freitas et al., 2005; Lopez-Rubio et al., 2009; Ralph et al., 2005; Voss et al., 2006).

A recent Hi-C study showed that depletion of *Pf*HP1, which leads to the de-repression of silenced *var* genes, also resulted in a loss of clustering among silenced *var* genes, suggesting that *var* gene organization is tightly linked to transcriptional status (Bunnik et al., 2018).

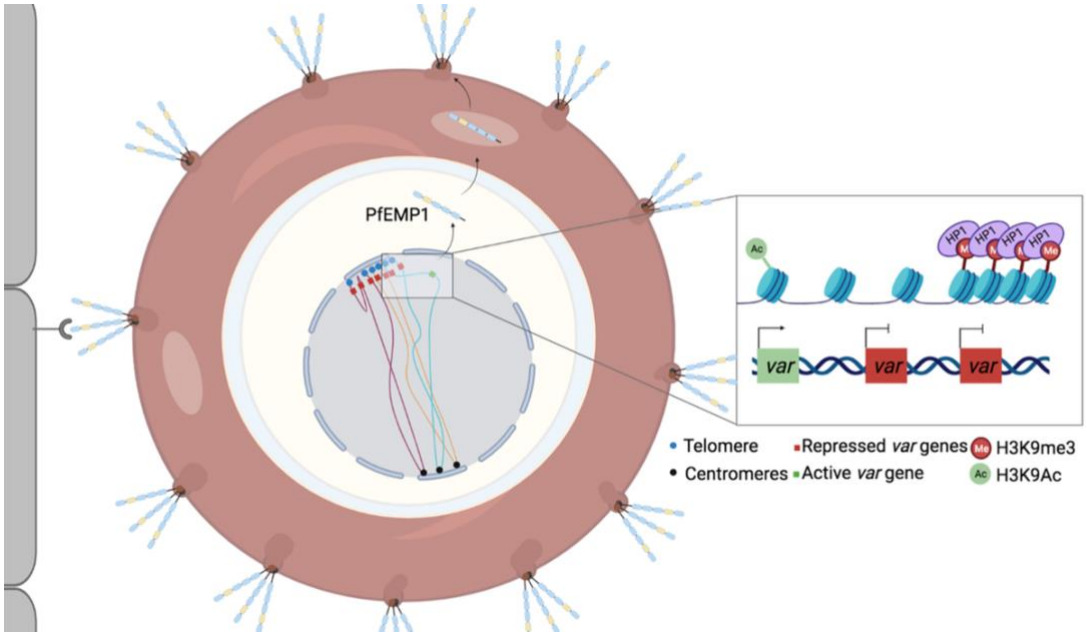

Figure 1.16. *P. falciparum* genome organization is important for *var* gene mutually exclusive transcription. Mutually exclusive expression of the 60-member *var* gene family, which codes for the immunodominant variant adhesion surface molecule *P. falciparum* Erythrocyte Membrane Protein 1 (*Pf*EMP1), is key for immune evasion and pathogenesis. Despite the wide distribution of *var* genes throughout the genome, transcription is coordinated so that all but one *var* gene are silenced in heterochromatic clusters (*Pf*HP1/ H3K9me3) at the nuclear periphery. The single active *var* gene is euchromatinized (H3K9Ac), with activation being associated with spatial separation from these repressive clusters and decompaction of chromatin.

1.3.1.4 Transcriptionally related genes

In addition to the significance of genome organization for mutually exclusive transcription of *var* genes (Fig. 1.15), a growing body of evidence indicates that genome organization may play role in the regulation of other transcriptional programs in *P. falciparum.*

In the context of RNA Pol II/III transcription, it has been shown that clustering of transcription foci increases during the transition from early to late stages of the *P. falciparum* IDC. In turn, these clusters resembled the transcription factories observed in model eukaryotes (Mancio-Silva et al., 2010). A follow-up study demonstrated that their increase in number over the course of the IDC correlates not with nuclear size, but with

total transcriptional activity (Moraes et al., 2013). Altogether, these studies indicate that transcription may be spatially organized into developmentally-regulated foci.

Indeed, assaying genome architecture at high resolution with Hi-C at multiple stages across the IDC revealed a correlation between chromosomal arrangements and transcriptional levels (Ay et al., 2014). It had previously been observed that the transition from ring to trophozoite stage is accompanied by 1) an increase in transcriptional activity, 2) decrease in nucleosome occupancy, and 3) an increase in the number of nuclear pores, facilitating the export of messenger RNA (mRNA) to the cytoplasm. Once the parasite enters schizogony, these changes are reversed (Weiner et al., 2011). The more recent Hi-C study confirmed that the genome adopted a more open conformation during trophozoite stage compared to ring and schizont stages, perhaps due to decreased nucleosome occupancy or in order to accommodate the increase in transcription (Ay et al., 2014).

Certain transcriptionally related genes appear to change their localization within the nucleus across developmental stages according to their transcriptional status. One example is the clustering of genes, such as *ap2-g*, that are exclusively transcribed in gametocytes and sporozoites, suggesting that repression during the IDC may be dependent on their nuclear positioning (Ay et al., 2014). Another example is the change in nuclear localization of invasion genes during the transmission from human to mosquito (early and late gametocytes), and from mosquito to human (sporozoites) (Bunnik et al., 2018). Although this growing body of evidence shows that specific genes and genomic features associate at specific times in the *P. falciparum* life cycle, with the exception of HP1-dependent genes, the factors responsible for this organization are largely unknown.

1.3.2 Proteins involved in genome organization

Genome organization is strongly affected by the physical interaction between DNA, chromatin, and architectural elements of the cell nucleus, such as the nuclear periphery and nuclear bodies. In higher eukaryotes, the nuclear envelope acts as a major constraint in the organization of genomes, and lamins are involved in the positioning of peripheral genomic regions (Zheng et al., 2018). Even though lamin orthologs and lamin-binding proteins exist in some species within the taxa Alveolata (Koreny & Field, 2016), no orthologs have been identified in Apicomplexa parasites. As for other nuclear compartments, the nucleolus is the most-well characterized in *P. falciparum*, defined by the presence of *Pf*Nop1 (or fibrillarin) and with *Pf*TERT (protein component of telomerase), which localizes in a subcompartment of the nucleolus (Figueiredo et al., 2005). However, a functional characterization is still needed to understand the role of these subnuclear compartment factors in transcription regulation and genome organization.

In *P. falciparum,* it has been shown that several aspects of genome organization are dynamic across the IDC (Chapter 1.3.1). In mammalian cells, it was observed that movement of a chromosome site from the nuclear periphery to an internal region appeared to be dependent on nuclear actin and myosin (Chuang et al., 2006). In *P. falciparum*, actin has provided the first link between a nuclear structural factor and transcriptional regulation, with perturbation of actin dynamics resulting in the loss of organization and mutually exclusive regulation of *var* genes (Q. Zhang et al., 2011).

The only architectural factor that has been functionally studied in *P. falciparum* is the high-mobility-group-box protein 1 (*Pf*HMGB1). It was found to play a role in the nuclear organization of centromeres, and knockdown led to defects in *var* gene transcription (Lu et al., 2021). While depletion of *Pf*HP1 led to the loss of *var* gene clustering, it is unclear if HP1 itself is the architectural protein that facilitates the higher

order organization of *var* genes at the nuclear periphery. Moreover, architectural factors linking chromosomal organization to the strict spatio-temporal transcriptional regulation of HP1-independent genes remain to be uncovered. Importantly, proteins such as CTCF or lamin, implicated in higher-order chromosome organization in other eukaryotes (Batsios et al., 2012; Heger et al., 2012), are absent in *P. falciparum*. However, the main components of the cohesin complex have been identified.

1.4. Cohesin: tying up loose ends?

Cohesin is a member of the structural maintenance of chromosome (SMC) protein family complexes, also including condensin and the SMC5-SMC6 complex, which are key regulators of chromosome structure in all living organisms, from bacteria to humans (Uhlmann, 2016). The most well-characterized role of cohesin is in holding replicated sister chromatids together to ensure faithful chromosome segregation during cell division (Guacci & Koshland, 1997; Michaelis et al., 1997); however, over recent years, roles in the DNA damage response, transcriptional regulation, and higher-order chromatin structure have been unveiled (Horsfield, 2022; Litwin et al., 2018; Nishiyama, 2019).

1.4.1 Cohesin complex composition and basic function

The core cohesin complex has a ring-like structure and is comprised of three subunits: SMC1, SMC3, and an α-kleisin protein, Scc1 (also known as Mcd1/Rad21 and hereafter referred as Rad21) (Haering et al., 2002, 2004; Haering & Hasmyth, 2003; Losada & Hirano, 2005) (Fig. 1.16). Each SMC subunit folds on itself by antiparallel coiled coil interactions, creating a globular hinge domain at one end and a functional adenosine triphosphate (ATP) nucleotide-binding domain (NBD) on the other. The NBD is formed when the SMC N-terminal Walker A motif (i.e. the phosphate-binding loop motif) dimerises with the C-terminal Walker B motif. The two SMC subunits associate with each other via their hinge domains, creating a V-shaped dimer. The characteristic ring-like structure emerges when Rad21 binds to and connects the SMC3 coiled coil region near the NBD and the SMC1 NBD (Gligoris et al., 2014; Gruber & Haering, 2003; Haering et al., 2002; Huis in ’t Veld et al., 2014) (Fig. 1.16).

Another component of the cohesin complex is a stromalin protein, Scc3 (also known as Psc3/SA/STAG and hereafter referred as STAG), which interacts with two regions of

the Rad21 C-terminus (Roig et al., 2014) (Fig.1.17). All eukaryotes have STAG orthologs, as this is a key regulatory subunit found to be involved in cohesin loading onto chromatin by stimulating cohesin's ATPase activity in yeast (Hu et al., 2011; Murayama & Uhlmann, 2014) and release from chromosomes in vertebrates (Hauf et al., 2005; Rowland et al., 2009). In human, there are two STAG paralogues (STAG 1 and 2), only one of which associates with any given cohesin complex. Thus, depletion of STAG1 or 2 leads to distinct consequences for chromosome cohesion and DNA repair (Canudas & Smith, 2009; Kong et al., 2014).

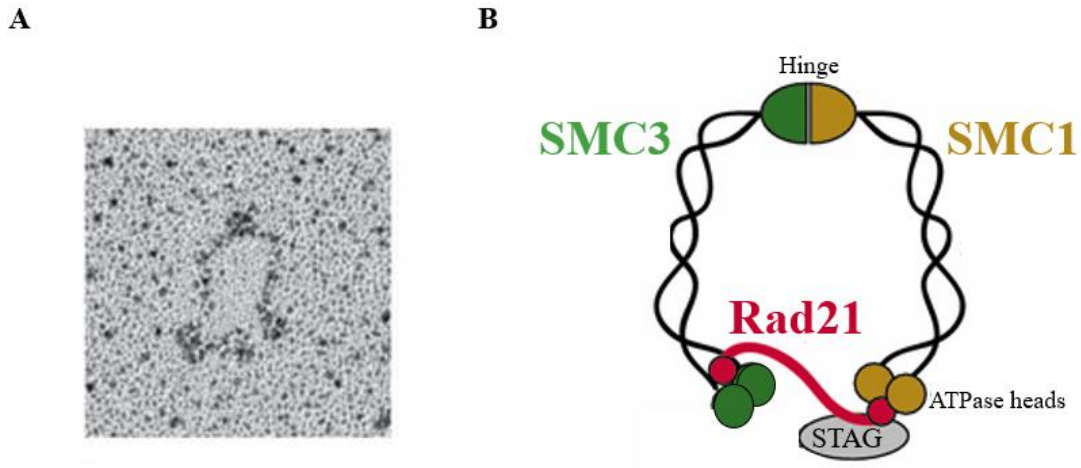

Figure 1.17. Structure of the cohesin complex. A. Representative micrograph of the human cohesin tetramer. Image taken from (Huis in 't Veld et al., 2014). **B**. Graphical representation of the cohesin complex ring (SMC3, SMC1, Rad21 and STAG). Image adapted from (Mirkovic & Oliveira, 2017)**.**

1.4.1.1 Cohesin engages with DNA

The structure that emerges from the SMC/Rad21 association has long raised the possibility that cohesin associates with chromosomal DNA by topological entrapment within the ring (Haering et al., 2008). In the context of sister chromatid cohesion, two main models of cohesin engagement with DNA have been described: (1) the ring model, whereby two sister chromatids are topologically entrapped inside the ring (Haering et al., 2008; Ivanov & Nasmyth, 2005) and (2) the handcuff model, in which each cohesin entraps a single chromatid, with cohesion achieved via dimerization of the cohesin complexes

(Huang et al., 2005; N. Zhang et al., 2008). More recently, a novel model has emerged whereby cohesin can engage chromatin both in a topological and a non-topological manner that does not involve encircling the DNA through the ring structure (Srinivasan et al., 2018).

However, cohesin not only holds sister chromatid together in post-replicative cells, but is also involved in organizing chromatid fibers during interphase (Rao et al., 2017). For performing this role, a novel mode of action has emerged for human cohesin: DNA loop extrusion, which is dependent on cohesin's ATPase activity (Davidson et al., 2019; Y. Kim et al., 2019). Indeed, this recent discovery shifted the role of cohesin from an apparently passive tethering factor to an active molecular motor.

1.4.1.2 The cohesin cycle and its regulatory proteins

Cohesin loading is not an evenly distributed event across the chromosomal landscape, as it is particularly enriched in centromeric and pericentromeric regions as well as specific loci in chromosomal arms (Blat & Kleckner, 1999; Glynn et al., 2004; Megee et al., 1999; Tanaka et al., 1999). Moreover, it has been shown that cohesin can translocate across the DNA. Thus, cohesin binding sites and cohesin loading sites do not necessary coincide (Hu et al., 2011; Lengronne et al., 2004). In fact, cohesin is loaded and unloaded from chromatin in a cycle that is regulated by various accessory proteins.

Scc2 and Scc4 (also known as NIPBL–MAU2 in humans) form a dimer and load cohesin onto chromatin (Gerlich et al., 2006; Guacci & Koshland, 1997; Losada et al., 1998; Michaelis et al., 1997). Involved in the maintenance of the cohesin complex in chromatin are Eco1, soronin, and the Pds5 (Ben-Shahar et al., 2008; Nishiyama et al., 2010). Shugoshin and PP2A protect cohesin from removal by WAPL (Q. Zhang & Liu, 2020). On the other hand, interaction of WAPL with Pds5 is involved in cohesin dissociation from chromatin (Nishiyama et al., 2010). Separase is also associated with

cohesin removal, with Securin inhibiting its action until the appropriate time (Lin et al., 2016) (Fig. 1.18).

In the process of cohesin removal from chromatin, several mitotic kinases phosphorylate key proteins in the cohesin cycle. The Aurora B kinase and Cyclin-Dependent kinase (Cdk1) have been shown to antagonize soronin, which results in cohesin dissociation from chromosomes (Nishiyama et al., 2013). The phosphorylation of STAG by Polo-like kinase 1 (PlK1) is also involved in cohesin removal (Hauf et al., 2005). Curiously, Aurora B and Cdk1 are also suggested to be involved in protecting cohesin from removal from chromatin (Q. Zhang & Liu, 2020) (Fig. 1.18).

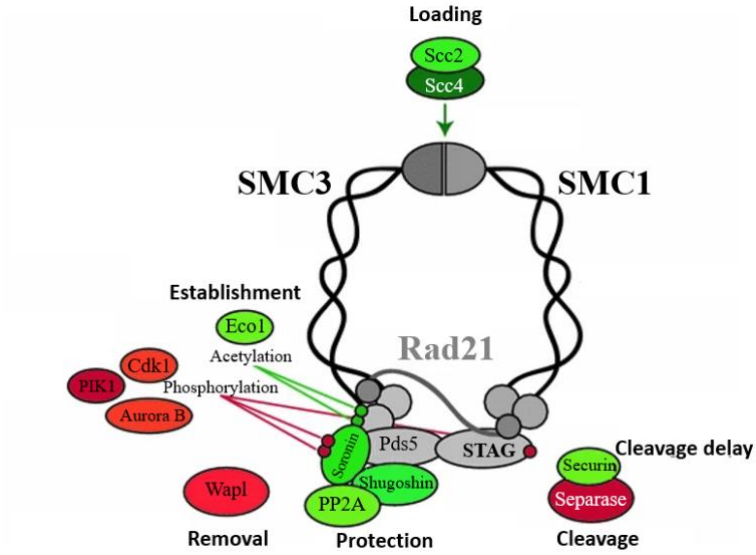

Figure 1.18. Cohesin and associated regulatory factors. The cohesin complex and different regulatory proteins regulate cohesin interaction with chromatin. Molecules are color-coded accordingly to their influence in the stabilty of cohesin's association with chromatin. Factors that promote cohesin association with chromatin are in green, those that antagonize this interaction are in red, and factors with a dual role both in promoting cohesin association and dissociation are in orange. Image adapted from (Mirkovic & Oliveira, 2017).

1.4.1.2.1 Cohesin and the cell cycle

Before DNA replication (G1 phase), cohesin interaction with chromatin is quite dynamic, with Wapl destabilizing and removing the complex from unreplicated chromatin (Eichinger et al., 2013; Gerlich et al., 2006). After G1 phase, cohesin interaction with

chromatin appears to correlate with the main role of the complex in sister chromatid cohesion (Fig. 1.19).

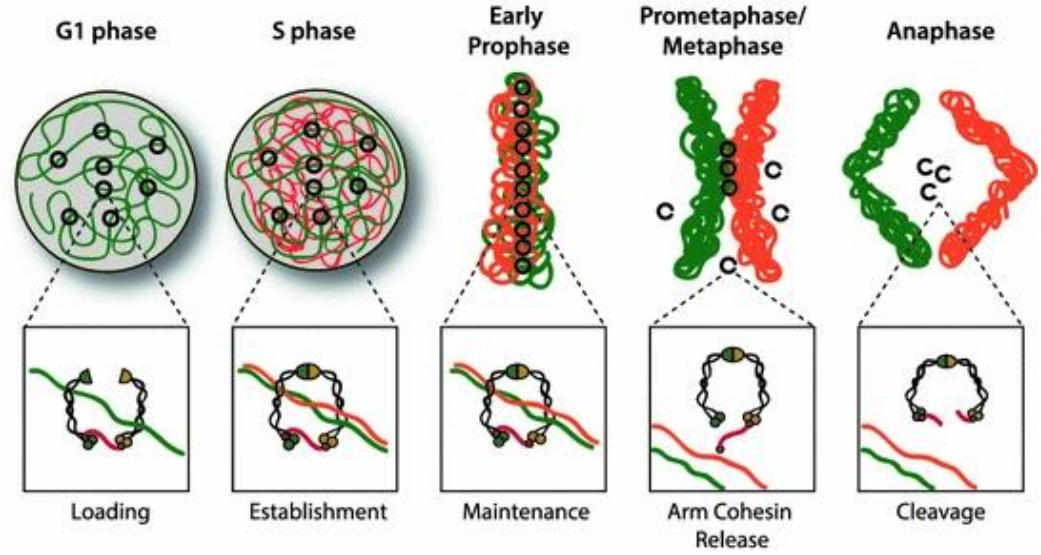

Figure 1.19. Overview of the cohesin cycle. Cohesin is loaded in telophase or G1 phase and dynamically associates with chromatin. Upon replication, cohesion is established, connecting two replicated strands. In metazoans cohesin is removed in a dual-step strategy, with non-centromeric cohesin removed from chromosome arms during prophase and the remaining cohesin pool removed at the onset of anaphase to allow separation of the sister chromatids. Image taken from (Mirkovic & Oliveira, 2017).

The initial association of cohesin with chromatin is mediated by the by Scc2/4 loading factor. In budding yeast, cohesin is loaded onto DNA at the end of G1 phase (Guacci & Koshland, 1997; Michaelis et al., 1997), while in metazoans the process initiates already in telophase (Gerlich et al., 2006; Losada et al., 1998). Following the onset of S phase, a fraction of cohesin molecules establishes effective cohesion between the newly replicated sister chromatids. Stabilization of the cohesin complex is suggested to occur via the acetylation of specific lysine residues on SMC3 by Eco1 and the recruitment of soronin to protect the complex from Wapl-mediated removal (Ben-Shahar et al., 2008; Nishiyama et al., 2010) (Fig.1.20).

During early mitosis, dramatic changes in cohesin distribution start to occur, with most cohesin being removed except for at centromeric and pericentromeric regions. Indeed,

it is the loss of cohesin at chromosomal arms, coupled with retention at (peri)centromeric regions that results in the classic "X" shape of metaphase chromosomes. In metazoans, this so-called "prophase pathway" of cohesin removal mainly depends on the action of WAPL, which forces the opening of the cohesin ring by disrupting the interaction between SMC3 and Rad21 (Buheitel & Stemmann, 2013; Eichinger et al., 2013). These events depend on the action of several mitotic kinases that phosphorylate key regulatory proteins. As soronin directly competes with WAPL for binding to Pds5, phosphorylation-mediated soronin release promotes WAPL binding and cohesin removal (Nishiyama et al., 2010). Additionally, one of these kinases is believed to participate in WAPL activation, directly leading to cohesin removal (Nishiyama et al., 2013). Finally, phosphorylation of STAG is also key for cohesin release during the prophase pathway (Hauf et al., 2005) (Fig. 1.20).

In parallel, centromeric cohesin is protected from the removal process via the action of Shugoshin in complex with the PP2A phosphatase (Kitajima et al., 2004; McGuinness et al., 2005). The same kinases that are involved in cohesin removal, phosphorylate, and thus activate Shugoshin, leading to its localization and maintenance to the centromere. Once there, Shugoshin/PP2A guards centromeric cohesin from WAPL-mediated removal by (1) antagonizing soronin phosphorylation, favoring soronin interaction with Pds5 and blocking WAPL binding and (2) counteracting phosphorylation of STAG (Mirkovic & Oliveira, 2017) (Fig. 1.20).

Finally, at the onset of anaphase, the remaining cohesin is removed via cleavage of Rad21 by a large cysteine protease called separase. This causes distancing of the SMC1 and SMC3 subunits, opening of the ring, and release of the sister DNA molecules. This process can only occur when separase inhibitors, namely Securin and the kinase Cyclin B, are degraded (via ubiquitination) and Shugoshin- PP2A are released from centromeres (Lin et al., 2016) (Fig. 1.20). In contrast to metazoans, budding yeast does not have a dual-step

process of cohesin removal, as cohesin at the chromosomal arms is not removed at the onset of mitosis. Instead, removal of the entire cohesin pool occurs in the metaphase-to-anaphase transition via separase-mediated Rad21 cleavage (Uhlmann et al., 1999).

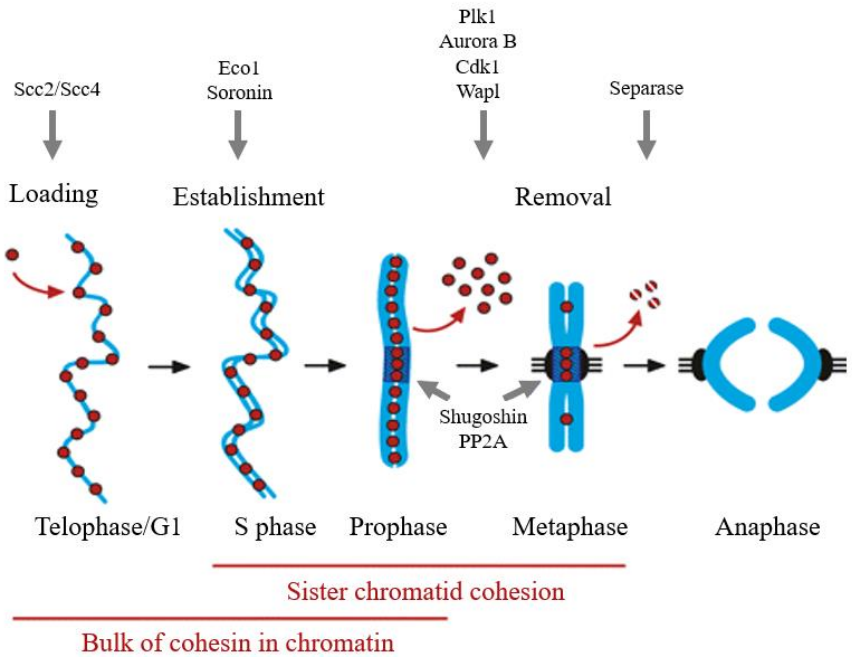

Figure 1.20. Regulation of sister chromatid cohesion during the metazoan cell cycle. Loading of cohesin onto chromatin occurs during telophase and G1 and requires the cohesin loading factors Scc2 and Scc4. During S phase, cohesion between sister chromatids is established, and this process depends on Eco1 and soronin recruitment. During prophase, Plk1, Aurora B kinase, CdK1 and WAPl lead to the dissociation of the bulk of cohesin chromatin. Cohesin at centromeres is protected by Sgo1 and PP2A. At the metaphase-to-anaphase transition, separase is activated and cleaves centromeric cohesin as well as residual cohesin on chromosome arms, enabling sister chromatid separation. Image adapted from (Peters et al., 2008).

1.4.2 The role of cohesin in transcriptional regulation

The discovery that cohesin plays a role in transcriptional regulation came from studies in *Drosophila* in the 1990s. It was found that expression of *cut*, a Notch-responsive gene that encodes a homeobox TF, was controlled by a distant enhancer 85 kb away (Jack et al., 1991; Jack & Delotto', 1995). Later, Nipped-B, an ortholog of the cohesin loading factor NIPBL, was found to be necessary for promoting enhancer-promoter contacts at *cut* (Rollins et al., 1999).

It was only in 2008 that a definitive role for cohesin in post-mitotic cells (i.e. independent of the cell cycle) was finally established. In the *Drosophila* model, it was found that cohesin was key for axon pruning in post-mitotic mushroom body neurons, possibly via regulation of the gene encoding the Ecdysone receptor (Schuldiner et al., 2008). In 2009, the finding that cohesin was transcribed in post-mitotic brain cells of zebrafish indicated that cohesin may also have cell-cycle independent roles in vertebrates (Mönnich et al., 2009).

The mechanisms whereby cohesin controls transcription and how these distinct strategies integrate with each other remains poorly understood. Cohesin has been studied the most in vertebrates in the context of its interaction with CTCF and the formation of TADs (Rao et al., 2017). However, it has also been suggested that cohesin can act in a CTCF-independent manner via the recruitment of transcriptional activators to transcriptional hotspots (Yan et al., 2013). Cohesin interactions with Mediator, which facilitates promoter-enhancer interactions (Kagey et al., 2010), and with the super-elongation complex (Izumi et al., 2015) have also been suggested to influence transcription.

1.4.2.1 Cohesin and CTCF

In 2008, pioneering studies in mammalian cells demonstrated that cohesin co-localized with CTCF, an 'insulator' protein known to demarcate the boundaries of TAD domains (Parelho et al., 2008; Stedman et al., 2008; Wendt et al., 2008). CTCF is not necessary for cohesin loading; however, it appears to localize cohesin to CTCF binding sites along the chromosome arms. Thus, it was proposed that cohesin mediated CTCF insulator activity (Wendt et al., 2008). Supporting the need for cohesin in domain formation, recent studies show that loss of cohesin-related factors result in loss of loop structures at different scales (Rao et al., 2017; Schwarzer et al., 2017). Although depletion of the cohesin subunit Rad21 and the release factor WAPL dramatically changes the 3D

genome structure, the impact on gene expression is comparably modest (Haarhuis et al., 2017; Rao et al., 2017). Thus, it is still unclear if CTCF and cohesin play an important global, or more specific, role in gene transcription.

It has been proposed that cohesin and CTCF anchor DNA loops that in turn constrain the topology of genes. Indeed, recent studies of human cohesin have described the ability of the complex to extrude DNA loops, with loop formation and maintenance dependent on cohesin's ATPase activity and its loading dimer (NIPBL-MAU2) (Davidson et al., 2019; Y. Kim et al., 2019). Cohesin and CTCF have been found to regulate several complex gene loci, either by facilitating or preventing enhancer-promoter contacts (Fig. 1.21). These include the Insulin-Like Growth Factor 2 (IGF2)/H19 region (Stedman et al., 2008), the β-globin locus (Chine et al., 2011), the proto-cadherin loci (Remeseiro et al., 2012), and the lymphocyte receptor loci (Seitan et al., 2012).

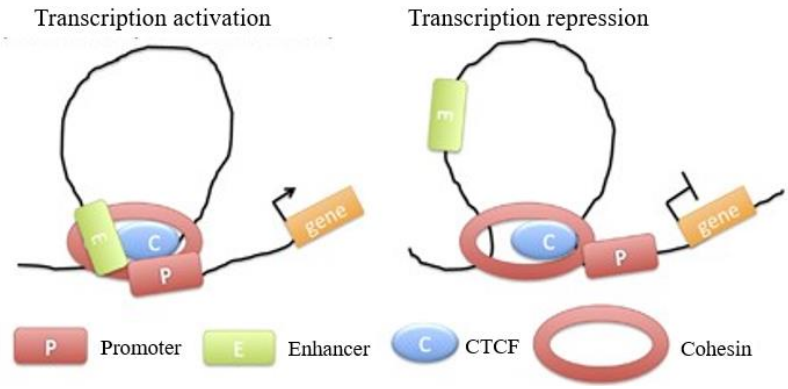

Figure 1.21. CTCF and the cohesin complex can lead to transcriptional activation or repression in a binding site-dependent manner. When CTCF and cohesin bind to their binding sites and create a chromatin loop that encompasses the enhancer and promoter, transcriptional activation occurs. Conversely, if CTCF and cohesin form a chromatin loop that prevents the enhancer from reaching the promoter, gene expression is repressed. Image adapted from (S. Kim et al., 2015).

The IGF2/H19 locus is well characterized in the context of gene imprinting, where the DNA of one allele is methylated and silenced while the other allele remains unmethylated and active. H19 is only expressed from the maternal allele whereas IGF2 is transcribed from the paternal allele and imprinting is dependent on the imprinting control

region (ICR) that lies between the two genes. On the maternal chromosome, CTCF protein binds to the ICR and through cohesin establishes a transcriptional insulator that organizes the chromosome into loops that favor H19 expression but block interactions between the maternal IGF2 promoters and the downstream shared enhancers. It follows that the loss of insulation resulted in the activation of IGF2 transcription (Nativio et al., 2009).

A recent study in mammalian cells suggested that looping between enhancers and promoters could be mediated by low-affinity binding of CTCF at preferred promoters, which would then interact with enhancer-bound cohesin. This was indicative that "enhancer scanning" might occur within a contact domain (Oh et al., 2021).

1.4.2.2 Cohesin and transcription factors

Cohesin has been found to co-localize with tissue-specific transcription factors, which includes the oestrogen receptor in breast cancer cell lines, liver-specific factors in liver cells, and pluripotency factors in embryonic stem cells (Faure et al., 2012; Nitzsche et al., 2011; Schmidt et al., 2010). In mouse liver cells, it was found that cohesin was particularly abundant in multiply bound *cis*-regulatory regions with weaker TF-binding motifs, suggesting that cohesin may facilitate TF stabilization at these regulatory regions (Faure et al., 2012).

Another study that analysed genome-wide binding for 112 TFs and the core cohesin subunits in mammalian cells corroborated the previous findings. It was found that (1) regions with high TF density were often bound by cohesin, (2) sites of cohesin binding, with or without TF clusters or binding motifs, were depleted of nucleosomes (i.e. accessible to DNase I) (3) cohesin loss led to a decrease in DNase I accessibility and TF binding at cluster sites, (4) cohesin bound sister chromatids together at cluster sites, and (5) cohesin binding was maintained during S and M phases even though TFs are evicted in early M

phase. Altogether, these findings suggest that cohesin might facilitate inheritance of TF-binding patterns after DNA replication and chromatin condensation (Yan et al., 2013).

1.4.2.3 Cohesin and Mediator

Mediator is a large multiprotein complex that links sequence-specific TFs with the general transcription machinery (Kornberg, 2005). Cohesin, Mediator, and NIPBL have been found to co-occupy sites (without CTCF) at genes that are highly transcribed by RNA Pol II in mouse embryonic stem cells. In fact, Mediator and cohesin co-occupied different promoters in different cells, which generated cell-type specific DNA loops, suggesting a link to cell-specific gene expression programs (Kagey et al., 2010). In zebrafish, concomitant depletion of Mediator and NIPBL had a synergetic effect on gene expression and limb development, consistent with the two factors being part of the same pathway (Muto et al., 2014).

In yeast, Mediator was found to have a similar binding pattern to both a chromatin remodelling complex, RSC, and cohesin. In turn, these were bound to nucleosome-depleted regions and promoters of RNA Pol II-transcribed genes (Chereji et al., 2017). Recently, it was found that depletion of a subunit of the yeast Mediator complex resulted in both defects in sister chromatid cohesion and decreased binding of Scc2 (NIPBL in humans) at RNA Pol II-transcribed genes, suggesting involvement in mitosis and interphase (Mattingly et al., 2022).

1.4.2.4 Cohesin and the super-elongation complex

In *Drosophila*, it was observed that cohesin often associates with genes that have high levels of promoter-proximal paused Pol II. Pausing requires the negative elongation factor (NELF) and DRB sensitivity inducing factor (DSIF) complexes that interact with Pol II and the nascent RNA transcript. The presence of the super elongation complex (SEC)

and release of NELF is associated with the transition to transcription elongation. These studies deduced that cohesin could promote the transition of promoter-proximal paused Pol II to elongation at many of the genes that it bound; however, the mechanisms were unclear (Fay et al., 2011; Schaaf et al., 2013). Clues were found in the study of a human cohesinopaty - Cornelia de Lange syndrome (CdLS) – in which mutations are found in certain cohesin core subunits or regulators. One study found that a mutation in SMC1A led to increased cohesin binding at specific genes where the transition to Pol II transcriptional elongation was enhanced (Mannini et al., 2015).

1.4.3 Cohesin in *P. falciparum*

In *P. falciparum*, putative SMC3 (PF3D7_0414000), SMC1 (PF3D7_1130700), Rad21 (PF3D7_1440100), and a STAG domain-containing protein (PF3D7_1456500) have been identified (Gardner et al., 2002). Proteomics studies have confirmed that *Pf*SMC1, *Pf*SMC3, and *Pf*RAD21 exist in a complex (Hillier et al., 2019). Importantly, orthologs of other cohesin regulatory proteins, such as the loading complex NIPBL-MAU2, Pds5, or the unloading factor Wapl, have not been identified. While *Pf*SMC1 and *Pf*RAD21 are as of yet uncharacterized, a recent study has provided a preliminary characterization of *Pf*SMC3 (Batugedara et al., 2020). The authors found that *Pf*SMC3 localizes in a perinuclear focus that did not co-localize with HP1 and binds predominantly to centromeric regions. However, the function of cohesin in *P. falciparum*, especially with regard to transcription and genome organization, is unknown.

1.5 Thesis scope

The cohesin complex is key for sister chromatid cohesion during mitosis and is thus essential for survival. In addition, in non-replicating cells or during interphase, cohesin has been found to have numerous roles in gene regulation, particularly in the strict spatio-temporal control of transcription in developmental models. The *P. falciparum* life cycle is driven by a precisely timed transcriptional cascade; however, it is unclear how this is accomplished with so few TFs and without a general use of HP1 heterochromatin. While genome organization is believed to play a role in transcriptional control, the underlying mechanisms and the role of architectural proteins remain understudied.

This PhD project aimed to elucidate the biological role of cohesin in *P. falciparum*. The most important goal was to determine whether cohesin plays a role in transcription before the onset of DNA replication, with the following objectives:

1. Generate strains in which the endogenous cohesin subunit is epitope tagged and able to be inducibly knocked down (Results section 2.2.1).

2. Identify new components of the cohesin complex (Results section 2.2.1).

3. Characterize cohesin subnuclear and genome-wide localization across the IDC (Results section 2.2.1 and 2.2.2).

4. Evaluate the effect of cohesin depletion on transcription across the IDC (Results section 2.2.3 and 2.2.4).

PART TWO

COHESIN IS INVOLVED IN TRANSCRIPTIONAL REPRESSION OF STAGE-SPECIFC GENES IN THE HUMAN MALARIA PARASITE

Catarina Rosa[1-5], Parul Singh[1-4], Ameya Sinha[6,7], Peter R Preiser[6,7], Peter C Dedon[7,8], Sebastian Baumgarten[4,9], Artur Scherf[1-4], Jessica M Bryant[1-4]

[1] Biology of Host-Parasite Interactions Unit, Institut Pasteur, Paris, France

[2] INSERM U1201, Paris, France

[3] CNRS ERL9195, Paris, France

[4]Université Paris Cité, Paris, France

[5]Sorbonne Université, Ecole doctorale Complexité du Vivant ED515, Paris, France

[6]School of Biological Sciences, Nanyang Technological University, Singapore, Singapore

[7]Antimicrobial Resistance Interdisciplinary Research Group, Singapore-MIT Alliance for Research and Technology, Singapore, Singapore

[8]Department of Biological Engineering, Massachusetts Institute of Technology, Cambridge,

MA, USA

[9]Plasmodium RNA Biology Group, Institut Pasteur, Paris, France

2.1 Results

2.1.1 SMC3 is expressed across the intra-erythrocytic developmental cycle and localizes to HP1-independent nuclear foci

In the *P. falciparum* genome, three putative core cohesin subunits have been annotated: SMC1 (PF3D7_1130700), SMC3 (PF3D7_0414000), and a protein with the N-terminal Rad21/Rec8 domain (PF3D7_1440100) (Fig. 2.1A). A comparative sequence analysis showed that, of these three subunits, *Pf*SMC3 shares the highest sequence similarly and identity to its orthologues in *H. sapiens*, *D. melanogaster*, *S. cerevisiae*, *S. pombe*, and *A. thaliana* (Fig. 2.1B). A Pfam domain analysis (Mistry et al., 2021) showed an overall conserved domain architecture: an N-terminal Walker A motif-containing domain, a central hinge domain, and a C-terminal Walker B motif-containing domain (Fig. 2.1B). Given the conserved nature of *Pf*SMC3, we decided to investigate its function *in vivo*.

We used CRISPR/Cas9 genome editing (Ghorbal et al., 2014) to add a 3x hemagglutinin (3HA) epitope tag-encoding sequence followed by a *glmS* ribozyme-encoding sequence at the 3' end of *smc3* (SMC3-3HA-*glmS*), which allows for inducible knockdown (Prommana et al., 2013). Polymerase chain reaction (PCR) and sequencing confirmed the correct integration of the 3HA tag and *glmS* ribozyme sequences, first in the bulk transfectant culture and then in the clones obtained by limited dilution (Supp. Fig.1). The other core cohesin subunits, SMC1 and Rad21 were also endogenously tagged using different approaches, generating SMC1-3HA-ddFKBP and Rad21-GFP-sandwich parasites; however, we have only performed a preliminary characterization of these proteins (Appendix A).

Immunoprecipitation followed by liquid chromatography-mass spectrometry (IP LC-MS/MS) of SMC3-3HA confirmed the interaction of SMC1, SMC3, and RAD21 previously reported in *P. falciparum* (Hillier et al., 2019; Batugedara et al., 2020) (Supp.

Table 1, EV1). A Stromal Antigen (STAG) domain-containing protein (PF3D7_1456500) was also enriched in the SMC3-3HA IP LC-MS/MS, suggesting that a fourth cohesin subunit (STAG1/2 in *H. sapiens* and Scc3 in *S. cerevisiae*) is present in the *P. falciparum* cohesin complex (Table 1, EV1).

Western blot analysis of a synchronous bulk population of SMC3-3HA-*glmS* parasites showed that SMC3 is expressed across the IDC but increases in abundance from ring to schizont stage (Fig. 2.1C). The presence of SMC3 in both ring and trophozoite stages suggests that cohesin is playing a role in interphase parasites (i.e. outside schizogony) and perhaps even before the onset of S phase, which is believed to take place after 24 hpi (Arnot et al., 2011; Ganter et al., 2017; Stanojcic et al., 2017) (Fig. 2.1D). Immunofluorescence assay (IFA) corroborated the nuclear localization, revealing a focus of SMC3-3HA at the nuclear periphery in trophozoite and schizont stages (Fig. 2.1E), similar to the localization observed for SMC1-HA and Rad21-GFP (Appendix A). While these foci are reminiscent of the heterochromatic *var* gene clusters at the nuclear periphery, no co-localization was observed between SMC3 and HP1 foci in trophozoite stage (Fig. 2.1F). It was not possible to detect SMC3 in ring stage and early trophozoite parasites with IFA, possibly due to the low abundance of the protein at this stage (Fig. 2.1C).

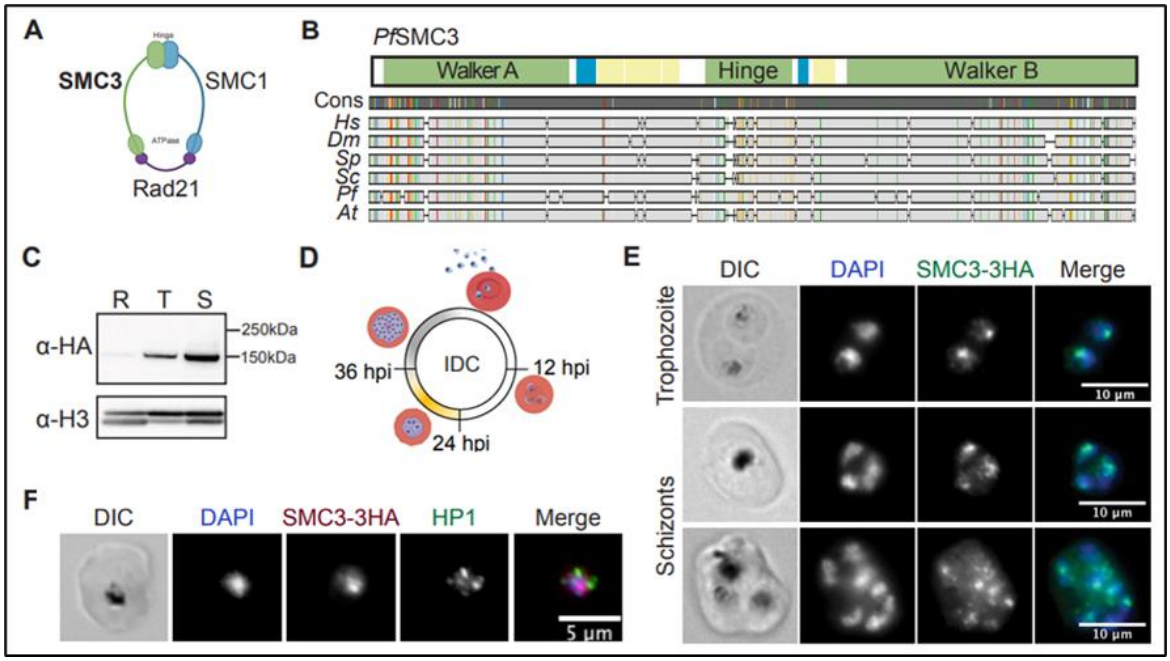

Figure 2.1. SMC3 is expressed across the intra-erythrocytic developmental cycle and localizes to HP1-independent nuclear foci. (A) Cohesin complex subunits annotated in *P. falciparum* (Gardner et al., 2002). Image prepared with BioRender.com. **(B)** Alignment of *P. falciparum* (*Pf*) SMC3 (*Pf*SMC3) with SMC3 protein sequences in *H. sapiens* (*Hs*), *D. melanogaster* (*Dm*), *S. pombe* (*Sp*), *S. cerevisiae* (*Sc*), and *A. thaliana* (*At*). A schematic of *Pf*SMC3 domain architecture is shown above. Coiled-coil domains are in yellow, low complexity regions are in blue, and other structured domains are annotated and in green. Sequence consensus ("Cons") is indicated by the grey bar with colors representing regions of 100 % agreement between the aligned sequences. Image prepared with Geneious Prime 2020.0.3. **(C)** Western blot analysis of nuclear extracts of ring (R), trophozoite (T), and schizont (S) stages from a synchronous population of SMC3-3HA-*glmS* parasites. SMC3-3HA is detected with an anti-HA antibody. An antibody against histone H3 is used as a control for the nuclear extract. Molecular weights are shown to the right. The SMC3-3HA has a predicted molecular weight of 147.3 kDa (3.3 kDa corresponding to the 3HA tag). **(D)** Schematic of *P. falciparum* intraerythrocytic developmental cycle (IDC). Yellow, approximate timing of DNA replication; Grey, approximate duration of schizogony (modified from (Ganter et al., 2017; H. Matthews et al., 2018). Time points in this study – 12 hpi (ring), 24 hpi (trophozoite), and 36 hpi (schizont) – are indicated. **(E)** and **(F)** Immunofluorescence assays of fixed RBCs infected with trophozoite or schizont stage SMC3-3HA-*glmS* parasites. DNA was stained with DAPI (blue) and SMC3-3HA was detected with anti-HA (green in E and magenta in F) antibody. HP1 was detected with anti-HP1 antibody (green in F). DIC, differential interference contrast. Scale bars equal 10 µm (**E**) and 5 µm (**F**)-

2.1.2 SMC3 binds stably to centromeres, but dynamically to other genes across the intra-erythrocytic developmental cycle

To determine the genome-wide binding pattern of SMC3 across the IDC, ChIP-seq was performed in a synchronous clonal population of SMC3-3HA-*glmS* parasites at 12 (ring), 24 (trophozoite), and 36 (schizont) hours post invasion (hpi). Using the macs2 peak calling algorithm (Y. Zhang et al., 2008), we obtained 1,164, 1,614, and 1,027 significant peaks at 12, 24, and 36 hpi, respectively (Table EV2). Most striking was the SMC3 enrichment at centromeric and pericentromeric regions at all time points, a phenomenon that was previously reported for trophozoite stages (Batugedara et al., 2020) (Fig. 2.2A, B). Comparison of the SMC3 peaks with the centromeric regions defined in (Hoeijmakers et al., 2012) revealed extensive overlap (Table EV3). SMC3 peak enrichment in centromeric regions was significantly higher than that of the peaks associated with the rest of the genome at 12, 24, and 36 hpi ($P < 0.0001$). Interestingly, we observed a decrease in SMC3 enrichment at the centromeric regions from 24 to 36 hpi, a time that corresponds to the transition into mitosis (Fig. 2.2C, Table EV3).

While quantification of the SMC3 peaks showed the largest enrichment in the centromeric and pericentromeric regions, there were significant SMC3 peaks across other genomic locations at all time points (Table EV2). Similarly, in *S. cerevisiae* - and to a lesser extent in *S. pombe* – besides being densely enriched at centromeric regions, cohesin was found to bind discrete sites along the chromosomal arms. Since these sites often corresponded to locations where transcription units converged (Lengronne et al., 2004), we evaluated the enrichment of SMC3 peaks within intergenic regions between converging versus diverging genes across the IDC. Although we observed a slightly higher enrichment of SMC3 peaks between convergent genes, the difference with those in intergenic regions between divergent genes was not significant (Supp. Fig. 2).

SMC3 peaks were found in both intergenic and intragenic regions closest to 767, 1,044, and 708 protein coding genes at 12, 24, and 36 hpi, respectively (Table EV4). Of all genes within ±500 base pairs (bp) of an SMC3 peak, 168 were bound by SMC3 across all three time points (Fig. 2.2D). However, most SMC3-bound genes showed a dynamic binding pattern, with a peak present at only one or two time points (Fig. 2.2B,D).

Gene ontology (GO) enrichment analysis showed that genes associated with SMC3 peaks at 12 hpi were not significantly represented by a specific GO term category (Table EV5). However, genes associated with SMC3 peaks at 24 and 36 hpi were most significantly represented by biological process categories such as "obsolete pathogenesis" (q = 1.2 x 10^{-19} and 3.3 x 10^{-21}, respectively), "cell-cell adhesion" (q = 1.2 x 10^{-19} and 4.7 x 10^{-23}, respectively), "response to host" (q = 1.21 x 10^{-11} and 1.43 x 10^{-13}, respectively), and "antigenic variation" (q = 8.1 x 10^{-12} and 2.7 x 10^{-13}, respectively) (Table EV5). These categories include many genes in common such as *var* and *rif* genes, which encode proteins that are exported to the surface of the host red blood cell to facilitate adhesion to the host microvasculature [reviewed in (Scherf et al., 2008)]. Genes associated with SMC3 peaks at 24 hpi were also significantly represented by the biological process categories "entry into host" (q = 0.014) and "exit from host" (q = 0.031). These categories include genes that are involved in invasion of or egress from the red blood cell such as *ralp1* (PF3D7_0722200) (Haase et al., 2008), *rhoph3* (PF3D7_0905400) (Sherling et al., 2017), and *msp1* (PF3D7_0930300)(O'Donnell et al., 2000, 2001).

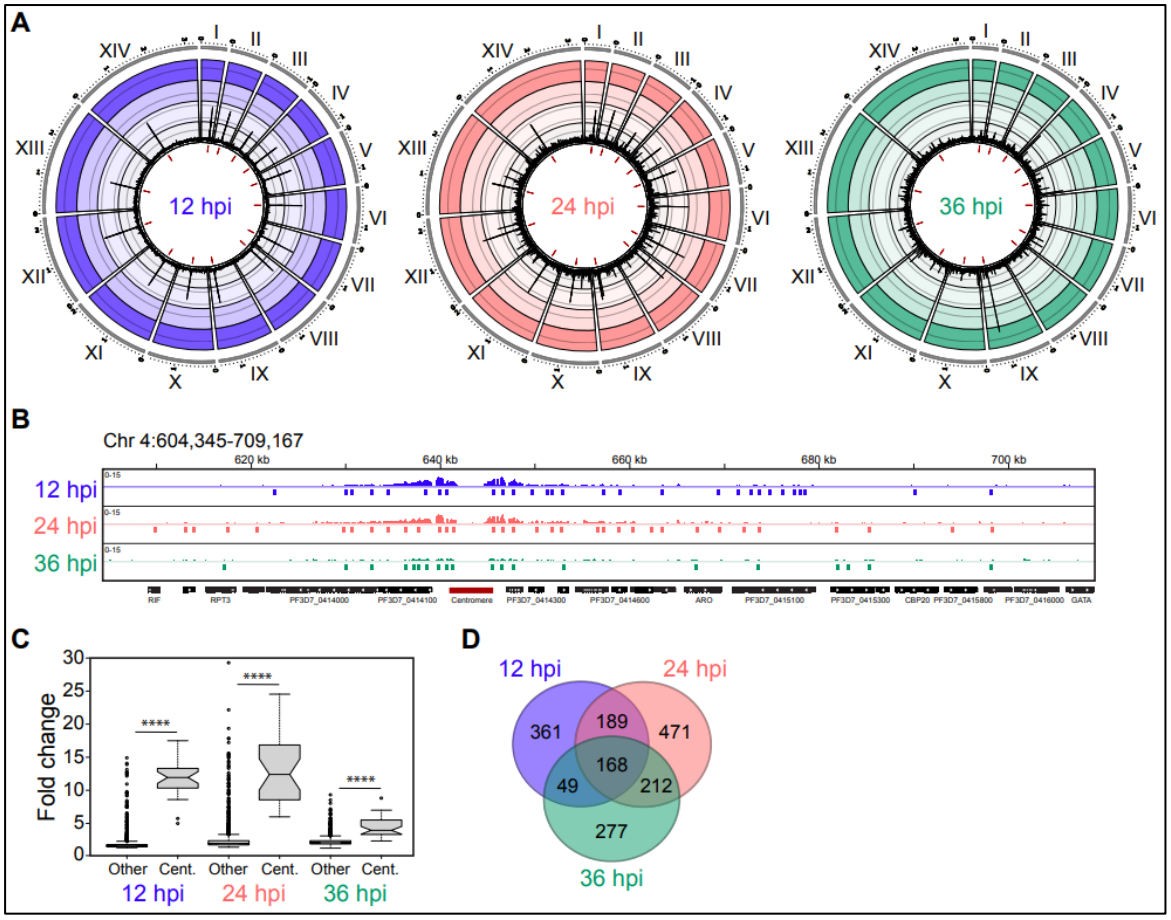

Figure 2.2. SMC3 binds stably to centromeres, but dynamically to other genes across the intra-erythrocytic developmental cycle. (A) Circos plot of ChIP-seq data showing genome-wide SMC3 binding across the IDC. For 12 (blue), 24 (coral), and 36 (green) hpi, the 14 chromosomes are represented circularly by the outer gray bars, with chromosome number indicated in roman numerals and chromosome distances (Mbp) indicated in Arabic numerals. Enrichment ratio (ChIP/input) is shown as average reads per million (RPM) over bins of 1,000 nucleotides. The maximum y-axis value is 24. Centromeric regions are represented by red bars in the innermost circle. **(B)** Zoomed-in view of ChIP-seq data corresponding to chromosome 4 (604,345 - 709,167 bp), including the centromere (represented with dark red line below the x-axis). For 12 (blue), 24 (coral), and 36 (green) hpi the y-axis is enrichment (ChIP/Input), with vertical lines below representing significant peaks obtained from peak calling algorithm macs2 (q-value < 0.05). The x-axis is DNA sequence, with genes represented by black boxes indented to delineate introns and labeled with white arrowheads to indicate transcription direction. **(C)** Box plot comparing the distribution of peak enrichment (fold change, ChIP/Input) between centromeric (Cent.) regions and extra-centromeric (Other) regions of the genome for 12, 24, and 36 hpi. Peaks were called with macs2 (*q*-value < 0.05). Center line, median; box limits, first and third quartiles; whiskers, 1.5× interquartile range. Wilcoxon test was used for statistical analysis. **** = adjusted *P*-value < 0.0001. **(D)** Venn diagram showing overlap between SMC3 peak-

associated genes at 12 (blue), 24 (coral), and 36 (green) hpi. Closest unique protein coding genes to the extended SMC3-3HA peak summit (+/- 500 bp) at 12, 24, and 36 hpi are shown in Table EV4.

While peak calling analysis is informative, the diverse functional categories of genes associated with SMC3 peaks makes it difficult to determine if SMC3 plays a specific role in transcriptional regulation or binds randomly throughout genic regions to facilitate a role in mitosis-related chromosome organization. Thus, functional analysis was required to elucidate a potential transcriptional function for SMC3 binding.

2.1.3 SMC3 is involved in transcriptional regulation of invasion-related genes

To gain insight into the role of SMC3 during interphase, we performed an inducible knockdown of SMC3 using the *glmS* ribozyme system (Prommana et al., 2013). An SMC3-3HA-*glmS* clone was tightly synchronized and split, and glucosamine was added to one half for 96 hours (two cell cycles), as knockdown at the protein level could not be achieved after a single cell cycle (Supp. Fig. 3). Simultaneously, a wild-type (WT) clone from the parent 3D7 strain was synchronized and treated in the same way to account for transcriptional changes due to the presence of glucosamine. After another round of synchronization, parasites were harvested at 12, 24 and 36 hpi, and western blot analysis revealed an SMC3-3HA knockdown at the protein level in nuclear extracts at all time points, although to a lesser extent at 36 hpi (Fig. 2.3A).

We then performed RNA-seq followed by differential expression analysis for the untreated and glucosamine-treated SMC3-3HA-*glmS* and WT parasites, which confirmed a significant knockdown of SMC3 at the transcript level in the SMC3-3HA-*glmS* parasites: 55 % (q = 8.5 x 10^{-3}) at 12 hpi, 69 % (q = 1.3 x 10^{-39}) at 24 hpi and 48% at 36 hpi (q = 4.14 x 10^{-54}) (Tables EV6, EV7 and EV8, Fig. 2.3B). Importantly, there was no significant difference between SMC3 transcript levels in SMC3-3HA-*glmS* and WT parasites,

confirming that the addition of an epitope-tag encoding sequence and *glmS* ribozyme did not affect the stability of *smc3* transcripts (Supp. Fig.4).

Comparison of our RNA-seq data to time course microarray data from (Bozdech et al., 2003), as in (Lemieux et al., 2009), showed that data from the untreated and glucosamine-treated WT and the SMC-3HA-*glmS* parasites showed approximately the same "transcriptional age" at the 12 and 24 hpi time points (Supp. Fig. 5). However, while the untreated and glucosamine-treated parasites were highly similar morphologically (Supp. Fig. 6), the glucosamine-treated WT parasites showed a significantly advanced "transcriptional age" compared to the untreated parasites at 36 hpi (Supp. Fig. 5).

To remove potential artifacts of glucosamine treatment, genes that were significantly up- or downregulated in the glucosamine-treated WT parasites at 12 and 24 hpi (Tables EV9 and EV10) were filtered out of the datasets for significantly up- and downregulated genes in the SMC-3HA-*glmS* parasites at the corresponding time points (Supp. Fig.7). We could not perform filtering of the SMC3-3HA-*glmS* data at 36 hpi because the glucosamine-treated WT parasites were substantially more advanced in the IDC than the other parasites at this time point (Supp. Fig. 5). After filtering at 12 and 24 hpi, 104 and 932 genes were significantly downregulated, respectively (Tables EV11 and EV12, Fig. 2.3 C,D), and 67 and 674 genes were significantly upregulated at 12 and 24 hpi, respectively (Tables EV11 and EV12, Fig. 2.3 C,D) in SMC3-3HA-*glmS* parasites.

To gain insight into the transcriptional function of SMC3, we performed a GO enrichment analysis of genes that were up- and downregulated specifically in response to SMC3 knockdown at 12 and 24 hpi. At 12 hpi, downregulated genes were most significantly represented by the biological process category of "protein insertion into membrane" (q = 0.017, Table EV13), whereas at 24 hpi downregulated genes were most

significantly represented by the categories of "chromosome organization" (q = 1.0 x 10-3, Table EV14) and "chromosome segregation" (q = 1.0 x 10-3, Table EV14).

For both time points, upregulated genes were most significantly represented by the biological process categories of "movement in host environment" (12 hpi: $q = 1.8 \times 10^{-7}$, Table EV13; 24 hpi: $q = 1.3 \times 10^{-5}$, Table EV14) and "entry into host" (12 hpi: $q = 1.8 \times 10^{-7}$, Table EV13; 24 hpi: $q = 1.3 \times 10^{-5}$, Table EV14). Genes included in these categories are involved in egress and invasion of the red blood cell [reviewed in (Cowman et al., 2012, 2017)]. Indeed, a substantial percentage of invasion-related genes defined in (Hu et al., 2010) were significantly upregulated upon SMC3 depletion at 12 and 24 hpi (Table EV15). Comparison of our RNA-seq data to the time course transcriptomics data from (Painter et al., 2018) revealed that SMC3 depletion at 12 hpi caused downregulation of genes that normally reach their peak expression in the trophozoite stage (18-30 hpi), with the majority of upregulated genes normally reaching their peak expression in the schizont and very early ring stages (40-2 hpi) (Fig. 2.3E). At 24 hpi, a similar trend is observed, with most downregulated genes normally peaking in expression in trophozoite stage (24-32 hpi) and the majority of upregulated genes peaking in expression at very early ring stage (2 hpi) (Fig. 2.3F).

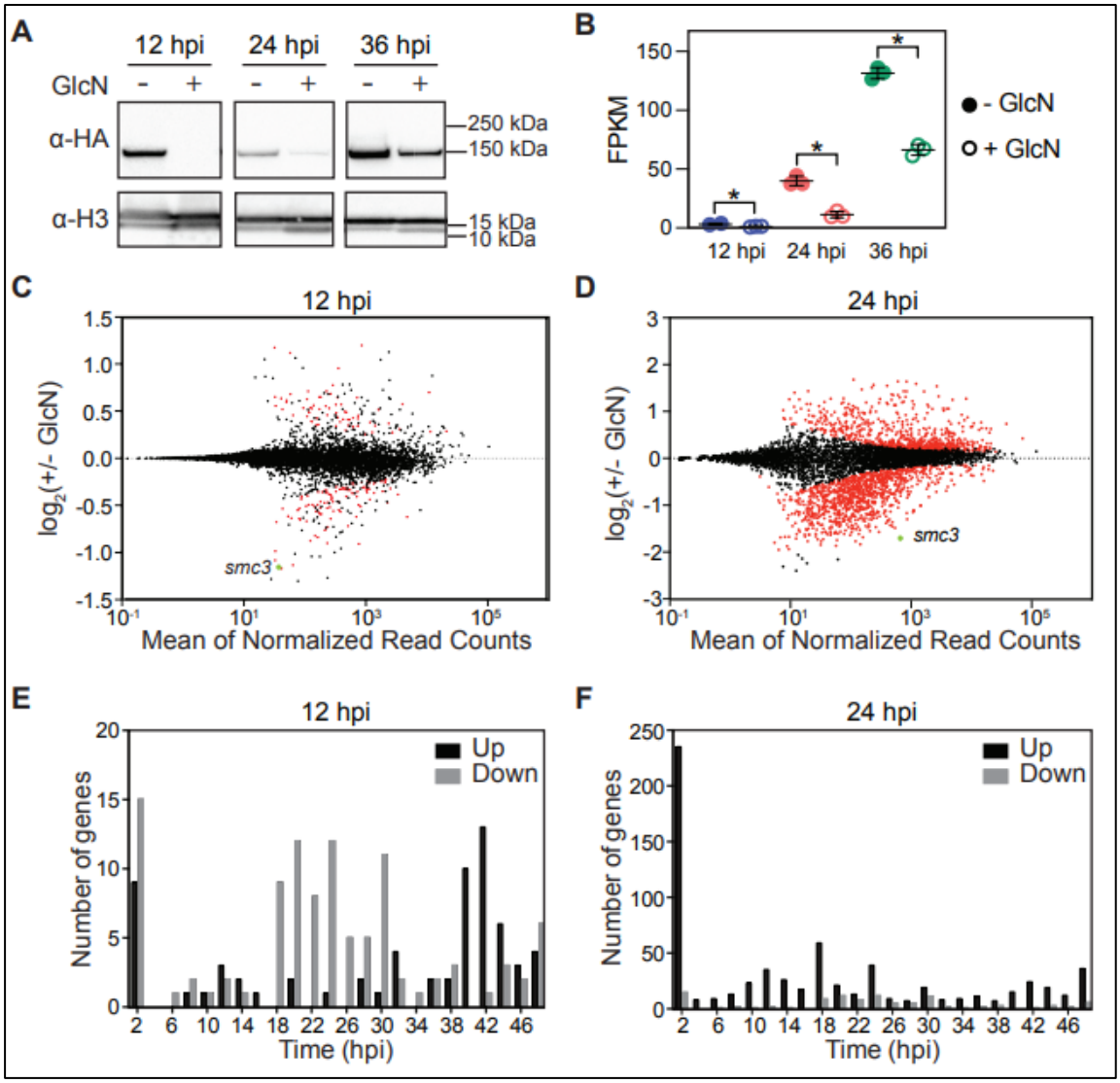

Figure 2.3. SMC3 inducible knockdown results in deregulation of genes in *P. falciparum*. (A) Western blot analysis of nuclear extracts at 12, 24 hpi and 36 hpi from a clonal population of SMC3-3HA-*glmS* parasites in the absence (-) or presence (+) of glucosamine (GlcN). SMC3-3HA is detected with an anti-HA antibody. An antibody against histone H3 is used as a control for the nuclear extract. Molecular weights are shown to the right. **(B)** RNA-seq of an SMC3-3HA-*glmS* clone shows smc3 transcript levels (FPKM) at 12 (q = 8.5 x 10^{-3}), 24 (q = 1.3 x 10^{-39}) and 36 hpi (q = 4.14 x 10^{-54}) in the absence (circles) or presence (squares) of glucosamine (GlcN). P-values are calculated with a Wald test for significance of coefficients in a negative binomial generalized linear model as implemented in DESeq2 (Love et al., 2014). q = Bonferroni corrected *P*-value. Corresponding data can be found in Tables 6 and 7. (C) and (D) MA plots of log2(glucosamine-treated/untreated, M) plotted over the mean abundance of each gene (A) at 12 hpi **(C)** and 24 hpi **(D).** Transcripts that were significantly higher (above x-axis) or lower (below x-axis) in abundance in the presence of glucosamine are highlighted in red ($q \leq 0.1$). *smc3* is highlighted in green. Three replicates were used for untreated and glucosamine-treated parasites, with the exception of the untreated 12 hpi parasites, for which there were two replicates. *P*-values were calculated with a Wald test for significance of coefficients in a negative binomial generalized linear model as implemented in DESeq2 (Love et al., 2014). q = Bonferroni

corrected *P*-value. **(E)** and **(F)** Frequency plots showing the time in the IDC (hpi) of peak transcript level (comparison to transcriptomics time course in (Painter et al., 2018) for genes that are significantly downregulated (grey) or upregulated (black) following SMC3 knockdown at 12 hpi **(E)** and 24 **(F)** hpi.

2.1.4 SMC3 dynamically binds to genes that are upregulated in its absence

To provide evidence for a direct function of SMC3 in the transcriptional regulation of these up- and downregulated genes, we compared our SMC3 ChIP-seq data to our RNA-seq data at 12 hpi and 24 hpi. Metagene analysis from the ChIP-seq data showed that SMC3 was absent from the promoter regions of genes that are downregulated in response to its knockdown (Fig. 2.4A, Supp. Fig. 8). In contrast, SMC3 was enriched in the promoter regions of genes that are upregulated in response to its knockdown (Fig. 2.4A, Supp. Fig. 8). Indeed, this enrichment of SMC3 at the promoters of upregulated genes was present at 12 and 24 hpi, but not 36 hpi (Fig. 2.4B). Our data suggest that SMC3 binding has a direct effect on the transcription of genes that are upregulated in its absence, whether naturally or via knockdown.

Because genes that are significantly upregulated upon SMC3 knockdown normally reach peak expression late in the cell cycle (Fig. 2.3E), are depleted of SMC3 at 36 hpi (Fig. 2.4B), and are most significantly represented by GO terms pertaining to invasion and egress (Tables EV13,14), we hypothesized that SMC3 helps to repress these genes until their appropriate time of expression late in the cell cycle. Indeed, all genes that are significantly up-regulated upon SMC3 knockdown at 12 hpi show an increase in chromatin accessibility [Assay for Transposase-Accessible Chromatin using sequencing (ATAC-seq) data from (Toenhake et al., 2018)] at their promoters at later stages of the IDC (Fig. 2.4C), the opposite trend of SMC3 binding (Fig. 2.4B).

Examples of invasion-related genes that are up-regulated upon SMC3 KD include the *rhoptry-associated protein 2* (*rap2*, PF3D7_0501600) and *glideosome-associated protein 45* (*gap45*, PF3D7_1222700). These genes show SMC3 enrichment at their

promoter regions at 12 and 24 hpi, but not at 36 hpi (Fig. 2.4D), and depletion of SMC3 resulted in upregulation at both 12 and 24 hpi (Fig. 4E). Comparison of the SMC3 ChIP-seq data with published ATAC-seq data (Toenhake et al., 2018) and mRNA dynamics data (Painter et al., 2018) from similar time points in the IDC revealed that SMC3 binding at the promoter regions of these genes inversely correlates with chromatin accessibility (Fig. 2.4D) and their mRNA levels (Fig. 2.4F), which both peak in schizont stages. These data are consistent with a role of SMC3 in repressing this gene subset until their appropriate time of expression in the IDC.

We also hypothesized that the upregulation of invasion-related genes upon SMC3 knockdown might result in higher rates of invasion. First, we attempted to determine if up-regulation of invasion-related gene transcription led to higher expression of the corresponding protein. Unfortunately, we could only gain access to an antibody against a single invasion-related protein – RAP2 – whose transcript level was significantly upregulated upon SMC3 depletion. RAP2 protein levels were not significantly different in protein extracts from untreated and glucosamine-treated SMC3-3HA-*glmS* parasites at 12 hpi, suggesting that the differential expression of this gene upon SMC3 KD, while significant at the transcript level, did not translate to a decrease in the corresponding protein (Supp. Fig 9). However, more proteins would need to be tested to determine if what is seen for RAP2 is a general trend.

Next, to determine if SMC3 knockdown affects parasite growth, we performed a growth curve analysis of untreated and glucosamine-treated WT and SMC3-3HA-*glmS* synchronous clonal parasite populations. We did not observe a significant difference in parasite growth between untreated and glucosamine-treated parasites, although there was a slight difference between WT and SMC3-3HA-*glmS* parasites regardless of treatment condition (Supp. Fig. 10). These results suggest that SMC3 knockdown to the level we

achieve with the *glmS* system does not affect parasite growth, either via the transcriptional changes it causes or effects on mitosis/schizogony.

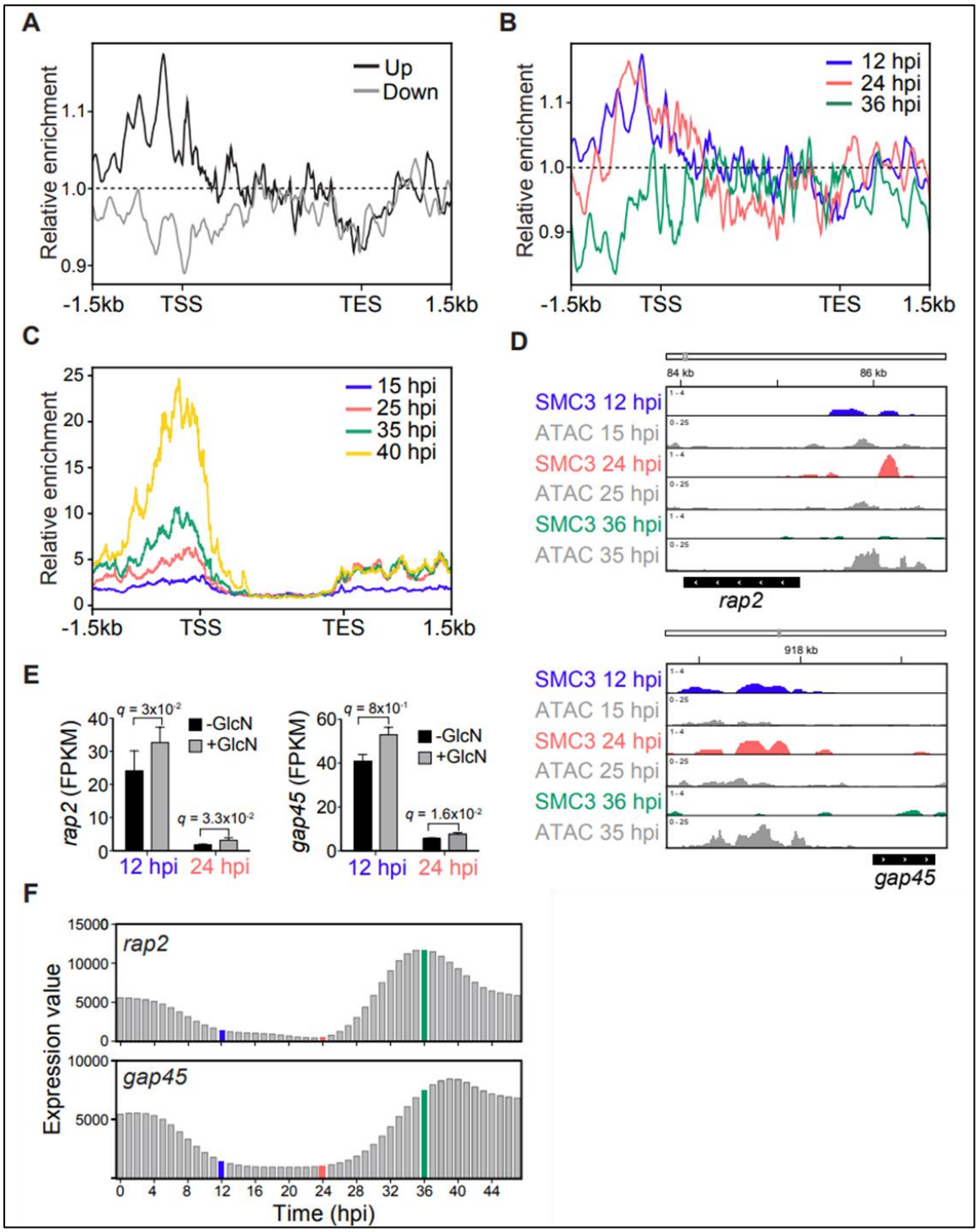

Figure 2.4. Cohesin is involved in transcriptional regulation of invasion-related genes. (A) Metagene plot showing average SMC3 enrichment (*y*-axis = ChIP/Input) in clonal SMC3-3HA-*glmS* parasites at 12 hpi from 1.5 kb upstream of the transcription start site (TSS) to 1.5 kb downstream of the transcription end site (TES) for genes that are significantly down- (grey) or

upregulated (black) upon SMC3 knockdown. **(B)** Metagene plot showing average SMC3 enrichment (*y*-axis = ChIP/Input) in clonal SMC3-3HA-*glmS* parasites at 12 (blue), 24 (coral), and 36 hpi (green) from 1.5 kb upstream of the transcription start site (TSS) to 1.5 kb downstream of the transcription end site (TES) for genes that are significantly upregulated upon SMC3 knockdown at 12 hpi. **(C)** Metagene plot showing average chromatin accessibility [ATAC-seq (RPM)/gDNA (RPM)] from (Toenhake et al., 2018) across the IDC from 1.5 kb upstream of the transcription start site (TSS) to 1.5 kb downstream of the transcription end site (TES) for genes that are significantly upregulated upon SMC3 knockdown at 12 hpi. **(D)** ChIP-seq data showing enrichment of SMC3 (ChIP/Input) at 12 (blue), 24 (coral), and 36 (green) hpi in clonal SMC3-3HA-*glmS* parasites at the *rhoptry-associated protein 2* (*rap2*, PF3D7_0501600) and the *glideosome-associated protein 45* (*gap45*, PF3D7_1222700) gene loci. The *x*-axis is DNA sequence, with the gene represented by a black box with white arrowheads to indicate transcription direction. ATAC-seq data from closely corresponding time points (15, 25, and 35 hpi) from (Toenhake et al., 2018) are shown in grey, with the *y*-axis representing ATAC-seq (RPM)/gDNA(RPM). **(E)** RNA-seq of an SMC3-3HA-*glmS* clone shows transcript levels (FPKM) for *rap2* (PF3D7_0501600) at 12 ($q = 3 \times 10^{-2}$) and 24 ($q = 3.3 \times 10^{-2}$) hpi and *gap45* (PF3D7_1222700) at 12 ($q = 8 \times 10^{-1}$) and 24 ($q = 1.6 \times 10^{-2}$) hpi in the absence (black) or presence (grey) of glucosamine (GlcN). *P*-values are calculated with a Wald test for significance of coefficients in a negative binomial generalized linear model as implemented in DESeq2 (Love et al., 2014). *q* = Bonferroni corrected *P*-value. Corresponding data can be found in Tables 6 and 7. **(F)** Expression values of *rap2* (PF3D7_0501600) and *gap45* (PF3D7_1222700) genes across the IDC (indicated on the *x*-axis by hpi) from the transcriptomics time course in (Painter et al., 2018). Data corresponding to 12 (blue), 24 (coral), and 36 (green) hpi time points are highlighted.

2.2 Supplementary data

2.2.1 Supplementary Figures

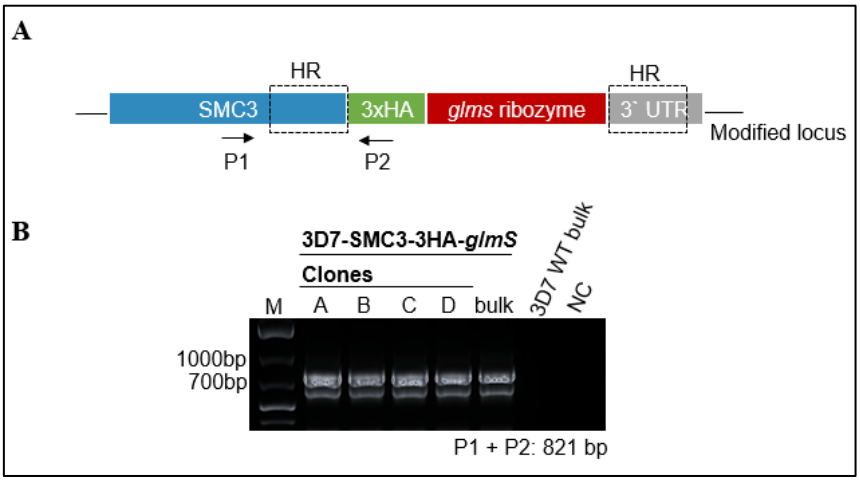

Supplementary Figure 1. CRISPR/Cas9-mediated integration of 3HA tag and *glmS* ribozyme at SMC3 C-terminus. A. SMC3 modified locus after CRISPR/Cas9-mediated 3HA tagging and *glmS* ribozyme integration at the C-terminus. HR: Homology Region. **B.** PCR analysis of gDNA from the parasite lines indicated above each gel. Primers used are as indicated below the gel and annealing sites are defined in (A). M, Molecular weight marker. NC, Negative Control.

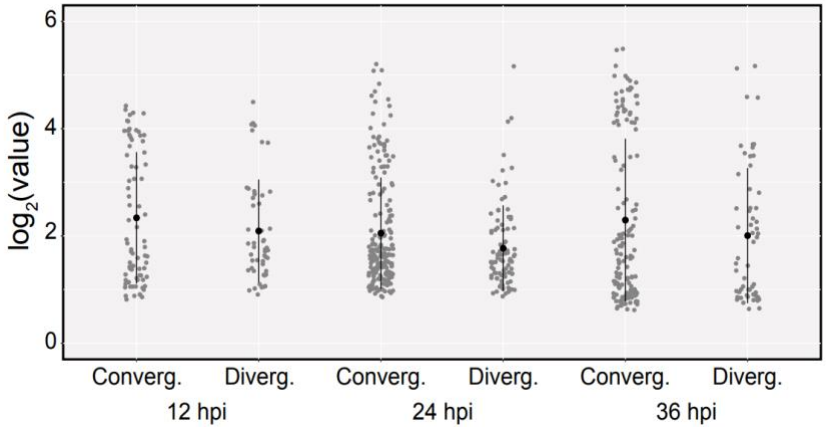

Supplementary Figure 2. SMC3 peak enrichment at intergenic regions between convergent and divergent genes. Plot comparing SMC3 peak enrichment [log2(ChIP/Input)] between regions between convergent ("Converg.") and divergent ("Diverg.") genes for 12, 24, and 36 hpi. SMC3 peaks were shared between two replicates (clones A and B) called with macs2 (*q*-value < 0.05). Center black dot, median; central vertical line, standard deviation.

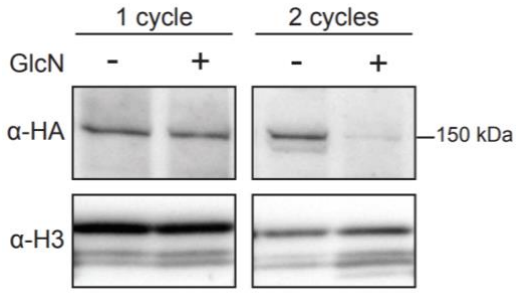

Supplementary Figure 3. SMC3 knockdown occurs after two cell cycles of glucosamine treatment. Western blot analysis of nuclear extracts from a synchronous clonal population of SMC3-3HA-*glmS* ring stage parasites in the absence (-) or presence (+) of glucosamine (GlcN) for 48 and 96 hr (one and two IDC cycles, respectively). SMC3-3HA is detected with an anti-HA antibody. An antibody against histone H3 is used as a control for the nuclear extract. Molecular weights are shown to the right.

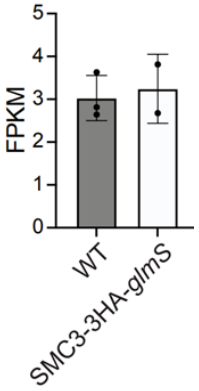

Supplementary Figure 4. Levels of smc3 transcription do not change between WT and SMC3-3HA-*glmS* parasites. RNA-seq of a WT and SMC3-3HA-*glmS* clone shows no significant difference in *smc3* transcript levels (FPKM) at 12 hpi in the absence of glucosamine.

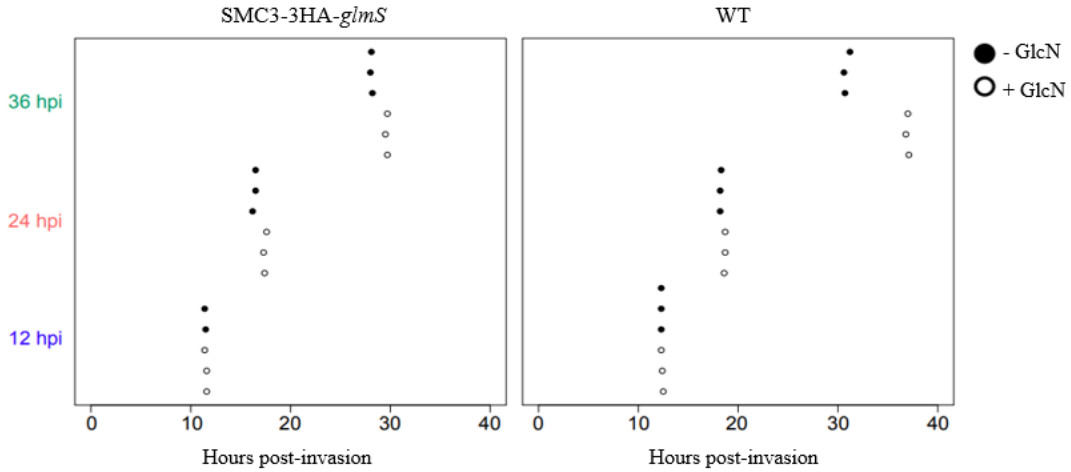

Supplementary Figure 5. Cell cycle progression of SMC3-3HA-*glmS* and 3D7 WT at 12, 24 and 36 hpi. Cell cycle progression estimation of a synchronous, clonal SMC3-3HA-*glmS* and 3D7 population in the absence (− GlcN) or presence (+ GlcN) of glucosamine. RNA-seq data from synchronized parasites harvested

at 12 (blue), 24 (coral) and 36 (green) hpi were compared to microarray data from (Bozdech et al., 2003) as in (Lemieux et al., 2009) to determine the approximate time point in the IDC (*x*-axis). Replicates are represented with circles.

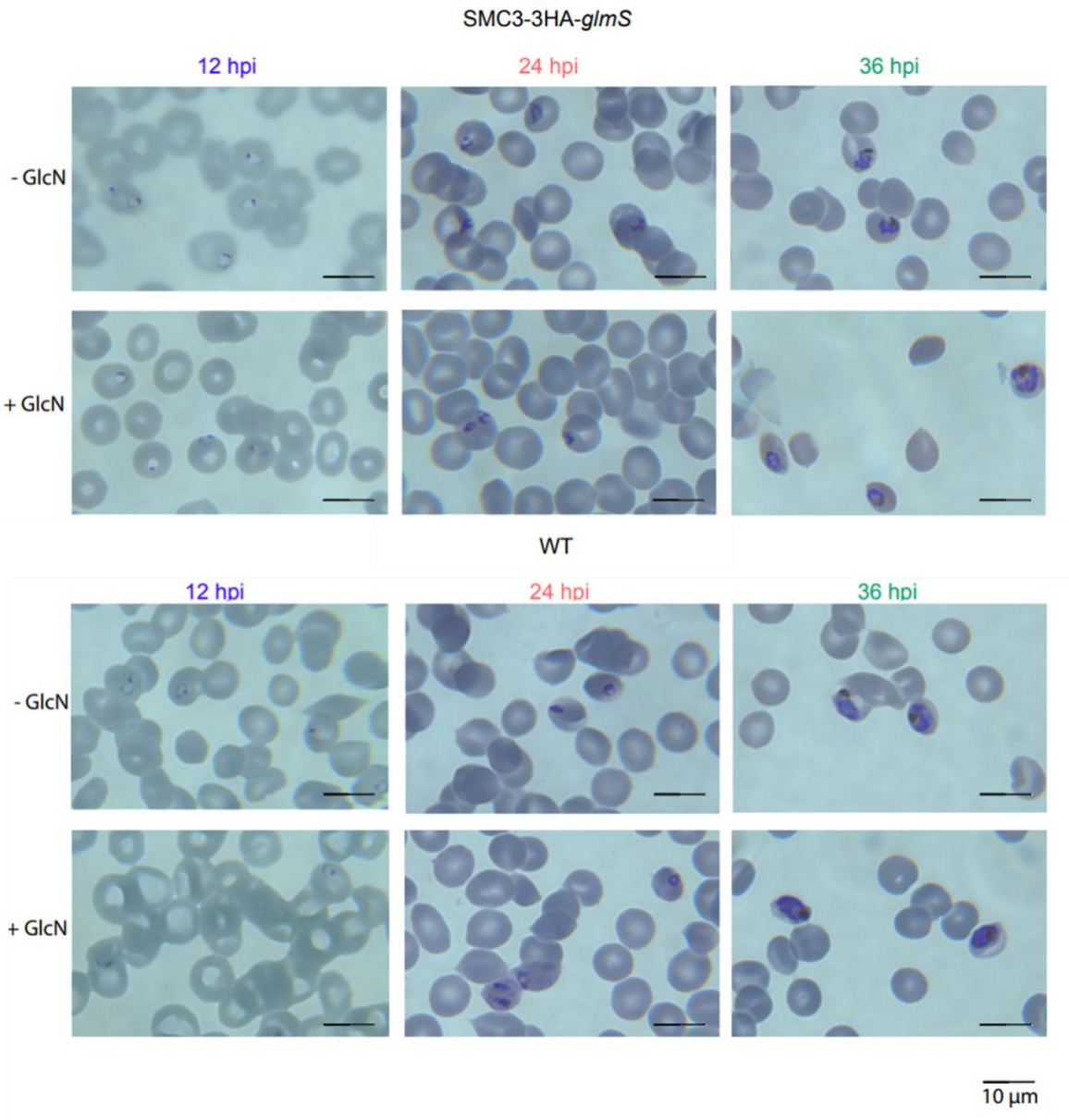

Supplementary Figure 6. Representative pictures of SMC3-3HA-*glmS* and 3D7 WT at 12, 24 and 36 hpi. Giemsa staining showing morphology of clonal SMC3-3HA-*glmS* and 3D7 WT population in the absence (− GlcN) and presence (+ GlcN) of glucosamine for the synchronized parasites harvested at 12 (blue), 24 (coral) and 36 (green) hpi for RNA-seq.

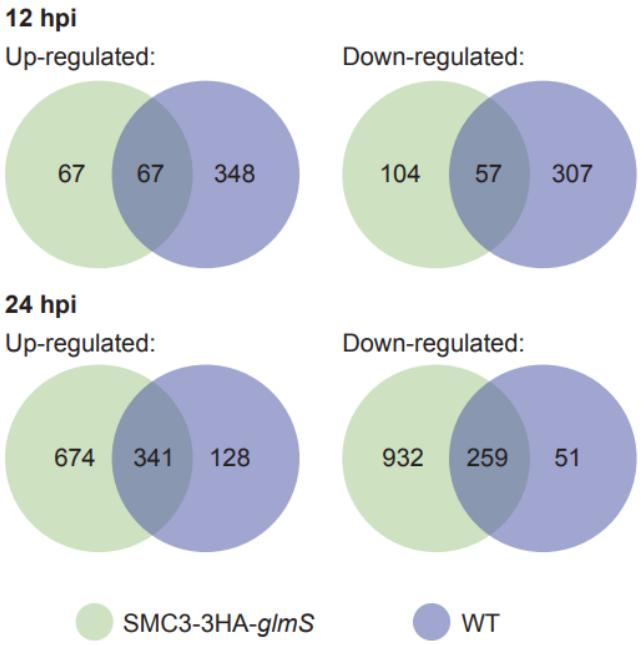

Supplementary Figure 7. Strategy for determining expression changes due to glucosamine treatment. Venn diagram showing the number of unique or shared significantly up- or downregulated genes after two cycles of glucosamine treatment in synchronous, clonal populations of SMC3-3HA-*glmS* (green) and WT (purple) parasites at 12 and 24 hpi.

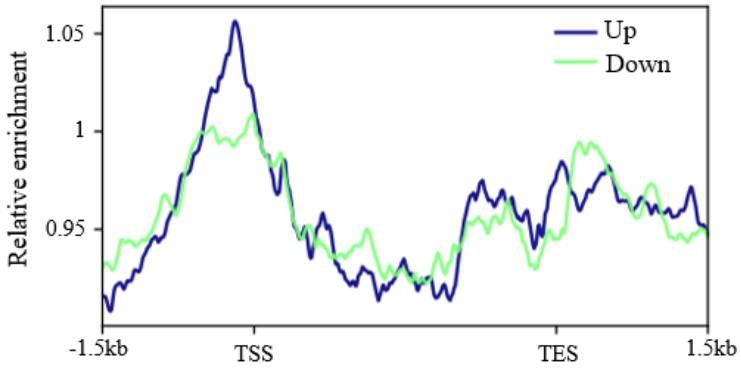

Supplementary Figure 8. SMC3 is enriched in the promoter regions of genes that are upregulated in response to its knockdown at 24 hpi. Metagene plot showing average SMC3 enrichment (y-axis = ChIP/Input) in clonal SMC3-3HA-*glmS* parasites at 24 hpi from 1.5 kb upstream of the transcription start site (TSS) to 1.5 kb downstream of the transcription end site (TES) for genes that are significantly down- (green) or upregulated (blue) upon SMC3 knockdown.

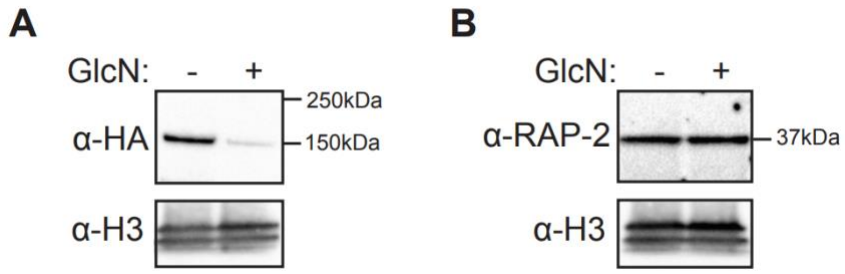

Supplementary Figure 9. SMC3 depletion does not affect protein levels of rhoptry-associated protein 2. Western blot analysis of total from a synchronous clonal population of SMC3-3HA-*glmS* trophozoite stage parasites in the absence (-) or presence (+) of glucosamine (GlcN). **A.** SMC3-3HA is detected with an anti-HA antibody. **B.** RAP2 is detected with and anti-RAP2 antibody (3A9/48). An antibody against histone H3 is used as a control for the nuclear extract. Molecular weights are shown to the right.

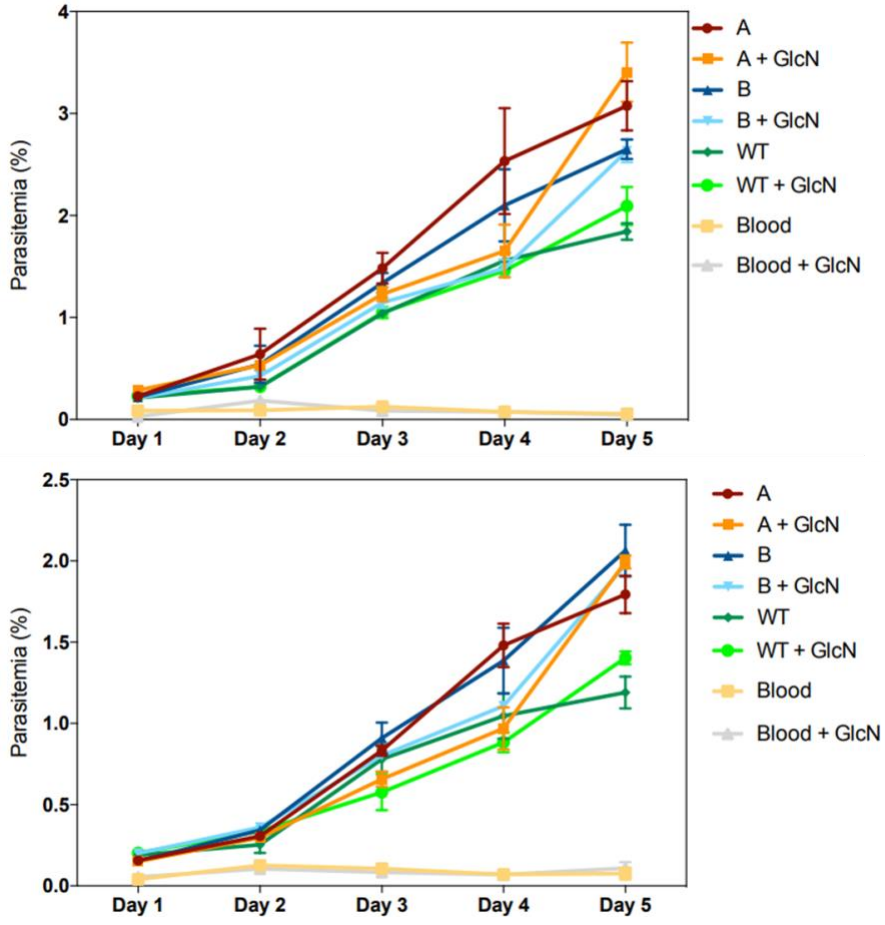

Supplementary Figure 10. SMC3 depletion does not affect growth of SMC3-3HA-*glmS* parasites. Growth curves over five days of two clonal SMC3-3HA-*glmS* (A and B) and WT parasites in the absence or presence of glucosamine (GlcN) in blood of two different donors (upper and bottom panel). Glucosamine treatment was started 96 h (two cycles) before Day 1 to ensure SMC3 knockdown during the days sampled (Supp. Fig. 2A). Uninfected red blood cells (Blood) served as reference of background and right and Error bars indicate standard deviation of three technical replicates.

2.2.2 Supplementary Table

Gene ID	Protein ID	Description
PF3D7_0414000	Q8I1U7	structural maintenance of chromosomes protein 3
PF3D7_1130700	Q8II57	structural maintenance of chromosomes protein 1, putative
PF3D7_1456500	Q8IKR4	STAG domain-containing protein, putative
PF3D7_1470100	Q8IKD7	conserved Plasmodium protein, unknown function
PF3D7_0708800	Q8IC01	heat shock protein 110
PF3D7_0108700	Q8I255	secreted ookinete protein, putative
PF3D7_0918000	Q8I2X3	glideosome-associated protein 50
PF3D7_1470800	Q8IKD0	conserved Plasmodium protein, unknown function
PF3D7_0321700	O97291	conserved Plasmodium protein, unknown function
PF3D7_0319400	O97277	kinesin-8X
PF3D7_0527500	Q8I3J0	Hsc70-interacting protein
PF3D7_0608300	C6KST1	heptatricopeptide repeat-containing protein, putative
PF3D7_0621900	C6KT56	signal recognition particle subunit SRP68, putative
PF3D7_0720700	Q8IBP4	phosphoinositide-binding protein PX1
PF3D7_0804500	A0A143ZZV5	conserved Plasmodium membrane protein, unknown function
PF3D7_0806400	Q8IAQ4	UDP-N-acetylglucosamine transferase subunit ALG13, putative
PF3D7_1029100	Q8IJB4	conserved Plasmodium protein, unknown function
PF3D7_1036900	A0A143ZYL5	conserved Plasmodium protein, unknown function
PF3D7_1203300	Q8I612	TBCC domain-containing protein, putative
PF3D7_1221700	Q8I5J6	FbpA domain protein, putative
PF3D7_1329000	Q8IE49	DNA-directed RNA polymerase III subunit RPC1, putative
PF3D7_1338300	Q8IDV0	elongation factor 1-gamma, putative
PF3D7_1434300	A0A144A2J9	Hsp70/Hsp90 organizing protein
PF3D7_1440100	Q8IL69	cohesin complex subunit, putative
PF3D7_1449700	Q8IKX8	Exosome complex exonuclease RRP6

Supplementary Table 1. LC-MS/MS analysis of SMC3-3HA-*glmS* immunoprecipitation in late stage parasites. Proteins listed were exclusively found in SMC3-3HA immunoprecipitations (see table EV1). Predicted members of the cohesin complex are highlighted in grey based on (Hillier et al., 2019; Batugedara et al., 2020).

2.2.3 Expanded view Tables

Additional tables generated in this study could not be included due to their large size. Each table is followed by the corresponding legend and a description of contents.

Table EV1. LC-MS/MS analysis of SMC3-3HA immunoprecipitation. LC-MS/MS results of the SMC3-3HA immunoprecipitation in late stage parasites. Total (TotPep) and unique (UniPep) peptide counts for the proteins listed are shown for three replicates each of the SMC3-3HA and 3D7 WT control immunoprecipitations. Predicted members of the cohesin complex are highlighted in grey based on (Hillier et al., 2019; Batugedara et al., 2020).

Table EV2. MACS2 peak calling results for SMC3-3HA ChIP-seq at 12, 24, and 36 hpi. The paired end deduplicated ChIP and input BAM files were used as treatment and control, respectively, for peak calling algorithm macs2 command callpeak. Significant peaks ($q < 0.05$) are shown for each time point, along with their chromosomal coordinates, fold enrichment (ChIP/Input), and $-\log_{10}$(*q*-value).

Table EV3. SMC3-3HA peak enrichment at centromeric regions at 12, 24, and 36 hpi. List of significant SMC3 peaks ($q < 0.05$, Table 2) that overlap with centromeres, as defined by peaks of CenH3 (Hoeijmakers et al., 2012) at 12, 24, and 36 hpi. Significant SMC3 peaks and their overlapping centromeric regions are shown for each time point, along with their chromosomal coordinates, fold enrichment (ChIP/Input), and $-\log_{10}$ (*q*-value).

Table EV4. List of SMC3-3HA peak-associated genes at 12, 24, and 36 hpi. Protein-coding genes that are closest to the SMC3-3HA peak summit (+/- 500 bp) at 12, 24, and 36 hpi (defined in Table EV2).

Table EV5. Gene Ontology analysis for SMC3 peak-associated genes. GO enrichment analysis (biological process) of genes associated with an SMC3 peak at 12, 24, or 36 hpi (defined in Table EV4). Number of significantly enriched genes within each "biological process" term (Result count), number of genes with this term divided by the total number of annotated genes with this term in the *P. falciparum* genome (Fold enrichment), odds ratio statistics from the Fisher's exact test, *P*-value (calculated using a Fisher's exact test), and Benjamini-corrected *P*-value are shown (*q*-value). Only GO terms with $P < 0.05$ are shown. Analysis was performed using the GO enrichment tool at PlasmoDB.org (Aurrecoechea et al., 2017).

Table EV6. Differential gene expression analysis at 12 hpi of glucosamine-treated over untreated SMC3-3HA-*glmS* parasites. Analysis was performed for n=3153 genes (ID and chromosome locations are given) with two and three replicates for untreated and glucosamine-treated SMC3-3HA-*glmS* parasites, respectively. SMC3 is highlighted in grey. $\log_2$(FoldChange) = Fold change of baseMean (average of the normalized read counts across all samples and replicates for this gene) in glucosamine-treated/untreated parasites ($\log_2$). *P*-values are calculated with a Wald test for significance of coefficients in a negative binomial generalized linear model as implemented in DESeq2 (Love et al., 2014). *q* = Bonferroni corrected *P*-value.

Table EV7. Differential gene expression analysis at 24 hpi of glucosamine-treated over untreated SMC3-3HA-*glmS* parasites. Analysis was performed for n=4822 genes (ID and chromosome locations are

given) with three replicates for untreated and glucosamine-treated SMC3-3HA-*glmS* parasites. SMC3 is highlighted in grey. log_2(FoldChange) = Fold change of baseMean (average of the normalized read counts across all samples and replicates for this gene) in glucosamine-treated/untreated parasites (log_2). *P*-values are calculated with a Wald test for significance of coefficients in a negative binomial generalized linear model as implemented in DESeq2 (Love et al., 2014) *q* = Bonferroni corrected *P*-value.

Table EV8. Differential gene expression analysis at 36 hpi of glucosamine-treated over untreated SMC3-3HA-*glmS* parasites. Analysis was performed for n=4936 genes (ID and chromosome locations are given) with three replicates for untreated and glucosamine-treated SMC3-3HA-*glmS* parasites. SMC3 is highlighted in grey. log_2(FoldChange) = Fold change of baseMean (average of the normalized read counts across all samples and replicates for this gene) in glucosamine-treated/untreated parasites (log_2). *P*-values are calculated with a Wald test for significance of coefficients in a negative binomial generalized linear model as implemented in DESeq2 (Love et al., 2014) *q* = Bonferroni corrected *P*-value.

Table EV9. Differential gene expression analysis at 12 hpi of glucosamine-treated over untreated 3D7 WT parasites. Analysis was performed for n=3668 genes (ID and chromosome locations are given) with three replicates for untreated and glucosamine-treated 3D7 WT parasites, respectively. log_2(FoldChange) = Fold change of baseMean (average of the normalized read counts across all samples and replicates for this gene) in glucosamine-treated/untreated parasites (log_2). *P*-values are calculated with a Wald test for significance of coefficients in a negative binomial generalized linear model as implemented in DESeq2 (Love et al., 2014). *q* = Bonferroni corrected *P*-value.

Table EV10. Differential gene expression analysis at 24 hpi of glucosamine-treated over untreated 3D7 WT parasites. Analysis was performed for n=4734 genes (ID and chromosome locations are given) with three replicates for untreated and glucosamine-treated 3D7 WT parasites. log_2(FoldChange) = Fold change of baseMean (average of the normalized read counts across all samples and replicates for this gene) in glucosamine-treated/untreated parasites (log_2). *P*-values are calculated with a Wald test for significance of coefficients in a negative binomial generalized linear model as implemented in DESeq2 (Love et al., 2014). *q* = Bonferroni corrected *P*-value.

Table EV11. List of differentially expressed genes in SMC3-3HA-*glmS* parasites after filtering of significantly differentially expressed genes in the 3D7 WT upon glucosamine treatment at 12 hpi (Supp. Fig. 7). log_2(FoldChange) = Fold change of baseMean (average of the normalized read counts across all samples and replicates for this gene) in glucosamine-treated/untreated parasites (log_2). *P*-values are calculated with a Wald test for significance of coefficients in a negative binomial generalized linear model as implemented in DESeq2 (Love et al., 2014). *q* = Bonferroni corrected *P*-value. SMC3 is highlighted in grey.

Table EV12. List of differentially expressed genes in SMC3-3HA-*glmS* parasites after filtering of significantly differentially expressed genes in the 3D7 WT upon glucosamine treatment at 24hpi (Supp. Fig. 7). log_2(FoldChange) = Fold change of baseMean (average of the normalized read counts across all samples and replicates for this gene) in glucosamine-treated/untreated parasites (log_2). *P*-values are calculated with a Wald test for significance of coefficients in a negative binomial generalized linear model as implemented in DESeq2 (Love et al, 2014). *q* = Bonferroni corrected *P*-value. SMC3 is highlighted in grey.

Table EV13: Gene Ontology analysis of significantly up- and downregulated genes in SMC3 knockdown at 12 hpi. GO enrichment analysis (biological process) of genes significantly and specifically up- or downregulated upon SMC3 knockdown at 12 hpi (as defined in Table 10). Number of significantly enriched genes within each "biological process" term (Result count), number of genes with this term divided by the total number of annotated genes with this term in the *P. falciparum* genome (Fold enrichment), odds ratio statistics from the Fisher's exact test, *P*-value (calculated using a Fisher's exact test), and Benjamini-corrected *P*-value (*q*-value). Only GO terms with $P < 0.05$ are shown. Analysis was performed using the GO enrichment tool at PlasmoDB.org (Aurrecoechea et al., 2017).

Table EV14: Gene Ontology analysis of significantly up- and downregulated genes in SMC3 knockdown at 24 hpi. GO enrichment analysis (biological process) of genes significantly and specifically up- or downregulated upon SMC3 knockdown at 12 hpi (as defined in Table 11). Number of significantly enriched genes within each "biological process" term (Result count), number of genes with this term divided by the total number of annotated genes with this term in the *P. falciparum* genome (Fold enrichment), odds ratio statistics from the Fisher's exact test, *P*-value (calculated using a Fisher's exact test), and Benjamini-corrected *P*-value (*q*-value). Only GO terms with a $P < 0.05$ are shown. Analysis was performed using the GO enrichment tool at PlasmoDB.org (Aurrecoechea et al., 2017).

Table EV15: List of invasion-related genes that are significantly upregulated in SMC3 knockdown at 12 and 24 hpi. List of genes significantly and specifically upregulated at 12 and 24 hpi in response to SMC3 depletion that overlap with a list of "invasion-related genes," as defined in (Hu et al., 2010). Gene IDs and chromosome locations are given. $\log_2$(FoldChange) = Fold change of baseMean (average of the normalized read counts across all samples and replicates for this gene) in glucosamine-treated/untreated parasites ($\log_2$). *P*-values are calculated with a Wald test for significance of coefficients in a negative binomial generalized linear model as implemented in DESeq2 (Love et al., 2014). *q* = Bonferroni corrected *P*-value.

2.3 Material and Methods

2.3.1 Parasite culture

Blood stage 3D7 *P. falciparum* parasites were cultured as previously described in (Lopez-Rubio et al., 2009). Briefly, parasites were cultured in human RBCs supplemented with 10% v/v Albumax I (Thermo Fisher 11020), hypoxanthine (0.1 mM final concentration, C.C.Pro Z-41-M) and 10 mg gentamicin (Sigma G1397) at 4% hematocrit and under 5% O2, 5% CO2 at 37 °C. Parasites were synchronized by sorbitol (5%, Sigma S6021) lysis during ring stage followed by a plasmagel (Plasmion, Fresenius Kabi) enrichment for late blood stages 24 hours later. Another sorbitol treatment 6 h afterwards places the 0 h time point 3 h after the plasmagel enrichment. Parasite development was monitored by Giemsa staining. Parasites were harvested at 1–5% parasitemia.

2.3.2 Generation of strains

The SMC3-3HA-*glms* strain was generated using a two-plasmid system (pUF1 and pL7) based on the CRISPR/Cas9 system previously described in (Ghorbal et al., 2014). A 3D7 wild-type bulk ring stage culture was transfected with 25 µg pUF1-Cas9 and 25 µg of pL7-*Pf*SMC3-3HA-*glmS* containing the single guide RNA (sgRNA) -encoding sequence 5'-CCTAGAAAATTAGAACAATT-3' targeting the 3' UTR of PF3D7_0414000. The pL7-*Pf*SMC3-3HA-*glmS* plasmid also contained the homology repair construct 5'-

AGATAGAGAGAGTTATATATCTAAAGGAACAAAGAATGAGGCCTACGAAATT
ATTAGCATTGTATAAAAAAAAAAAGAAAAAAAAAAGAAAAAAAAAAAAGAT
TATATATATAATATATGTTGACAATTAATAAATATATTTGTATATATCTGTTAA
CTAATTATGAAAATTTTTGAATCAATAAATTTTTTAAATAACAAAAAAAAAAA
AAAATATATATATTATATATATATTTTATATTTTATATTTTCTTGTAATTTTTGT
TTTTTTAGGAGGAAAAACATGCCCTAGAAAATggcggtggaTACCCTTACGATGTG

CCTGATTACGCGTAtCCcTAtGAcGTaCCaGAcTAtGCGTACCCtTAtGAcGTtCCgG
ATTAtGCtcacggggtgTAAGCGGCCGCGGTCTTGTTCTTATTTTCTCAATAGGAAA
AGAAGACGGGATTATTGCTTTACCTATAATTATAGCGCCCGAACTAAGCGCC
CGGAAAAAGGCTTAGTTGACGAGGATGGAGGTTATCGAATTTTCGGCGGATG
CCTCCCGGCTGAGTGTGCAGATCACAGCCGTAAGGATTTCTTCAAACCAAGG
GGGTGACTCCTTGAACAAAGAGAAATCACATGATCTTCCAAAAAACATGTAG
GAGGGGACAACAATTTGGTTTTGTTTTTTTCTTTAGGTTTTGAGAAAAACAAA
TAGGAAATACAAAAAAAAAAAAAAAAAAAAAAAAAAAAAAAAAAAATG
TATTTTTACATATGCACTTGGATTATTTTATTTTTATTATTTTTCTTTATATAAA
GTAAAAATATACATAAGTATGCTTATTTATTACATAAGAGTTTATTTAAGAAA
GGTTTCTTTTTCATAATATTGTGTGCATGAGTTTTTTTTTATTTTATTTTTTTTTT
TTATTTCTGTAACGAAAAGGATATTAAAAAAAATAATAAAA-3’ (synthesized by GenScript Biotech [Piscataway, NJ, USA]). This homology repair construct comprises a 3 x Hemaglutinin (3HA) - encoding sequence followed by a *glmS* ribozyme-encoding sequence (Prommana et al., 2013), which are flanked by 300 bp homology repair regions upstream and downstream of the Cas9 cut site, excluding the gene STOP codon. The sgRNA sequence was designed using Protospacer (MacPherson & Scherf, 2015). The sgRNA sequence uniquely targeted a single sequence in the genome. As the sgRNA sequence encompasses the STOP codon, its modification via the addition of the 3HA and *glmS*-encoding sequences renders the modified parasites refractory to further dCas9 cleavage at this locus.

All cloning was performed using KAPA HiFi DNA Polymerase (Roche 07958846001), In-Fusion HD Cloning Kit (Clontech 639649), and XL10-Gold Ultracompetent E. coli (Agilent Technologies 200315). After transfection, drug selection was applied for five days at 2.67 nM WR99210 (Jacobus Pharmaceuticals) and 1.5 μM

DSM1 (MR4/BEI Resources). Parasites reappeared approximately three weeks after transfection, and 5-fluorocytosine was used to negatively select the pL7 plasmid. Parasites were cloned by limiting dilution, and the targeted genomic locus was sequenced to confirm epitope tag and ribozyme integration.

2.3.3 SMC3 immunoprecipitation and mass spectrometry

An SMC3-3HA-*glms* clone ($n = 3$ technical replicates) and wild-type culture ($n = 3$ technical replicates), as a negative control, were synchronized. Late stage parasites (1.5×10^9 parasites) were enriched using Percoll density gradient separation and then cross-linked with 1 mL 0.5 mM dithiobissuccinimidyl propionate (DSP; Thermo Fisher 22585) in DPBS for 60 min at 37°C (as in (Mesén-Ramírez et al., 2016)). Cross-linked parasites were centrifuged at 4,000 *g* for 5 min at 4°C, and the pellet was washed twice with DPBS at 4°C. The pellet was lysed with 10 volumes of RIPA buffer (10 mM Tris–HCl pH 7.5, 150 mM NaCl, 0.1% SDS, 1% Triton) containing protease and phosphatase inhibitor cocktail (Thermo Fisher 78440) and 1 U/µL of Benzonase (Merck 71206). The lysates were cleared by centrifugation at 16,000 *g* for 10 min at 4°C. Supernatants were incubated with 25 µL of anti-HA Dynabeads (Thermo Fisher 88836) overnight with rotation at 4°C. Beads were collected with a magnet and washed five times with 1 mL RIPA buffer, then five times with 1 mL DPBS, and then once with 1 mL 25 mM NH_4HCO_3 (Sigma 09830). The beads were reduced with 100 mM dithiothreitol (Sigma D9779), alkylated with 55 mM iodoacetamide (Sigma I1149), and subjected to on-bead digestion using 1 µg of trypsin (Thermo Fisher 90059). The resulting peptides were desalted using C18 ziptips (Merck ZTC04S096) and sent for MS analysis.

Peptides were separated by reverse phase HPLC (Thermo Fisher Easy-nLC1000) using an EASY-Spray column, 50 cm × 75 µm ID, PepMap RSLC C18, 2 µm (Thermo Fisher ES803A) over a 70-min gradient before nanoelectrospray using a Q Exactive HF-X

mass spectrometer (Thermo Fisher). The mass spectrometer was operated in a data-dependent mode. The parameters for the full scan MS were as follows: resolution of 60,000 across 350–1,500 *m/z*, AGC $1e^5$ (as in (Kensche et al., 2016)), and maximum injection time (IT) 150 ms. The full MS scan was followed by MS/MS for the top 15 precursor ions in each cycle with an NCE of 30 and dynamic exclusion of 30 s and maximum IT of 96 ms. Raw mass spectral data files (.raw) were searched using Proteome Discoverer 2.3.0.523 (Thermo Fisher) with the SEQUEST search engine. The search parameters were as follows: 10 ppm mass tolerance for precursor ions; 0.8 Da fragment ion mass tolerance; two missed cleavages of trypsin; fixed modification was carbamidomethylation of cysteine; and variable modifications were methionine oxidation, CAMthiopropanoyl on lysine or protein N-terminal, and serine, threonine, and tyrosine phosphorylation. Only peptide spectral matches (PSMs) with an XCorr score greater than or equal to 2 and an isolation interference less than or equal to 30 were included in the data analysis.

2.3.4 Protein fractionation and western blot analysis

Parasites were washed once with Dulbecco's phosphate-buffered saline (DPBS, Thermo Fisher 14190), then resuspended in cytoplasmic lysis buffer (25 mM Tris–HCl pH 7.5, 10 mM NaCl, 1.5 mM $MgCl_2$, 1% IGEPAL CA-630, and 1× protease inhibitor cocktail [“PI”, Roche 11836170001]) at 4°C and incubated on ice for 30 min. The cytoplasmic lysate was cleared with centrifugation (13,500 *g*, 10 min, 4°C). The pellet (containing the nuclei) was resuspended in 3.3 times less volume of nuclear extraction buffer (25 mM Tris–HCl pH 7.5, 600 mM NaCl, 1.5 mM $MgCl_2$, 1% IGEPAL CA-630, PI) than cytoplasmic lysis buffer at 4°C, transferred to 1.5 mL sonication tubes (Diagenode C30010016, 300 µL per tube), and sonicated for five min total (10 cycles of 30 s on/off) in a Diagenode Pico Bioruptor at 4°C. This nuclear lysate was cleared with centrifugation (13,500 *g*, 10 min, 4°C). Protein samples were supplemented with NuPage Sample Buffer (Thermo Fisher

NP0008) and NuPage Reducing Agent (Thermo Fisher NP0004) and denatured for 10 min at 70°C. Proteins were separated on a 4–12% Bis-Tris NuPage gel (Thermo Fisher NP0321) and transferred to a PVDF membrane with a Trans-Blot Turbo Transfer system (Bio-Rad). The membrane was blocked for 1 h with 1% milk in PBST (PBS, 0.1% Tween 20) at 25°C. HA-tagged proteins and histone H3 were detected with anti-HA (Abcam ab9110, 1:1,000 in 1% milk-PBST) and anti-H3 (Abcam ab1791, 1:2,500 in 1% milk-PBST) primary antibodies, respectively, followed by donkey anti-rabbit secondary antibody conjugated to horseradish peroxidase ("HRP", Sigma GENA934, 1:5,000 in 1% milk-PBST). Aldolase was detected with anti-aldolase-HRP (Abcam ab38905, 1:5,000 in 1% milk-PBST). HRP signal was developed with SuperSignal West Pico Plus chemiluminescent substrate (Thermo Fisher 34580) and imaged with a ChemiDoc XRS+ (Bio-Rad).

2.3.5 Immunofluorescence assays and image acquisition

iRBCs were washed once with DPBS (Thermo Fisher 14190) at 37°C and fixed in suspension in 4% paraformaldehyde (EMS 15714) with 0.0075% glutaraldehyde (EMS 16220) in PBS for 20 min at 25°C, as described previously (Tonkin et al., 2004). The subsequent steps were performed at 25 °C as described in (Mehnert et al., 2019), with minor changes. After washing once with PBS, cells were permeabilized with 0.1% Triton-X 100 for 10 min followed by three PBS washes. Free aldehyde group were quenched with 50 mM NH_4Cl for 10 min, followed by two PBS washes. Cells were blocked with 3% bovine serum albumin (BSA) (Sigma A4503-50G) in PBS for 30 min. Cells were incubated with anti-HA (Abcam ab9110, 1:1,000 in 3% BSA in PBS) primary antibody for one hour followed by three 10 min washes with 0.5% Tween® 20/PBS. Cells were incubated with anti-rabbit Alexa Fluor 488- or 633-conjugated secondary antibodies (Invitrogen A-11008 or A-21070, 1:2,000 in 3% BSA in PBS) with DAPI (FluoProbes FP-CJF800, 1 μg/mL) for 45 min followed by three 10 min washes with 0.5% Tween® 20/PBS. Cells were washed

once more with PBS and placed onto polyethyleneimine-coated slides (Thermo Scientific 30-42H-RED-CE24). Once adhered to the slide, cells were washed twice and mounted with VectaShield® (Vector Laboratories). Images were acquired using a Deltavision Elite imaging system (GE Healthcare), and Fiji (http://fiji.sc) was used for analysis using the least manipulation possible.

2.3.6 SMC3 chromatin immunoprecipitation sequencing and data analysis

A clonal population of SMC3-3HA-*glmS* parasites were tightly synchronized and harvested at 12 (10^{10} parasites), 24 (4.3 x 10^8 parasites) and 36 hpi (3.6 x 10^8 parasites). Parasite culture was centrifuged at 800 *g* for 3 min at 25ºC. Medium was removed and the RBCs were lysed with 10 mL 0.075% saponin (Sigma S7900) in DPBS at 37ºC. The parasites were centrifuged at 3,250 *g* for 3 min at 25°C and washed with 10 mL DPBS at 37°C. The supernatant was removed, and the parasite pellet was resuspended in 10 mL of PBS at 25ºC. The parasites were cross-linked by adding methanol-free formaldehyde (Thermo Fisher 28908) (final concentration 1%) and incubating with gentle agitation for 10 min at 25°C. The cross-linking reaction was quenched by adding glycine (final concentration 125 mM, Sigma G8899) and incubating with gentle agitation for 5 min at 25°C. Parasites were centrifuged at 3,250 *g* for 5 min at 4°C and the supernatant removed. The pellet was washed with DPBS and centrifuged at 3,250 *g* for 5 min at 4°C. The supernatant was removed, and the cross-linked parasite pellet were snap-frozen.

For each time-point, 200 µL of Protein G Dynabeads (Invitrogen 10004D) were washed twice with 1 mL ChIP dilution buffer (16.7 mM Tris–HCl pH 8, 150 mM NaCl, 1.2 mM EDTA pH 8, 1% Triton X-100, 0.01% SDS) using a DynaMag magnet (Thermo Fisher 12321D). The beads were resuspended in 1 mL ChIP dilution buffer with 8 µg of anti-HA antibody (Abcam ab9110) and incubated on a rotator at 4°C for 6 h.

The cross-linked parasites were resuspended in 4 mL of lysis buffer (10 mM HEPES pH 8, 10 mM KCl, 0.1 mM EDTA pH 8, PI) at 4°C, and 10% Nonidet-P40 was added (final concentration 0.25%). The parasites were lysed in a prechilled dounce homogenizer (200 strokes for 12 hpi parasites and 100 strokes for 24 and 36 hpi parasites). The lysates were centrifuged for 10 min at 13,500 *g* at 4°C, the supernatant was removed, and the pellet was resuspended in SDS lysis buffer (50 mM Tris–HCl pH 8, 10 mM EDTA pH 8, 1% SDS, PI) at 4°C (3.6 mL for the 12 hpi sample and 1.8 mL for the 24 ad 36 hpi samples). The liquid was distributed into 1.5 mL sonication tubes (Diagenode C30010016, 300 µL per tube) and sonicated for 12 min total (24 cycles of 30 s on/off) in a Diagenode Pico Bioruptor at 4°C. The sonicated extracts were centrifuged at 13,500 *g* for 10 min at 4°C and the supernatant, corresponding to the chromatin fraction, was kept. The DNA concentration for each time point was determined using the Qubit dsDNA High Sensitivity Assay Kit (Thermo Fisher Scientific Q32851) with a Qubit 3.0 Fluorometer (Thermo Fisher Scientific). For each time point, chromatin lysate corresponding to 100 ng of DNA was diluted in SDS lysis buffer (final volume 200 µL) and kept as "input" at −20°C. Chromatin lysate corresponding to 19 µg (12 hpi), 2 µg (24 hpi) and 3 µg (36 hpi) of DNA was diluted 1:10 in ChIP dilution buffer at 4°C.

Using a DynaMag magnet, the antibody-conjugated Dynabeads were washed twice with 1 mL ChIP dilution buffer and resuspend in 100 µL of ChIP dilution buffer at 4°C. Then the washed antibody-conjugated Dynabeads were added to the diluted chromatin sample and incubated overnight with rotation at 4°C. The beads were collected on a DynaMag into eight different tubes per sample, the supernatant was removed, and the beads in each tube were washed for 5 min with gentle rotation with 1 mL of the following buffers, sequentially:

- Low salt wash buffer (20 mM Tris–HCl pH 8, 150 mM NaCl, 2 mM EDTA pH 8, 1% Triton X-100, 0.1% SDS) at 4°C.
- High salt wash buffer (20 mM Tris–HCl pH 8, 500 mM NaCl, 2 mM EDTA pH 8, 1% Triton X-100, 0.1% SDS) at 4°C.
- LiCl wash buffer (10 mM Tris–HCl pH 8, 250 mM LiCl, 1 mM EDTA pH 8, 0.5% IGEPAL CA-630, 0.5% sodium deoxycholate) at 4°C.
- TE wash buffer (10 mM Tris–HCl pH 8, 1 mM EDTA pH 8) at 25°C.

After the washes, the beads were collected on a DynaMag, the supernatant was removed, and the beads for each time point were resuspended in 800 µL of elution buffer and incubated at 65°C for 30 min with agitation (1000 rpm 30 s on/off). The beads were collected on a DynaMag and the eluate, corresponding to the "ChIP" samples, was transferred to a different tube.

For purification of the DNA, both "ChIP" and "Input" samples were incubated for approximately 10 h at 65°C to reverse the crosslinking. 200 µL of TE buffer followed by 8 µL of RNaseA (Thermo Fisher EN0531) (final concentration of 0.2 mg/mL) were added to each sample, which was then incubated for 2 h at 37 °C. 4 µL Proteinase K (New England Biolabs P8107S) (final concentration of 0.2 mg/mL) were added to each sample, which was then incubated for 2 h at 55°C. 400 µL phenol:chloroform:isoamyl alcohol (25:24:1) (Sigma, 77617) were added to each sample, which was then mixed with vortexing and centrifuged for 10 min at 13,500 *g* at 4°C to separate phases. The aqueous top layer was transferred to another tube and mixed with 30 µg glycogen (Thermo Fisher 10814) and 5M NaCl (200 mM final concentration). 800 µL 100% EtOH at 4°C were added to each sample, which was then incubated at −20°C for 30 min. The DNA was pelleted by centrifugation for 10 min at 13,500 *g* at 4°C, washed with 500 µL 80% EtOH at 4°C, and centrifuged for 5 min at 13,500 *g* at 4°C. After removing the EtOH, the pellet was dried at

25 °C and all DNA for each sample was resuspended in 30 µL 10 mM Tris–HCl, pH 8 total. The DNA concentration and average size of the sonicated fragments was determined using a DNA high sensitivity kit and the Agilent 2100 Bioanalyzer. Libraries for Illumina Next Generation Sequencing were prepared with the MicroPlex library preparation kit (Diagenode C05010014), with KAPA HiFi polymerase (KAPA biosystems) substituted for the PCR amplification. Libraries were sequenced on the NextSeq 500 platform (Illumina).

Sequenced reads (150 bp paired end) were mapped to the *P. falciparum* genome (Gardner et al., 2002) (plasmoDB.org, version 3, release 55) using "bwa mem" (Li & Durbin, 2009) allowing a read to align only once to the reference genome (option "–c 1"). Alignments were subsequently filtered for duplicates and a mapping quality ≥ 20 using samtools (Li et al., 2009). The paired end deduplicated ChIP and input BAM files were used as treatment and control, respectively, for peak calling with the macs2 command callpeak default settings (Y. Zhang et al., 2008). Obtained peaks with *q*-value cutoff 0.05 for each time point were visualized in Integrative Genomics Viewer (Robinson et al., 2011) along with ChIP-Input ratio coverage obtained from deeptool's bamCompare command (Ramírez et al., 2016). To map SMC3 binding to nearby protein coding genes, peak summits were extended 150 bp upstream and downstream, and bedtools closest command (Quinlan & Hall, 2010) were used with *P. falciparum* reference genome feature file (gff) (plasmoDB.org, version 3, release 56). Only regions 500 bp upstream or downstream near to the protein coding genes were considered further for downstream analysis. Centromeric regions (from (Hoeijmakers et al., 2012) were corrected for changes in genome annotation. These regions were overlapped with SMC3 peaks dataset using bedtools intersect command (Quinlan & Hall, 2010). Fold change quantification and statistical analysis for all peaks and peaks in centromeric regions was performed in R (R Core Team, 2021).

2.3.7 RNA extraction, stranded RNA sequencing and analysis

A WT and SMC3-3HA-*glmS* clone were synchronized simultaneously and each culture was split into two at 12 hpi. Glucosamine (Sigma G1514, final concentration 2.5 nM) was added to one half of the culture for two rounds of parasite replication (approximately 96 h). Parasites were then re-synchronized and three technical replicates (with and without glucosamine) were harvested at 12, 24, and 36 hpi. RBCs were lysed in 0.075 % saponin (Sigma S7900) in PBS at 37°C, centrifuged at 3,250 *g* for 5 min, washed in PBS, centrifuged at 3,250 g for 5 min, and resuspended in 700 µL QIAzol reagent (Qiagen 79306). RNA was extracted using an miRNeasy Mini kit (Qiagen 1038703) with the recommended on-column DNase treatment. Total RNA was poly (A) selected using the Dynabeads mRNA Purification Kit (Thermo Fischer Scientific 61006).

Library preparation was performed with the NEBNext® Ultra™ II Directional RNA Library Prep Kit for Illumina® (New England Biolabs E7760S) and paired end sequencing was performed on the Nextseq 550 platform (Illumina). Sequenced reads (150 bp paired end) were mapped to the *P. falciparum* genome (Gardner et al., 2002) (plasmoDB.org, version 3, release 55) using "bwa mem" (Li & Durbin, 2009), allowing a read to align only once to the reference genome (option "–c 1"). Alignments were subsequently filtered for duplicates and a mapping quality ≥ 20 using samtools (Li et al., 2009). Gene counts were quantified with htseq-count (Anders et al., 2015), and differentially expressed genes were identified in R (R Core Team, 2021) using package DESeq2 (Love et al., 2014).

2.3.8 Estimation of cell cycle progression

RNA-seq-based cell cycle progression was estimated in R by comparing the normalized expression values (i.e., RPKM, reads per kilobase per exon per one million

mapped reads) of each sample to the microarray data from (Bozdech et al., 2003) using the statistical model as in (Lemieux et al., 2009).

2.3.9 Parasite growth assay

Parasite growth was measured as described previously (Vembar et al., 2015). Briefly, an SMC3-3HA-*glmS* clone and a WT clone were tightly synchronized. Each culture was split and glucosamine (Sigma G1514) was added (2.5 mM final concentration) to one half for approximately 96 h before starting the growth curve. The parasites were tightly re-synchronized and diluted to 0.3% parasitemia (5% hematocrit) at ring stage using the blood of two different donors. The growth curve was performed in a 96-well plate (200 µL culture per well) with three technical replicates per condition per blood. Every 24 h, 5 µL of the culture were fixed in 45 µL of 0.025% glutaraldehyde in PBS for 1h at 4°C. After centrifuging at 800 *g* for 5 min, free aldehyde groups were quenched by re-suspending the iRBC pellet in 200 µL of 15 mM NH_4Cl in PBS. A 1:10 dilution of the quenched iRBC suspension was incubated with Sybr Green I (Sigma S9430) to stain the parasite nuclei. Quantification of the iRBCs was performed in a CytoFLEX S cytometer (Beckman Coulter) and analysis with FlowJo™ Software.

2.3.10 Data availability

All data sets generated in this study are available in the following databases:

- ChIP-seq data: NCBI BioProject accession # PRJNA854331
- RNA-seq data: NCBI BioProject accession # PRJNA854331
- SMC3-3HA Proteomics data: PRIDE repository accession # PXD035225 (DOI: 10.6019/PXD035225, Username**:** reviewer_pxd035225@ebi.ac.uk, Password**:** agXjJYP4)

PART THREE

DISCUSSION

Genome organization is key to transcriptional control and genome integrity. The human malaria parasite *P. falciparum* executes complex transcriptional programs and has a sophisticated genome organization considering that it encodes relatively few specific TFs and lacks key canonical genome organizing factors such as CTCF and lamins (Batsios et al., 2012; Heger et al., 2012; Ay et al., 2014; Bunnik et al., 2019). To investigate potential links between transcription and genome organization in this parasite, we have characterized SMC3, a key and conserved subunit of the multi-protein ring-shaped complex cohesin. In the organisms studied so far, cohesin plays diverse roles in genome organization such as sister chromatid cohesion during mitosis, transcription, and DNA damage repair (Horsfield, 2022; Litwin et al., 2018; Nishiyama, 2019).

In the present study we used genome-wide approaches to elucidate the function of the cohesin subunit SMC3 during the IDC of *P. falciparum*. While in model systems, such as yeast, there is the need to perform cell cycle arrest to study cohesin outside the essential role in mitosis; the use of tightly synchronized *P. falciparum* parasites has allowed us to address the role of cohesin in both mitosis/schizogony and transcription in a less perturbed biological context.

3.1 Cohesin and mitosis/schizogony

The most well-described role of cohesin is in holding sister chromatids together until their separation in anaphase (Guacci & Koshland, 1997; Michaelis et al., 1997). It is essential for mitotic fidelity, as it counteracts the bipolar tension produced by the mitotic spindle, preventing premature chromatid individualization and random genome segregation (Oliveira et al., 2010; Tanaka et al., 2000). In *P. falciparum*, DNA replication debuts approximately halfway through the IDC and is followed by repeated asynchronous rounds of nuclear division during schizont stage. Nuclear multiplication finishes with a relatively synchronous round of nuclear division and the formation of a multinucleated syncytium before cytokinesis (Arnot et al., 2011; Francia & Striepen, 2014; Ganter et al., 2017; Klaus et al., 2022).

Cohesin subunit *Pf*SMC3 was found to be most enriched in centromeric and peri-centromeric regions of all the chromosomes (Fig. 2.2A, B). In other eukaryotes, cohesin is also mostly enriched around the centromeres relative to the chromosome arms (Holzmann et al., 2019; Tanaka et al., 1999; Tomonaga et al., 2000). Centromeric binding was found to decrease in late-stage parasites (Fig. 2.1A-C), which might be due to the need for cohesin removal during the separation of sister chromatids, as has been observed in model eukaryotes (Uhlmann et al., 1999; Waizenegger et al., 2000). While *Plasmodium* does have a clear anaphase during which sister chromatids separate (Gerald et al., 2011), asynchronous mitosis may lead to a mixed population of parasites in which cohesin is present or absent from centromeres to facilitate sister chromatid cohesion or separation, respectively.

Our observation that *Pf*SMC3 depletion does not inhibit parasite growth (Supp. Fig. 10) agrees with reports in *S. cerevisiae* and *D. melanogaster* in which normal growth and sister chromatid cohesion were achieved despite an 87% and 80% decrease in Rad21,

respectively (Carvalhal et al., 2018; Heidinger-Pauli et al., 2010). These studies and ours suggest that only a small fraction of cohesin is needed to successfully complete mitosis. Thus, even though *Pf*SMC3 is predicted to have an essential function (M. Zhang et al., 2018) and our inducible knockdown system was fairly efficient (Fig.2.3 A,B), there might still be sufficient protein levels to facilitate mitosis (Gerlich et al., 2006; Laugsch et al., 2013).

While before S phase there is dynamic turnover of cohesin, after DNA replication cohesin can stably bound chromatin until anaphase (Gerlich et al., 2006). Indeed, two cell cycles of inducible knockdown treatment were needed to observe *Pf*SMC3 depletion at the protein level in our system (Supp. Fig. 3). While we could attempt an inducible knockout system of *Pf*SMC3 in the future, the amount of time it takes to deplete *Pf*SMC3 from chromatin could allow for any parasites in which the inducible knockout was not achieved to overtake the mutant parasites.

Given that 1) depletion of SMC3 has been found to affect the stability of SMC1 (Laugsch et al., 2013), 2) mutations in SMC1A and SMC3 are associated with a milder variant of CdLS (Deardorff et al., 2007) and 3) *Pf*SMC3 loss may be compensated by another factor; in the future, parasite strains will be generated in which we can perform inducible knockout or knockdown of multiple members of the core cohesin complex.

Also, to confirm that *Pf*SMC3 functions within the cohesin complex, it will be vital to perform ChIP-seq and RNA-seq in these strains to explore the binding patterns of *Pf*SMC1 and *Pf*RAD21 in the presence or absence of *Pf*SMC3 depletion.

3.2 Cohesin and transcriptional regulation

Cohesin has been shown to play a role in transcriptional regulation in multiple eukaryotic model systems [reviewed in (Horsfield, 2022)]. In our study, we observed that SMC3 regulates specific cohorts of genes during interphase, many of which are involved in parasite RBC invasion. *Pf*SMC3 binds dynamically at extra-centromeric genomic locations over the course of the IDC (Fig. 2.2, Table EV2). We observed stage specific SMC3 binding across the genome, including at genes that were then upregulated upon SMC3 depletion during interphase. In contrast, genes that were downregulated upon SMC3 depletion were not enriched for SMC3, suggesting an indirect effect (Fig. 2.4A,B, Supp. Fig. 8, Tables EV2, EV11, EV12).

Differential expression analysis under *Pf*SMC3 depletion revealed upregulated genes that are, in general, highly expressed in late-stage parasites (Fig. 2.3E, Fig. 2.4F) which is the stage when we observed natural depletion of *Pf*SMC3 at their promoters and chromatin accessibility (Fig. 2.4B-D). Importantly, while we observed a decrease in *Pf*SMC3 binding at centromeric and pericentromeric regions in late-stage parasites, this was not a general trend across all SMC3 binding sites (Fig. 2.2C). These data suggest that *Pf*SMC3 is specifically recruited to and evicted from specific subsets of genes to facilitate their repression and transcription, respectively, over the course of the IDC.

Genes that were significantly upregulated upon SMC3 depletion during interphase were enriched for GO terms related to egress from and invasion of the RBC (Tables EV15) (Cowman et al., 2012, 2017). Indeed, out of a list of 63 invasion-related genes (Hu et al., 2010), 50% were among the genes that were upregulated upon SMC3 depletion during interphase (Table EV15). However, for at least one of these genes – RAP2 – we did not see a significant upregulation at the protein level upon SMC3 depletion. One possibility is that the transcript is translationally repressed and needs specific stage-specific RNA binding

proteins for translation. Other possibility, is that we did not achieve a high enough level of *Pf*SMC3 knockdown with our system to result in more substantial upregulation of *Pf*SMC3-bound genes. Also, other factor, such as *Pf*SMC1, may have redundant function with *Pf*SMC3. Again, the use of strains in which multiple core cohesin complex subunits are epitope-tagged and capable of being inducibly depleted would allow us to determine the role of the entire cohesin complex in the regulation of these specific genes.

The mechanism by which *Pf*SMC3 could repress specific genes in a stage-specific manner is unclear. Only in the context of interaction with CTCF, cohesin has been suggested to impact transcription in opposite ways, by either preventing enhancer-promoter interactions (Nativio et al., 2009; Wendt et al., 2008) or by mediating specific enhancer-promoter loops (Guo et al., 2012; Kubo et al., 2021). In *P. falciparum*, the current genome-wide chromosome conformation capture (Hi-C) datasets do not provide evidence of typical enhancer-promoter interactions found in other eukaryotes (Ay et al., 2014; Bunnik et al., 2019).

It is possible that in *P. falciparum*, cohesin binding to a promoter prevents binding of activating transcription factors or complexes. A study in TF1 cells – a human Erythroleukemic cell line from blood – characterized regions with differential chromatin accessibility in WT and SMC1A or Rad21 mutants (Mazumdar et al., 2015). Motif analysis at the TSS of regions with higher chromatin accessibility in SMC1A and Rad21 mutants revealed a strong enrichment in binding motifs for three TFs that are critical regulators of hematopoietic stem/progenitor cells (HSPCs). It was also reported with ChIP-seq analysis that increase in binding of two of these TFs inversely correlated inversely with the presence of the cohesin complex. A second study in mouse hematopoietic cells showed that KD of a non-core cohesin subunit (STAG2) led to up-regulation of genes involved in the myeloid differentiation program and increased chromatin accessibility at their promoters

(Mullenders et al., 2015). These genes had a DNA motif in their promoter regions for a TF that is the master regulator of primitive and definitive hematopoiesis.

Similar to these two studies, we observed a negative correlation between *Pf*SMC3 binding and chromatin accessibility at the promoters of genes that are upregulated upon *Pf*SMC3 depletion (Fig. 2.4A, Supp. Fig 8). However, it is unclear how *Pf*SMC3 achieves binding specificity and how it is evicted from binding sites at specific times in the IDC. In other organisms studied, cohesin may need a DNA-binding factor to achieve sequence-specific binding (Kagey et al., 2010; Rubio et al., 2008; Wendt et al., 2008). A search for a specific binding motif within the promoter sequences of invasion-related genes bound by *Pf*SMC3 yielded no clear results, indicating that *Pf*SMC3 may associate with multiple factors to achieve specific binding.

In *P. falciparum*, the AP2-I transcription factor (PF3D7_1007700) is involved in transcription of invasion-related genes via binding to the GTGCA motif, likely by interaction with the bromodomain protein 1 (*Pf*BDP1, PF3D7_1033700) (Santos et al., 2017). This complex could evict SMC3 from gene promoters or simply bind in its absence (Fig. 3.1). Even though SMC3 depletion resulted in the upregulation of AP2-I-independent invasion-related genes such as RONs, EBLs and Rhs, which have an ACAACT motif in their promoter regions (Young et al., 2008), these may be activated by an as-yet unidentified transcription factor. Because we performed our *Pf*SMC3 IP LC-MS/MS experiment in late stage parasites, it is possible that we missed an associated specificity factor that targets SMC3 in earlier (interphase) parasite stages.

In the future, we will perform IP LC-MS/MS for *Pf*SMC1/3 and *Pf*RAD21 to identify more associated proteins that could potentially confer specificity to the cohesin complex. Moreover, comparison between *Pf*SMC3 interacting proteins between multiple

stages of the IDC will enable us to find other members of the cohesin complex that could not be identified by domain homology.

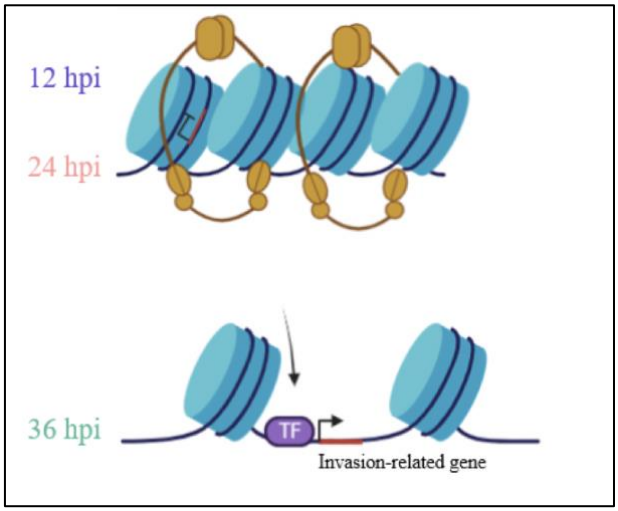

Figure 3.1. Hypothetical model of cohesin role in the transcriptional repression of invasion-related genes across the intraerythrocytic developmental cycle. Cohesin binding maintains chromatin inaccessibility at promoter regions of invasion-related genes preventing binding of activating transcription factors or complexes until the appropriate moment of transcription.

3.3 Cohesin and genome organization

It has been demonstrated that cohesin plays a role in interphase genome organization in other model eukaryotes [reviewed in (Rowley & Corces, 2018)]. Our study of *Pf*SMC3 in *P. falciparum* provides evidence for the involvement of cohesin in centromere organization, but also hints at a role in organizing genes that are transcriptionally related.

3.3.1 Cohesin at the centromeres

We showed that *Pf*SMC3 was most enriched at centromeric regions in interphase parasites (Fig. 2.2A-C) and was present in a foci at the nuclear periphery that did not overlap with HP1 (a marker of subtelomeric region) (Fig. 2.1F). In the future, we will perform IFA with centromeric markers such as CenH3 and the core cohesin complex subunits to investigate whether these foci are centromeric clusters. Centromeric clustering in interphase nuclei has been observed in several eukaryotes including *S. cerevisiae, D. melanogaster*, and *H. sapiens* [reviewed in (Muller et al., 2019)]. The functional importance of this spatial arrangement remains poorly understood; however, it has been shown that centromeric clustering is a relevant topological constraint that can affect transcription by preventing intrachromosomal arm interactions (Tolhuis et al., 2011). Studies in *P. falciparum* have demonstrated centromere clustering before and during schizogony, suggesting that this organization is needed during interphase and mitosis (Ay et al., 2014; Hoeijmakers et al., 2012).

One architectural factor, *Pf*HMGB1, was recently shown to play a direct role in centromere organization in the nucleus (Lu et al., 2021). Although *Pf*HMGB1 binds predominantly to centromeres, its depletion led to the de-regulation of many different genes to which it was not bound, suggesting that global genome organization is important for

transcriptional control at the local chromatin level (Lu et al., 2021). *Pf*HMGB1 knockout did not lead to blood stage parasite growth inhibition, indicating that other proteins, such as cohesin or *Pf*CenH3, play a role in centromere organization and mitosis.

Upon *Pf*SMC3 depletion, we observed significant up- and downregulation of many genes, suggesting that, as with *Pf*HMGB1, loss of *Pf*SMC3 at centromeric regions could lead to de-regulation of genes that are not directly bound by *Pf*SMC3. Future mass spectrometry studies of *Pf*SMC1, *Pf*SMC3, and *Pf*RAD21 in interphase parasites will reveal interacting partners that could target cohesin to centromeric regions. In addition, we will perform IFA with centromeric markers in parasites in which one or multiple cohesin core subunits have been knocked down/out to determine if cohesin is involved in centromere organization in *P. falciparum*.

3.3.2 Cohesin-mediated repression via tethering

Akin to the findings that cohesin plays a role in regulating important genes that underlie stem cell renewal and differentiation in human and mouse, our study also provides a link between cohesin, chromatin accessibility, and the repression of stage-specific genes in *P. falciparum*. Two potentially related mechanisms may facilitate cohesin-mediated transcriptional repression. Simple binding of cohesin could lead to chromatin inaccessibility by blocking transcriptional machinery at the gene promoter. However, because cohesin facilitates higher organization of chromatin in other eukaryotes, it is also possible that it tethers genes that are co-regulated in a spatio-temporal manner in *P. falciparum*. Tethering of invasion-related genes into a cluster could render their promoters inaccessible to specific activating factors until the appropriate time of transcription.

In mouse and human, cohesin has been shown to play a role in maintaining transcription-related chromatin architecture together with CTCF. In mouse embryonic stem

cells, it was shown that cell identity genes are found within chromosome structures that result from looping of two interacting CTCF sites co-occupied by cohesin (Dowen et al., 2014). In turn, it has been suggested that these looped structures form insulated neighbourhoods and that loss of cohesin would result in de-repression of these genes. Another study, with human epithelial cancer cells, showed Rad21 depletion led to the transcriptional induction of genes that are involved in the transition between epithelial and mesenchymal cancer cells (Yun et al., 2016), and Rad21 binding at those genes was found to inversely correlate with their transcription. This study indicated that the decrease of Rad21 expression levels in mesenchymal cancer compared to epithelial has a role in inducing genes necessary for the epithelial-mesenchymal transition, possibly via the release of gene-specific intrachromosomal architecture. However, because *P. falciparum* lacks CTCF and associated chromatin loops, it is unclear if this model could apply to cohesin-mediated gene repression in the parasite.

One possibility is that cohesin binding to the promoter of a gene merely inhibits the assembly or movement of the transcriptional machinery. Considering the ability of cohesin to interact with DNA molecules an intriguing possibility is that it tethers invasion-related genes together in a cluster that renders their promoters inaccessible to specific activating factors until the appropriate time of transcription.

Recently, *in vitro* studies in *S. cerevisiae,* revealed that cohesin and DNA separate into stably condensed clusters that are surrounded by a more diluted phase. Cohesin was able to bridge distant points along the DNA, that in turn led to the recruitment of more cohesin complexes, suggestive of bridging-induced phase separation (Ryu et al., 2021). Importantly, loop extrusion and phase separation are likely to co-exist in shaping chromatin domains (Conte et al., 2022). Similar clustering, whether due to phase separation or not, could lead to transcriptional repression of *Pf*SMC3-bound genes in *P. falciparum*. While

future studies will provide a mechanistic insight in the role of cohesin in the regulation of stage-specific transcription, we propose a model that could explain the results obtained (Fig.3.2).

In *P. falciparum*, transcriptional activity has been correlated with genome architecture (Ay et al., 2014; Bunnik et al., 2018, 2019). The parasite transition from blood stage to mosquito stage is accompanied by transcriptional repression of genes with a role in RBC invasion (Bunnik et al., 2018). During this transition, Hi-C studies revealed a significant increase in interactions between invasion genes on chromosomes 2 and 10 and repressed subtelomeric genes. This suggests a re-organization of genes as they become repressed; however, the current Hi-C studies performed in *P. falciparum* lack the resolution required to determine the level of interaction of the genes we found to be bound and regulated by *Pf*SMC3 in our study.

Future high-resolution chromosome conformation capture studies in WT and cohesin single/double mutant parasites will reveal a potential link between spatial association and transcriptional regulation of these SMC3-controlled genes across the IDC. Our attempts to perform Hi-C in *P. falciparum* were hampered due the inefficient restriction enzyme digestion of the highly AT-rich genome (Appendix B). Thus, we are currently optimizing a Micro-C protocol in *P. falciparum*, which uses MNase, an enzyme able to digest the genome at the nucleosome level, creating less bias and higher resolution compared to the restriction enzymes used in Hi-C protocols.

3.4 Conclusion and working model

The present study offers insight into the role of cohesin in the temporal regulation of genes in *P. falciparum* IDC. While the role of H3K9me3/HP1 has been well established in the transcriptional repression of clonally variant gene families and *ap2-g*, this study identifies a new factor – *Pf*SMC3 – involved in the repression of HP1-independent, stage-specific genes. Given the architectural nature of cohesin, this research provides a potential link between genome organization and transcriptional control in *P. falciparum*. We propose a model in which cohesin binding to gene promoters tethers them in space to prevent binding of TFs and the transcriptional machinery until the appropriate time of expression (Fig. 3.2). Follow-up experiments with the application of Micro-C and ATAC-seq in WT and cohesin single/double mutant parasites will elucidate the role of cohesin in mediating spatio-temporal regulation and chromatin accessibility of invasion-related genes.

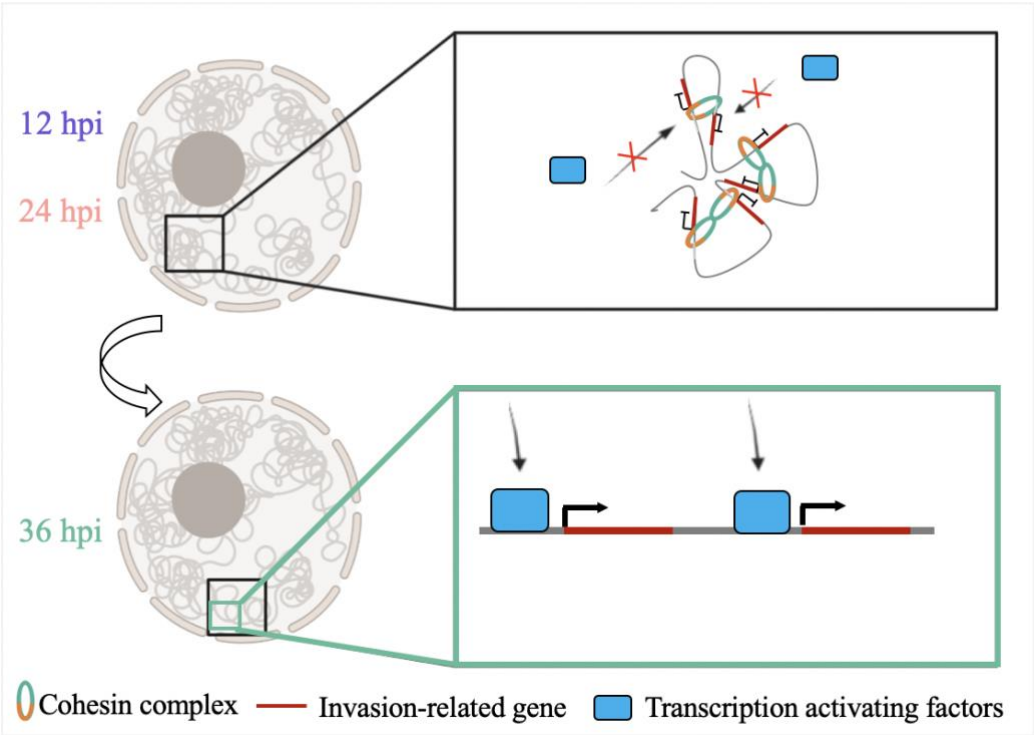

Figure 3.2. Working model - Cohesin regulates transcription via spatio-temporal regulation of the 3D genome. Image done with BioRender.

APPENDIX A

Additional preliminary results for Results section 2.1

Generation of strains for conditional knockdown of SMC1 and Rad21

Selection of parasites with genomic integrations can be achieved through a strategy termed selection-linked integration (SLI) (Birnbaum et al., 2017), by which an epitope tag construct is integrated at the 3' end of the gene and is followed by a skip peptide sequence and a promoterless selectable marker. A single-crossover recombination at the targeted locus drives expression of the selectable marker and the parasites carrying the integration can be positively selected with the corresponding drug. Alternatively, to the *glmS* inducible knockdown system, fusion of a FKBP destabilization domain (ddFKBP) to the N- or C-terminus allows destabilization of a protein of interest in the absence of the stabilizing Shield-1 ligand (Armstrong & Goldberg, 2007). We used this approach with SMC1, where sequences encoding a 3HA tag followed by the ddFKBP, a skip peptide, and the yDHODH resistance marker were inserted at the 3′ end of the corresponding gene (SMC1-3HA-ddFKBP) (Fig.1A). PCR followed by sequencing confirmed the correct integration of the construct (Fig. 1B).

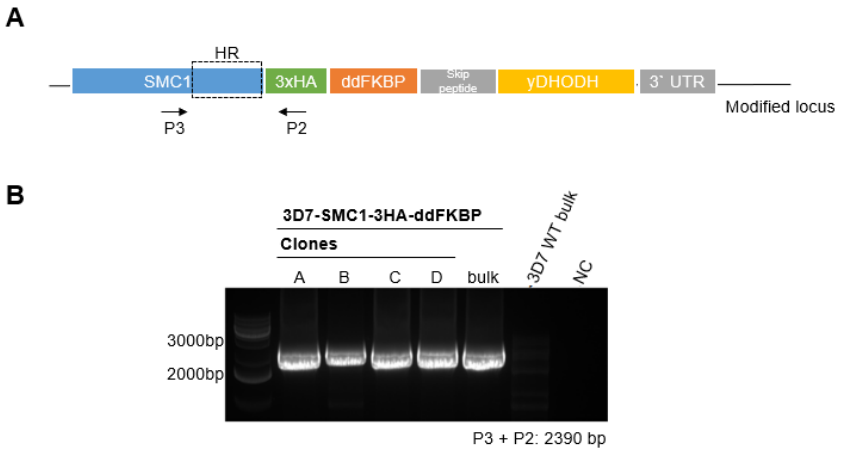

Figure A1. Generation of a strain for conditional knockdown of SMC1. A. Schematics of Selection-linked integration (SLI) strategy with integration of the 3HA tag and the FKBP destabilization domain

(ddFKBP) at SMC1 C-terminus. The yeast dihydroorotate Dehydrogenase (yDHODH) is only expressed after single crossover integration into the target locus allowing positive selection of the transgenic parasites upon addition of a molecule inhibited by yDHODH - DSM1.The presence of a ddFKBP domain allows to modulate SMC1-3HA protein levels. Fusion of the ddFKBP to SMC1-3HA dramatically interferes with the fused protein stability leading to rapid degradation in the proteasome. However, addition of a rapamycin-derived ligand (Shield-1), which causes ddFKBP to fold, results in the blockage of protein degradation. **B.** PCR analysis of gDNA from the parasite lines indicated above each gel. Primers used are as indicated below the gel and annealing sites are defined in (A). M, Molecular weight marker. NC, Negative Control.

To study the function of Rad21 we used the SLI strategy to add a green fluorescent protein (GFP) tag flanked on both sides by two FK506 binding protein (FKBP) domains to the C terminus of the endogenous *Rad21* gene (Rad21-GFP-sandwich) (Fig.2A). This system uses a knock sideways approach based on the ligand-induced dimerization of the FKBP domains fused to Rad21 and an FKBP-rapamycin binding protein (FRB), separately expressed and fused to a mislocalizer, anchored to the parasite plasma membrane (PPM) (Birnbaum et al., 2017). PCR followed by sequencing confirmed the integration of the construct (Fig.2B).

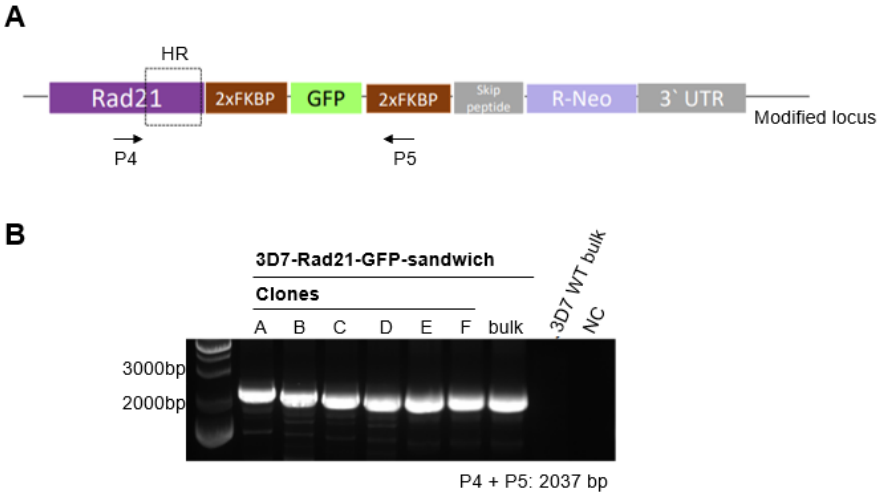

Figure A2. Generation of a strain for conditional knockdown of Rad21. A. Schematics of the selection-linked integration (SLI) strategy with integration of the green fluorescent protein (GFP) tag flanked either side by two FK506 binding protein (FKBP) domains at Rad21 C-terminus. **B.** PCR analysis of gDNA from the parasite lines indicated above each gel. Primers used are as indicated below the gel and annealing sites are defined in (A). M, Molecular weight marker. NC, Negative Control.

SMC1-3HA and Rad21-GFP localize to a perinuclear focus

Live cell imaging of Rad21-GFP-sandwich parasites (Fig.3A) and characterization of SMC1-3HA subcellular localization using IFA (Fig. 3B) revealed a perinuclear focus in trophozoite and schizont stages, similarly to those previously observed for SMC3-3HA.

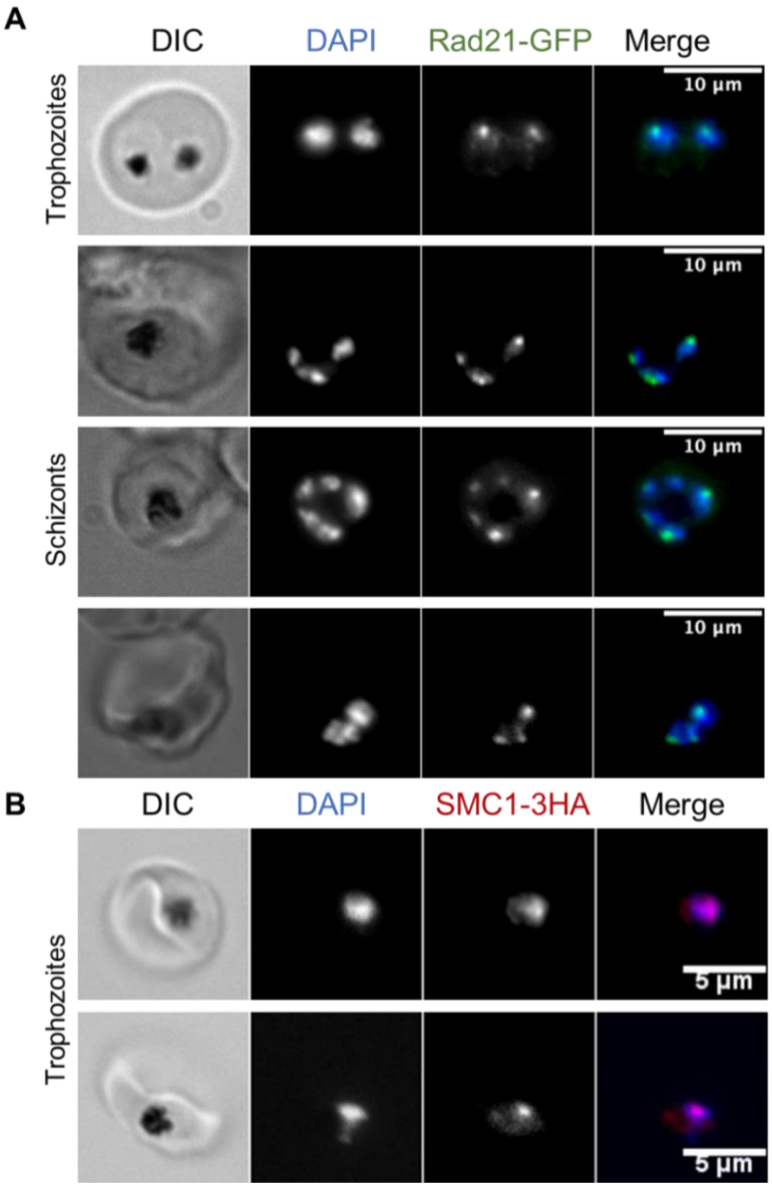

Figure A3. Live cell imaging and immunofluorescence assay show that cohesin subunits Rad21 and SMC1 localizes to a focus in the perinuclear periphery. (A) Live cell imaging of red blood cells (RBC) infected with trophozoite and schizont stages of Rad21-GFP-sandwich parasites. Scale bar, 10 µm. **(B)** Immunofluorescence analysis of fixed RBC infected with trophozoite stages of SMC1-3HA-ddFKBP parasites. DNA was stained with DAPI (blue), and SMC1-3HA-FKBP was detected with an anti-HA (red) antibody. Scale bars equal 10 µm (**A**) and 5 µm (**B**).

Material and Methods

Generation of strains

The SMC1-3HA-ddFKBP and Rad21-GFP-sandwich strains were generated using the method of selection-linked integration (SLI), previously described in (Birnbaum et al., 2017). For generation of SMC1-3HA-ddFKBP and Rad2-GFP-sandwich, an 894 bp and 672 bp fragment of the 3' coding sequence of the respective genes (excluding the STOP codon), flanked by 15 bp for InFusion cloning, was amplified from 3D7 genomic DNA using primer pairs P6/P7 and P8/P9, respectively. SMC1 was cloned into the NotI and AvrII sites of a plasmid containing the sequences encoding a 3HA epitope tag and a ligand-regulatable ddFKBP domain (Armstrong & Goldberg, 2007), followed by a skip peptide and the ubiquinone-independent dihydroorotate dehydrogenase (yDHODH) resistance marker (pSLI-SMC1-3HA-ddFKBP). Rad21 was cloned into the into the NotI and AvrII sites of the pSLI-sandwich (Addgene plasmid 85790) (pSLI-Rad21-GFP-sandwich) (Birnbaum et al., 2017).

A 3D7 wild-type bulk ring stage culture was transfected with 50 µg of either pSLI-SMC1-3HA-ddFKBP or pSLI-Rad21-GFP-sandwich. After, both were initially selected with 2.67 nM WR99210 (Jacobus Pharmaceuticals) until parasites reappeared, which occurred ~ 3 and ~ 5 weeks after transfection for SMC1-3HA-ddFKBP and Rad21-GFP-sandwich, respectively. SMC1-3HA-ddFKBP parasites were selected for integration via the addition 0.75 µM DSM1 (MR4/BEI Resources) and since the transfection were always kept with Shield-1 (Aoubious INC) at 500 nM. For Rad21-GFP-sandwich parasites, 400 µg/ml of G418 was added to the culture to select for integrants. After the second drug selection, gDNA of each integration cell line was collected using a commercial kit (DNeasy Blood & Tissue Kit) and checked by PCR to show that integration occurred at the correct

locus. From the bulk culture, clonal parasite populations were obtained by limited dilution and analysed for correct integration by PCR and sequencing.

Live cell imaging, immunofluorescence assays and image acquisition

For live cell imaging, 20 µl of iRBC were resuspended in PBS with DAPI (FluoProbes FP-CJF800, 1 µg/mL) for 20 min followed by two washes with PBS before mounting. Unattached cells were washed out with PBS and finally covered with culture medium prepared with phenol red free RPMI 1640 (PAN BIOTECH P04-16515). Immunofluorescence assays and image acquisition were performed as described in section 2.3.5.

APPENDIX B

Optimization of an Hi-C protocol

Anticipating the need to perform Hi-C to determine if knockdown of *Pf*SMC3 results in alterations in chromatin contacts (e.g. in loop domain formation), we begun to optimize the Hi-C protocol in *P. falciparum* to obtain the highest resolution level possible on for a DNA-DNA contact map. With the Arima Hi-C Kit, parasites are cross-linked, and the cross-linked chromatin is digested using a restriction enzyme cocktail. The 5' overhangs are filled in with a biotinylated nucleotide, and digested DNA ends in close proximity to one another are ligated. The proximally ligated DNA is then purified, fragmented, and enriched with streptavidin beads.

After library preparation, next generation sequencing, and analysis of the data, a Hi-C contact map can be produced. For our analysis, we used the NF54 clone A11, which stably expresses a central *var* gene, PF3D7_1240900 (Bryant et al., 2018). As such, is also an attractive model for investigating DNA-DNA interactions associated with clustering of the repressed var genes and potential loop formation with the active var gene. After optimizing the number of parasites to put into the kit protocol, we generated a genome-wide contact map. The obtained genome-wide contact map showed the strong cis interactions along the lengths of each chromosome (Figure B1.B), however it was unsuccessful to demonstrate two major hallmarks of inter-chromosomal interactions in *P. falciparum*: the close association between telomeres and chromosome internal *var* genes which associate in heterochromatin clusters at the perinuclear periphery and the interactions between regions of chromosomes 5 and 7 containing A-type rDNA loci observed in previous studies (Ay et al., 2014; Bunnik et al., 2018).

One of Hi-C caveats is that the use of restriction enzymes can result in an uneven genome digestion and a consequent low-resolution map of DNA-DNA interactions. Recently, Micro-C, has emerged as a technique that can detect genome-wide contacts at high resolution (T. H. S. Hsieh et al., 2020). This protocol uses MNase digestion which can generate even fragmentation of the genome at the nucleosome level (~ 150 bp) and a higher resolution genome-wide map of DNA contacts then with Hi-C.

In the future, the adaptation of Micro-C to resolve genome-wide DNA contacts, especially in the presence and absence of *Pf*SMC3 can potentially unveil how spatio-temporal regulation of gene transcription is achieved in *P. falciparum*.

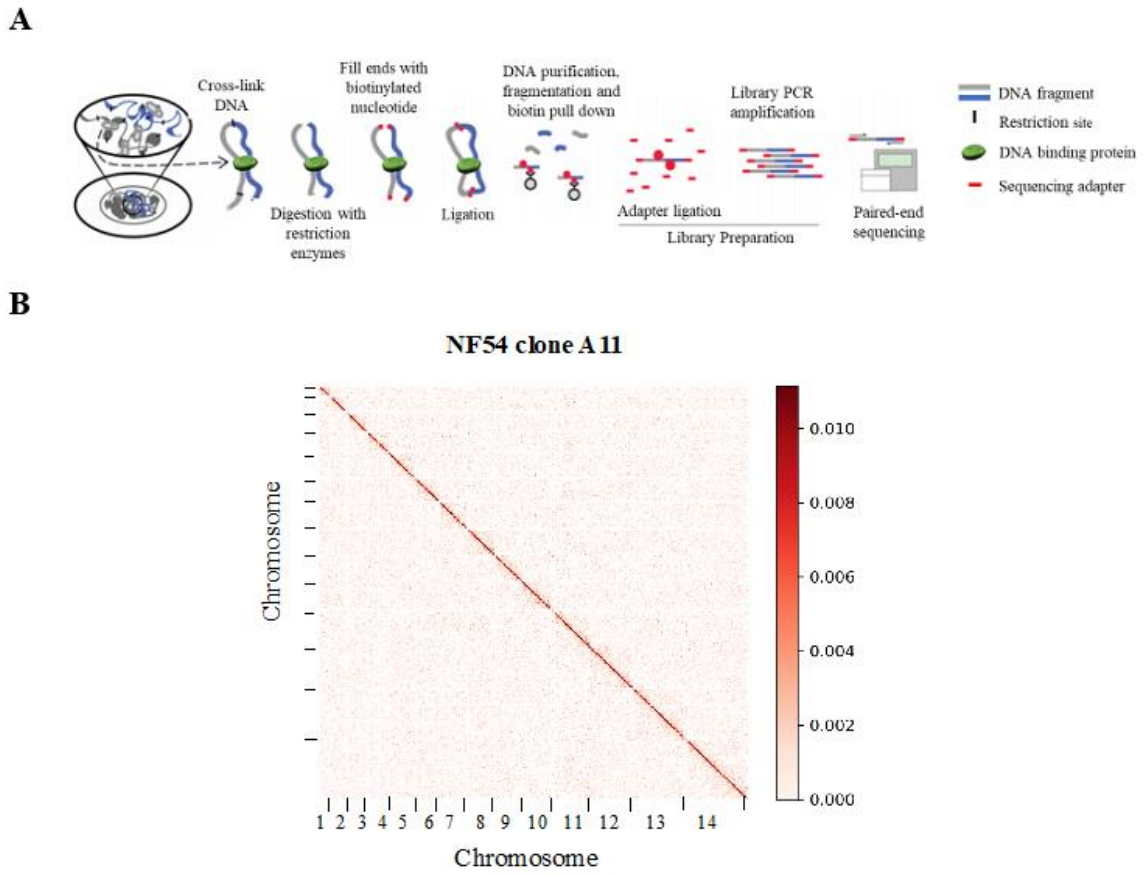

Figure B1. Hi-C protocol optimization in a *P. falciparum* NF54 clonal population. (A) Schematic of the Hi-C workflow. (B) Genome-wide DNA-DNA interaction matrix for all the 14 chromosomes constructed using the DpnII and HinfI restriction enzymes in the NF54 clone A11. Likelihood of DNA interaction increases with intensity of red color (scale shown at right).

Material and Methods

An NF54 clone – A11 – was tightly synchronized and harvested at 12 hpi. $4x10^9$ parasites were crosslinked in one of two ways: 1) they were cross-linked and saponin lysed as in the ChIP protocol ("fixed-lysed") or 2) they were lysed with saponin and then cross-linked ("lysed-fixed"). The estimation of DNA input from a serial dilution of cross-linked parasites ($1x10^6$, $1x10^7$ and $1x10^8$) and the Hi-C protocol were carried out using Arima-HiC Kit (Arima Genomics, San Diego, CA). For library preparation, the KAPA Hyper Prep Kit was used following Arima-HiC kit instructions. The *hicstuff* pipeline was used to generate the genome-wide DNA-DNA interaction matrix (Matthey-Doret et al., 2020).

REFERENCES

Amaratunga, C., Lim, P., Suon, S., Sreng, S., Mao, S., Sopha, C., Sam, B., Dek, D., Try, V., Amato, R., Blessborn, D., Song, L., Tullo, G. S., Fay, M. P., Anderson, J. M., Tarning, J., & Fairhurst, R. M. (2016). Dihydroartemisinin-piperaquine resistance in Plasmodium falciparum malaria in Cambodia: A multisite prospective cohort study. *The Lancet Infectious Diseases*, *16*(3), 357–365. https://doi.org/10.1016/S1473-3099(15)00487-9

Anders, S., Pyl, P. T., & Huber, W. (2015). HTSeq--a Python framework to work with high-throughput sequencing data. *Bioinformatics*, *31*(2), 166–169. https://doi.org/10.1093/bioinformatics/btu638

Andrews, K. T., Haque, A., & Jones, M. K. (2012). HDAC inhibitors in parasitic diseases. *Immunology and Cell Biology*, *90*(1), 66–77. https://doi.org/10.1038/icb.2011.97

Ariey, F., Witkowski, B., Amaratunga, C., Beghain, J., Langlois, A. C., Khim, N., Kim, S., Duru, V., Bouchier, C., Ma, L., Lim, P., Leang, R., Duong, S., Sreng, S., Suon, S., Chuor, C. M., Bout, D. M., Ménard, S., Rogers, W. O., Genton, B., … Ménard, D. (2014). A molecular marker of artemisinin-resistant *Plasmodium falciparum* malaria. *Nature*, *505*(7481), 50–55. https://doi.org/10.1038/nature12876

Armstrong, C. M., & Goldberg, D. E. (2007). An FKBP destabilization domain modulates protein levels in *Plasmodium falciparum*. *Nature Methods*, *4*(12), 1007–1009. https://doi.org/10.1038/nmeth1132

Arnot, D. E., Ronander, E., & Bengtsson, D. C. (2011). The progression of the intra-erythrocytic cell cycle of *Plasmodium falciparum* and the role of the centriolar plaques in asynchronous mitotic division during schizogony. *International Journal for Parasitology*, *41*(1), 71–80. https://doi.org/10.1016/j.ijpara.2010.07.012

Ashley, E. A., Dhorda, M., Fairhurst, R. M., Amaratunga, C., Lim, P., Suon, S., Sreng, S., Anderson, J. M., Mao, S., Sam, B., Sopha, C., Chuor, C. M., Nguon, C., Sovannaroth, S., Pukrittayakamee, S., Jittamala, P., Chotivanich, K., Chutasmit, K., Suchatsoonthorn, C., … White, N. J. (2014). Spread of Artemisinin Resistance in *Plasmodium falciparum* Malaria. *New England Journal of Medicine*, *371*(5), 411–423. https://doi.org/10.1056/nejmoa1314981

Asua, V., Conrad, M. D., Aydemir, O., Duvalsaint, M., Legac, J., Duarte, E., Tumwebaze, P., Chin, D. M., Cooper, R. A., Yeka, A., Kamya, M. R., Dorsey, G., Nsobya, S. L., Bailey, J., & Rosenthal, P. J. (2021). Changing Prevalence of Potential Mediators of Aminoquinoline, Antifolate, and Artemisinin Resistance across Uganda. *Journal of Infectious Diseases*, *223*(6), 985–994. https://doi.org/10.1093/infdis/jiaa687

Aurrecoechea, C., Barreto, A., Basenko, E. Y., Brestelli, J., Brunk, B. P., Cade, S., Crouch, K., Doherty, R., Falke, D., Fischer, S., Gajria, B., Harb, O. S., Heiges, M., Hertz-Fowler, C., Hu, S., Iodice, J., Kissinger, J. C., Lawrence, C., Li, W., … Zheng, J. (2017). EuPathDB: The eukaryotic pathogen genomics database resource. *Nucleic Acids Research*, *45*(1), 581–591. https://doi.org/10.1093/nar/gkw1105

Ay, F., Bunnik, E. M., Varoquaux, N., Bol, S. M., Prudhomme, J., Vert, J. P., Noble, W. S., & le Roch, K. G. (2014). Three-dimensional modeling of the *P. falciparum* genome during the erythrocytic cycle reveals a strong connection between genome architecture and gene expression. *Genome Research*, *24*(6), 974–988. https://doi.org/10.1101/gr.169417.113

Balaji, S., Madan Babu, M., Iyer, L. M., & Aravind, L. (2005). Discovery of the principal specific transcription factors of Apicomplexa and their implication for the evolution of the AP2-integrase DNA binding domains. *Nucleic Acids Research*, *33*(13), 3994–4006. https://doi.org/10.1093/nar/gki709

Bannister, L. H., & Dluzewski, A. R. (1990). The ultrastructure of red cell invasion in malaria infections: a review. *Blood cells*, *16*(2-3), 257–297.

Bártfai, R., Hoeijmakers, W. A. M., Salcedo-Amaya, A. M., Smits, A. H., Janssen-Megens, E., Kaan, A., Treeck, M., Gilberger, T. W., Franc ̧oijs, K. J., & Stunnenberg, H. G. (2010). H2A.Z demarcates intergenic regions of the *Plasmodium falciparum* epigenome that are dynamically marked by H3K9ac and H3K4me3. *PLoS Pathogens*, *6*(12). https://doi.org/10.1371/journal.ppat.1001223

Bartoloni, A., & Zammarchi, L. (2012). Clinical aspects of uncomplicated and severe malaria. *Mediterranean journal of hematology and infectious diseases*, *4*(1), e2012026. https://doi.org/10.4084/MJHID.2012.026

Batsios, P., Peter, T., Baumann, O., Stick, R., Meyer, I., & Gräf, R. (2012). A lamin in lower eukaryotes? *Nucleus (Austin, Tex.)*, *3*(3), 237–243. https://doi.org/10.4161/nucl.20149

Batugedara, G., Lu, X. M., Saraf, A., Sardiu, M. E., Cort, A., Abel, S., Prudhomme, J., Washburn, M. P., Florens, L., Bunnik, E. M., & le Roch, K. G. (2020). The chromatin bound proteome of the human malaria parasite. *Microbial Genomics*, *6*(2). https://doi.org/10.1099/mgen.0.000327

Becker, J. S., Nicetto, D., & Zare, K. S. (2016). H3K9me3-Dependent Heterochromatin: Barrier to Cell Fate Changes. *Trends in Genetics*, *32*(1), 29–41. https://doi.org/10.1016/j.physbeh.2017.03.040

Bednar, J., Horowitz, R. A., Grigoryev, S. A., Carruthers, L. M., Hansen, J. C., Koster, A. J., & Woodcock, C. L. (1998). Nucleosomes, linker DNA, and linker histone form a unique structural motif that directs the higher-order folding and compaction of chromatin. *Proceedings of the National Academy of Sciences of the United States of America*, *95*(24), 14173–14178. https://doi.org/10.1073/pnas.95.24.14173

Ben-Shahar, T. R., Heeger, S., Lehane, C., East, P., Flynn, H., Skehel, M., & Uhlmann, F. (2008). Eco1-Dependent Cohesin Acetylation During Establishment of Sister Chromatid Cohesion. *Science*, *321*(5888), 563–566. https://doi.org/10.1126/science.1157774

Berger, S. L., Kouzarides, T., Shiekhattar, R., & Shilatifard, A. (2009). An operational definition of epigenetics. *Genes and Development*, *23*(7), 781–783. https://doi.org/10.1101/gad.1787609

Bersaglieri, C., & Santoro, R. (2019). Genome organization in and around the nucleolus. *Cells*, *8*(6). https://doi.org/10.3390/cells8060579

Birnbaum, J., Flemming, S., Reichard, N., Soares, A. B., Mesén-Ramírez, P., Jonscher, E., Bergmann, B., & Spielmann, T. (2017). A genetic system to study *Plasmodium falciparum* protein function. *Nature Methods*, *14*(4), 450–456. https://doi.org/10.1038/nmeth.4223

Bischoff, E., & Vaquero, C. (2010). In silico and biological survey of transcription-associated proteins implicated in the transcriptional machinery during the erythrocytic

development of *Plasmodium falciparum*. *BMC Genomics*, *11*(1). https://doi.org/10.1186/1471-2164-11-34

Blat, Y., & Kleckner, N. (1999). Cohesins bind to preferential sites along yeast chromosome III, with differential regulation along arms versus the centric region. *Cell*, *98*(2), 249–259. https://doi.org/10.1016/s0092-8674(00)81019-3

Bloom, K. S. (2014). Centromeric Heterochromatin: The Primordial Segregation Machine. *Annual Review of Genetics*, *48*(1), 457–484. https://doi.org/10.1146/annurev-genet-120213-092033

Bozdech, Z., Llinás, M., Pulliam, B. L., Wong, E. D., Zhu, J., & DeRisi, J. L. (2003). The transcriptome of the intraerythrocytic developmental cycle of *Plasmodium falciparum*. *PLoS Biology*, *1*(1). https://doi.org/10.1371/journal.pbio.0000005

Branco, M. R., & Pombo, A. (2007). Chromosome organization: new facts, new models. *Trends in Cell Biology*, *17*(3), 127–134. https://doi.org/10.1016/j.tcb.2006.12.006

Brancucci, N. M. B., Bertschi, N. L., Zhu, L., Niederwieser, I., Chin, W. H., Wampfler, R., Freymond, C., Rottmann, M., Felger, I., Bozdech, Z., & Voss, T. S. (2014). Heterochromatin protein 1 secures survival and transmission of malaria parasites. *Cell Host and Microbe*, *16*(2), 165–176. https://doi.org/10.1016/j.chom.2014.07.004

Bryant, J. M., Baumgarten, S., Dingli, F., Loew, D., Sinha, A., Claës, A., Preiser, P. R., Dedon, P. C., & Scherf, A. (2020). Exploring the virulence gene interactome with CRISPR / dC as9 in the human malaria parasite. *Molecular Systems Biology*, *16*(8), 1–22. https://doi.org/10.15252/msb.20209569

Bryant, J. M., Baumgarten, S., Lorthiois, A., Scheidig-Benatar, C., Claës, A., & Scherf, A. (2018). *De Novo* Genome Assembly of a *Plasmodium falciparum* NF54 Clone Using Single-Molecule Real-Time Sequencing. *Genome announcements*, *6*(5), e01479-17. https://doi.org/10.1128/genomeA.01479-17

Buheitel, J., & Stemmann, O. (2013). Prophase pathway-dependent removal of cohesin from human chromosomes requires opening of the Smc3-Scc1 gate. *The EMBO journal*, *32*(5), 666–676. https://doi.org/10.1038/emboj.2013.7

Bunnik, E. M., Cook, K. B., Varoquaux, N., Batugedara, G., Prudhomme, J., Cort, A., Shi, L., Andolina, C., Ross, L. S., Brady, D., Fidock, D. A., Nosten, F., Tewari, R., Sinnis, P., Ay, F., Vert, J. P., Noble, W. S., & le Roch, K. G. (2018). Changes in genome organization of parasite-specific gene families during the *Plasmodium* transmission stages. *Nature Communications*, *9*(1), 1910. https://doi.org/10.1038/s41467-018-04295-5

Bunnik, E. M., Polishko, A., Prudhomme, J., Ponts, N., Gill, S. S., Lonardi, S., & le Roch, K. G. (2014). DNA-encoded nucleosome occupancy is associated with transcription levels in the human malaria parasite *Plasmodium falciparum*. *BMC Genomics*, *15*(1), 1–15. https://doi.org/10.1186/1471-2164-15-347

Bunnik, E. M., Venkat, A., Shao, J., McGovern, K. E., Batugedara, G., Worth, D., Prudhomme, J., Lapp, S. A., Andolina, C., Ross, L. S., Lawres, L., Brady, D., Sinnis, P., Nosten, F., Fidock, D. A., Wilson, E. H., Tewari, R., Galinski, M. R., ben Mamoun, C., … le Roch, K. G. (2019). Comparative 3D genome organization in apicomplexan parasites. *Proceedings of the National Academy of Sciences*, *116*(8), 3183–3192. https://doi.org/10.1073/pnas.1810815116

Calderón, F., Wilson, D. M., & Gamo, F. J. (2013). Antimalarial drug discovery: recent progress and future directions. *Progress in medicinal chemistry*, *52*, 97–151. https://doi.org/10.1016/B978-0-444-62652-3.00003-X

Campbell, T. L., de Silva, E. K., Olszewski, K. L., Elemento, O., & Llinás, M. (2010). Identification and Genome-Wide Prediction of DNA Binding Specificities for the ApiAP2 family of regulators from the malaria parasite. *PLoS Pathogens*, *6*(10). https://doi.org/10.1371/journal.ppat.1001165

Canudas, S., & Smith, S. (2009). Differential regulation of telomere and centromere cohesion by the Scc3 homologues SA1 and SA2, respectively, in human cells. *Journal of Cell Biology*, *187*(2), 165–173. https://doi.org/10.1083/jcb.200903096

Carmo-Fonseca, M., Mendes-Soares, L., & Campos, I. (2000). To be or not to be in the nucleolus. *Nature cell biology*, *2*(6), 107–112. https://doi.org/10.1038/35014078

Caro, F., Ahyong, V., Betegon, M., & DeRisi, J. L. (2014). Genome-wide regulatory dynamics of translation in the *Plasmodium falciparum* asexual blood stages. *ELife*, *3*, 1–24. https://doi.org/10.7554/elife.04106

Carvalhal, S., Tavares, A., Santos, M. B., Mirkovic, M., & Oliveira, R. A. (2018). A quantitative analysis of cohesin decay in mitotic fidelity. *Journal of Cell Biology*, *217*(10), 3343–3353. https://doi.org/10.1083/JCB.201801111

Chaal, B. K., Gupta, A. P., Wastuwidyaningtyas, B. D., Luah, Y. H., & Bozdech, Z. (2010). Histone deacetylases play a major role in the transcriptional regulation of the *Plasmodium falciparum* life cycle. *PLoS Pathogens*, *6*(1). https://doi.org/10.1371/journal.ppat.1000737

Chereji, R. v., Bharatula, V., Elfving, N., Blomberg, J., Larsson, M., Morozov, A. v., Broach, J. R., & Björklund, S. (2017). Mediator binds to boundaries of chromosomal interaction domains and to proteins involved in DNA looping, RNA metabolism, chromatin remodeling, and actin assembly. *Nucleic Acids Research*, *45*(15), 8806–8821. https://doi.org/10.1093/nar/gkx491

Chien, R., Zeng, W., Kawauchi, S., Bender, M. A., Santos, R., Gregson, H. C., Schmiesing, J. A., Newkirk, D. A., Kong, X., Ball, A. R., Calof, A. L., Lander, A. D., Groudine, M. T., & Yokomori, K. (2011). Cohesin mediates chromatin interactions that regulate mammalian β-globin expression. *Journal of Biological Chemistry*, *286*(20), 17870–17878. https://doi.org/10.1074/jbc.M110.207365

Chuang, C. H., Carpenter, A. E., Fuchsova, B., Johnson, T., de Lanerolle, P., & Belmont, A. S. (2006). Long-Range Directional Movement of an Interphase Chromosome Site. *Current Biology*, *16*(8), 825–831. https://doi.org/10.1016/j.cub.2006.03.059

Clapier, C. R., Iwasa, J., Cairns, B. R., & Peterson, C. L. (2017). Mechanisms of action and regulation of ATP-dependent chromatin-remodelling complexes. *Nature reviews. Molecular cell biology*, *18*(7), 407–422. https://doi.org/10.1038/nrm.2017.26

Coetzee, N., Sidoli, S., van Biljon, R., Painter, H., Llinás, M., Garcia, B. A., & Birkholtz, L. M. (2017). Quantitative chromatin proteomics reveals a dynamic histone post-translational modification landscape that defines asexual and sexual *Plasmodium falciparum* parasites. *Scientific Reports*, *7*(1), 1–12. https://doi.org/10.1038/s41598-017-00687-7

Coleman, B. I., Skillman, K. M., Jiang, R. H. Y., Childs, L. M., Altenhofen, L. M., Ganter, M., Leung, Y., Goldowitz, I., Kafsack, B. F. C., Marti, M., Llinás, M., Buckee, C. O., & Duraisingh, M. T. (2014). A *Plasmodium falciparum* Histone Deacetylase regulates antigenic variation and gametocyte conversion. *Cell Host and Microbe*, *16*(2), 177–186. https://doi.org/10.1016/j.chom.2014.06.014

Collins, C. R., Hackett, F., Strath, M., Penzo, M., Withers-Martinez, C., Baker, D. A., & Blackman, M. J. (2013). Malaria Parasite cGMP-dependent Protein Kinase Regulates Blood Stage Merozoite Secretory Organelle Discharge and Egress. *PLoS Pathogens*, *9*(5). https://doi.org/10.1371/journal.ppat.1003344

Conte, M., Irani, E., Chiariello, A. M., Abraham, A., Bianco, S., Esposito, A., & Nicodemi, M. (2022). Loop-extrusion and polymer phase-separation can co-exist at the single-molecule level to shape chromatin folding. *Nature Communications*, *13*(1). https://doi.org/10.1038/s41467-022-31856-6

Cosgrove, M. S., Boeke, J. D., & Wolberger, C. (2004). Regulated nucleosome mobility and the histone code. *Nature structural & molecular biology*, *11*(11), 1037–1043. https://doi.org/10.1038/nsmb851

Cowman, A. F., Berry, D., & Baum, J. (2012). The cellular and molecular basis for malaria parasite invasion of the human red blood cell. *Journal of Cell Biology*, *198*(6), 961–971. https://doi.org/10.1083/jcb.201206112

Cowman, A. F., & Crabb, B. S. (2006). Invasion of red blood cells by malaria parasites. *Cell*, *124*(4), 755–766. https://doi.org/10.1016/j.cell.2006.02.006

Cowman, A. F., Tonkin, C. J., Tham, W. H., & Duraisingh, M. T. (2017). The Molecular Basis of Erythrocyte Invasion by Malaria Parasites. *Cell Host and Microbe*, *22*(2), 232–245. https://doi.org/10.1016/j.chom.2017.07.003

Cox, F. E. (2010). History of the discovery of the malaria parasites and their vectors. *Parasites & vectors*, *3*(1), 5. https://doi.org/10.1186/1756-3305-3-5

Cui, L., Fan, Q., Cui, L., & Miao, J. (2008). Histone lysine methyltransferases and demethylases in *Plasmodium falciparum*. *International Journal for Parasitology*, *38*(10), 1083–1097. https://doi.org/10.1016/j.ijpara.2008.01.002

Cui, L., & Miao, J. (2010). Chromatin-Mediated epigenetic regulation in the malaria parasite *Plasmodium falciparum*. *Eukaryotic Cell*, *9*(8), 1138–1149. https://doi.org/10.1128/EC.00036-10

Davidson, I. F., Bauer, B., Goetz, D., Tang, W., Wutz, G., & Peters, J. M. (2019). DNA loop extrusion by human cohesin. *Science*, *366*(6471), 1338–1345. https://doi.org/10.1126/science.aaz3418

Deardorff, M. A., Kaur, M., Yaeger, D., Rampuria, A., Korolev, S., Pie, J., Gil-Rodríguez, C., Arnedo, M., Loeys, B., Kline, A. D., Wilson, M., Lillquist, K., Siu, V., Ramos, F. J., Musio, A., Jackson, L. S., Dorsett, D., & Krantz, I. D. (2007). Mutations in cohesin complex members SMC3 and SMC1A cause a mild variant of cornelia de Lange syndrome with predominant mental retardation. *American journal of human genetics*, *80*(3), 485–494. https://doi.org/10.1086/511888

de Monerri, N. C. S., Flynn, H. R., Campos, M. G., Hackett, F., Koussis, K., Withers-Martinez, C., Skehel, J. M., & Blackman, M. J. (2011). Global identification of multiple substrates for *Plasmodium falciparum* SUB1, an essential malarial processing protease. *Infection and Immunity*, *79*(3), 1086–1097. https://doi.org/10.1128/IAI.00902-10

de Silva, E. K., Gehrke, A. R., Olszewski, K., León, I., Chahal, J. S., Bulyk, M. L., & Llinás, M. (2008). Specific DNA-binding by Apicomplexan AP2 transcription factors. *Proceedings of the National Academy of Sciences of the United States of America*, *105*(24), 8393–8398. https://doi.org/10.1073/pnas.0801993105

Deitsch, K. W., & Dzikowski, R. (2017). Variant Gene Expression and Antigenic Variation by Malaria Parasites. *Annual Review of Microbiology*, *71*(1), 625–641. https://doi.org/10.1146/annurev-micro-090816-093841

Deitsch, K. W., Lukehart, S. A., & Stringer, J. R. (2009). Common strategies for antigenic variation by bacterial, fungal and protozoan pathogens. *Nature reviews. Microbiology*, *7*(7), 493–503. https://doi.org/10.1038/nrmicro2145

Dekker, J., Rippe, K., Dekker, M., & Kleckner, N. (2002). Capturing chromosome conformation. *Science*, *295*(5558), 1306–1311. https://doi.org/10.1126/science.1067799

Deng, W., Lee, J., Wang, H., Miller, J., Reik, A., Gregory, P. D., Dean, A., & Blobel, G. A. (2012). Controlling long-range genomic interactions at a native locus by targeted tethering of a looping factor. *Cell*, *149*(6), 1233–1244. https://doi.org/10.1016/j.cell.2012.03.051

Dixon, J. R., Selvaraj, S., Yue, F., Kim, A., Li, Y., Shen, Y., Hu, M., Liu, J. S., & Ren, B. (2012). Topological domains in mammalian genomes identified by analysis of chromatin interactions. *Nature*, *485*(7398), 376–380. https://doi.org/10.1038/nature11082

Doerig, C., Rayner, J. C., Scherf, A., & Tobin, A. B. (2015). Post-translational protein modifications in malaria parasites. *Nature Reviews Microbiology*, *13*(3), 160–172. https://doi.org/10.1038/nrmicro3402

Dondorp, A. M., Nosten, F., Yi, P., Das, D., Phyo, A. P., Tarning, J., Lwin, K. M., Ariey, F., Hanpithakpong, W., Lee, S. J., Ringwald, P., Silamut, K., Imwong, M., Chotivanich, K., Lim, P., Herdman, T., An, S. S., Yeung, S., Singhasivanon, P., … White, N. J. (2009). Artemisinin Resistance in *Plasmodium falciparum* Malaria. *New England Journal of Medicine*, *361*(5), 455–467. https://doi.org/10.1056/nejmoa0808859

Dowen, J. M., Fan, Z. P., Hnisz, D., Ren, G., Abraham, B. J., Zhang, L. N., Weintraub, A. S., Schuijers, J., Lee, T. I., Zhao, K., & Young, R. A. (2014). Control of cell identity genes occurs in insulated neighborhoods in mammalian chromosomes. *Cell*, *159*(2), 374–387. https://doi.org/10.1016/j.cell.2014.09.030

Duraisingh, M. T., & Skillman, K. M. (2018). Epigenetic Variation and Regulation in Malaria Parasites. *Annual review of microbiology*, *72*, 355–375. https://doi.org/10.1146/annurev-micro-090817-062722

Duraisingh, M. T., Voss, T. S., Marty, A. J., Duffy, M. F., Good, R. T., Thompson, J. K., Freitas, L. H., Scherf, A., Crabb, B. S., & Cowman, A. F. (2005). Heterochromatin silencing and locus repositioning linked to regulation of virulence genes in *Plasmodium falciparum*. *Cell*, *121*(1), 13–24. https://doi.org/10.1016/j.cell.2005.01.036

Eichinger, C. S., Kurze, A., Oliveira, R. A., & Nasmyth, K. (2013). Disengaging the Smc3/kleisin interface releases cohesin from *Drosophila* chromosomes during interphase and mitosis. *EMBO Journal*, *32*(5), 656–665. https://doi.org/10.1038/emboj.2012.346

Fang, J., & McCutchan, T. F. (2002). Thermoregulation in a parasite's life cycle. *Nature*, *418*(6899), 742. https://doi.org/10.1038/418742a

Faure, A. J., Schmidt, D., Watt, S., Schwalie, P. C., Wilson, M. D., Xu, H., Ramsay, R. G., Odom, D. T., & Flicek, P. (2012). Cohesin regulates tissue-specific expression by stabilizing highly occupied cis-regulatory modules. *Genome Research*, *22*(11), 2163–2175. https://doi.org/10.1101/gr.136507.111

Fay, A., Misulovin, Z., Li, J., Schaaf, C. A., Gause, M., Gilmour, D. S., & Dorsett, D. (2011). Cohesin selectively binds and regulates genes with paused RNA polymerase. *Current Biology*, *21*(19), 1624–1634. https://doi.org/10.1016/j.cub.2011.08.036

Figueiredo, L. M., Freitas-Junior, L. H., Bottius, E., Olivo-Marin, J. C., & Scherf, A. (2002). A central role for *Plasmodium falciparum* subtelomeric regions in spatial positioning and telomere length regulation. *EMBO Journal*, *21*(4), 815–824. https://doi.org/10.1093/emboj/21.4.815

Figueiredo, L. M., Rocha, E. P. C., Mancio-Silva, L., Prevost, C., Hernandez-Verdun, D., & Scherf, A. (2005). The unusually large *Plasmodium* telomerase reverse-transcriptase localizes in a discrete compartment associated with the nucleolus. *Nucleic Acids Research*, *33*(3), 1111–1122. https://doi.org/10.1093/nar/gki260

Filarsky, M., Fraschka, S. A., Niederwieser, I., Brancucci, N. M. B., Carrington, E., Carrió, E., Moes, S., Jenoe, P., Bártfai, R., & Voss, T. S. (2018). GDV1 induces sexual commitment of malaria parasites by antagonizing HP1-dependent gene silencing. *Science*, *359*(6381), 1259–1263. https://doi.org/10.1126/science.aan6042

Flueck, C., Bartfai, R., Niederwieser, I., Witmer, K., Alako, B. T. F., Moes, S., Bozdech, Z., Jenoe, P., Stunnenberg, H. G., & Voss, T. S. (2010). A major role for the *Plasmodium falciparum* ApiAP2 protein *Pf*SIP2 in chromosome end biology. *PLoS Pathogens*, *6*(2). https://doi.org/10.1371/journal.ppat.1000784

Flueck, C., Bartfai, R., Volz, J., Niederwieser, I., Salcedo-Amaya, A. M., Alako, B. T. F., Ehlgen, F., Ralph, S. A., Cowman, A. F., Bozdech, Z., Stunnenberg, H. G., & Voss, T. S. (2009). *Plasmodium falciparum* heterochromatin protein 1 marks genomic loci linked to phenotypic variation of exported virulence factors. *PLoS Pathogens*, *5*(9). https://doi.org/10.1371/journal.ppat.1000569

Francia, M. E., & Striepen, B. (2014). Cell division in apicomplexan parasites. *Nature Reviews. Microbiology*, *12*(2), 125–136. https://doi.org/10.1038/nrmicro3184

Fraschka, S. A., Filarsky, M., Hoo, R., Niederwieser, I., Yam, X. Y., Brancucci, N. M. B., Mohring, F., Mushunje, A. T., Huang, X., Christensen, P. R., Nosten, F., Bozdech, Z., Russell, B., Moon, R. W., Marti, M., Preiser, P. R., Bártfai, R., & Voss, T. S. (2018). Comparative Heterochromatin Profiling Reveals Conserved and Unique Epigenome Signatures Linked to Adaptation and Development of Malaria Parasites. *Cell Host and Microbe*, *23*(3), 407-420.e8. https://doi.org/10.1016/j.chom.2018.01.008

Fraschka, S. A., Henderson, R. W., & Bártfai, R. (2016). H3.3 demarcates GC-rich coding and subtelomeric regions and serves as potential memory mark for virulence gene expression in *Plasmodium falciparum*. *Scientific reports*, *6*, 31965. https://doi.org/10.1038/srep31965

Freitas, L. H., Hernandez-Rivas, R., Ralph, S. A., Montiel-Condado, D., Ruvalcaba-Salazar, O. K., Rojas-Meza, A. P., Mâncio-Silva, L., Leal-Silvestre, R. J., Gontijo, A. M., Shorte, S., & Scherf, A. (2005). Telomeric heterochromatin propagation and histone acetylation control mutually exclusive expression of antigenic variation genes in malaria parasites. *Cell*, *121*(1), 25–36. https://doi.org/10.1016/j.cell.2005.01.037

Freitas-Junior, L. H., Bottius, E., Pirrit, L. A., Deitsch, K. W., Scheidig, C., Guinet, F., Nehrbass, U., Wellems, T. E., & Scherf, A. (2000). Frequent ectopic recombination of virulence factor genes in telomeric chromosome clusters of *P. falciparum*. *Nature*, *407*(6807), 1018–1022. https://doi.org/10.1038/35039531

Ganter, M., Goldberg, J. M., Dvorin, J. D., Paulo, J. A., King, J. G., Tripathi, A. K., Paul, A. S., Yang, J., Coppens, I., Jiang, R. H. Y., Elsworth, B., Baker, D. A., Dinglasan, R. R., Gygi, S. P., & Duraisingh, M. T. (2017). *Plasmodium falciparum* CRK4 directs continuous rounds of DNA replication during schizogony. *Nature Microbiology*, *2*. https://doi.org/10.1038/nmicrobiol.2017.17

Gardner, M. J., Hall, N., Fung, E., White, O., Berriman, M., Hyman, R. W., Carlton, J. M., Pain, A., Nelson, K. E., Bowman, S., Paulsen, I. T., James, K., Eisen, J. A., Rutherford, K., Salzberg, S. L., Craig, A., Kyes, S., Chan, M.-S., Nene, V., … Barrell, B. (2002). Genome sequence of the human malaria parasite *Plasmodium falciparum*. *Nature*, *419*(6906), 498–511. https://doi.org/10.1038/nature01097

Garg, S., Agarwal, S., Kumar, S., Shams Yazdani, S., Chitnis, C. E., & Singh, S. (2013). Calcium-dependent permeabilization of erythrocytes by a perforin-like protein during egress of malaria parasites. *Nature Communications*, *4*, *1736*. https://doi.org/10.1038/ncomms2725

Gerald, N., Mahajan, B., & Kumar, S. (2011). Mitosis in the human malaria parasite *Plasmodium falciparum*. *Eukaryotic Cell*, *10*(4), 474–482. https://doi.org/10.1128/EC.00314-10

Gerlich, D., Koch, B., Dupeux, F., Peters, J. M., & Ellenberg, J. (2006). Live-Cell Imaging Reveals a Stable Cohesin-Chromatin Interaction after but Not before DNA Replication. *Current Biology*, *16*(15), 1571–1578. https://doi.org/10.1016/j.cub.2006.06.068

Ghorbal, M., Gorman, M., MacPherson, C. R., Martins, R. M., Scherf, A., & Lopez-Rubio, J. J. (2014). Genome editing in the human malaria parasite *Plasmodium falciparum* using the CRISPR-Cas9 system. *Nature Biotechnology*, *32*(8), 819–821. https://doi.org/10.1038/nbt.2925

Gilson, P. R., & Crabb, B. S. (2009). Morphology and kinetics of the three distinct phases of red blood cell invasion by *Plasmodium falciparum* merozoites. *International Journal for Parasitology*, *39*(1), 91–96. https://doi.org/10.1016/j.ijpara.2008.09.007

Gligoris, T. G., Scheinost, J. C., Bürmann, F., Petela, N., Chan, K. L., Uluocak, P., Beckouët, F., Gruber, S., Nasmyth, K., & Löwe, J. (2014). Closing the cohesin ring: Structure and function of its Smc3-kleisin interface. *Science*, *346*(6212), 963–967. https://doi.org/10.1126/science.1256917

Glynn, E. F., Megee, P. C., Yu, H. G., Mistrot, C., Unal, E., Koshland, D. E., DeRisi, J. L., & Gerton, J. L. (2004). Genome-wide mapping of the cohesin complex in the yeast *Saccharomyces cerevisiae*. *PLoS Biology*, *2*(9). https://doi.org/10.1371/journal.pbio.0020259

Greenwood, D. (1992). The quinine connection. *The Journal of antimicrobial chemotherapy*, *30*(4), 417–427. https://doi.org/10.1093/jac/30.4.417

Gruber, S., Haering, C. H., & Nasmyth, K. (2003). Chromosomal cohesin forms a ring. *Cell*, *112*(6), 765–777. https://doi.org/10.1016/s0092-8674(03)00162-4

Guacci, V., Koshland, D., & Strunnikov, A. (1997). A direct link between sister chromatid cohesion and chromosome condensation revealed through the analysis of MCD1 in *S. cerevisiae*. *Cell*, *91*(1), 47–57. https://doi.org/10.1016/s0092-8674(01)80008-8

Guizetti, J., & Scherf, A. (2013). Silence, activate, poise and switch! Mechanisms of antigenic variation in *Plasmodium falciparum*. *Cellular Microbiology*, *15*(5), 718–726. https://doi.org/10.1111/cmi.12115

Guo, Y., Monahan, K., Wu, H., Gertz, J., Varley, K. E., Li, W., Myers, R. M., Maniatis, T., & Wu, Q. (2012). CTCF/cohesin-mediated DNA looping is required for protocadherin α promoter choice. *Proceedings of the National Academy of Sciences of the United States of America*, *109*(51), 21081–21086. https://doi.org/10.1073/pnas.1219280110

Gupta, A. P., Chin, W. H., Zhu, L., Mok, S., Luah, Y. H., Lim, E. H., & Bozdech, Z. (2013). Dynamic Epigenetic Regulation of Gene Expression during the Life Cycle of Malaria Parasite *Plasmodium falciparum*. *PLoS Pathogens*, *9*(2). https://doi.org/10.1371/journal.ppat.1003170

Haarhuis, J. H. I., van der Weide, R. H., Blomen, V. A., Yáñez-Cuna, J. O., Amendola, M., van Ruiten, M. S., Krijger, P. H. L., Teunissen, H., Medema, R. H., van Steensel, B., Brummelkamp, T. R., de Wit, E., & Rowland, B. D. (2017). The Cohesin Release Factor WAPL Restricts Chromatin Loop Extension. *Cell*, *169*(4), 693-707.e14. https://doi.org/10.1016/j.cell.2017.04.013

Haase, S., Cabrera, A., Langer, C., Treeck, M., Struck, N., Herrmann, S., Jansen, P. W., Bruchhaus, I., Bachmann, A., Dias, S., Cowman, A. F., Stunnenberg, H. G., Spielmann, T., & Gilberger, T. W. (2008). Characterization of a conserved rhoptry-associated leucine zipper-like protein in the malaria parasite *Plasmodium falciparum*. *Infection and Immunity*, *76*(3), 879–887. https://doi.org/10.1128/IAI.00144-07

Haering, C. H., Farcas, A. M., Arumugam, P., Metson, J., & Nasmyth, K. (2008). The cohesin ring concatenates sister DNA molecules. *Nature*, *454*(7202), 297–301. https://doi.org/10.1038/nature07098

Haering, C. H., & Nasmyth, K. (2003). Building and breaking bridges between sister chromatids. *BioEssays: news and reviews in molecular, cellular and developmental biology*, *25*(12), 1178–1191. https://doi.org/10.1002/bies.10361

Haering, C. H., Löwe, J., Hochwagen, A., & Nasmyth, K. (2002). Molecular architecture of SMC proteins and the yeast cohesin complex. *Molecular cell*, *9*(4), 773–788. https://doi.org/10.1016/s1097-2765(02)00515-4

Haering, C. H., Schoffnegger, D., Nishino, T., Helmhart, W., Nasmyth, K., & Löwe, J. (2004). Structure and stability of cohesin's Smc1-kleisin interaction. *Molecular cell*, *15*(6), 951–964. https://doi.org/10.1016/j.molcel.2004.08.030

Hahn, S., & Young, E. T. (2011). Transcriptional regulation in *Saccharomyces cerevisiae*: Transcription factor regulation and function, mechanisms of initiation, and roles of activators and coactivators. *Genetics*, *189*(3), 705–736. https://doi.org/10.1534/genetics.111.127019

Haldar, K., Bhattacharjee, S., & Safeukui, I. (2018). Drug resistance in *Plasmodium*. *Nature Reviews. Microbiology*, *16*(3), 156–170. https://doi.org/10.1038/nrmicro.2017.161

Hauf, S., Roitinger, E., Koch, B., Dittrich, C. M., Mechtler, K., & Peters, J. M. (2005). Dissociation of cohesin from chromosome arms and loss of arm cohesion during early mitosis depends on phosphorylation of SA2. *PLoS Biology*, *3*(3), 0419–0432. https://doi.org/10.1371/journal.pbio.0030069

Heger, P., Marin, B., Bartkuhn, M., Schierenberg, E., & Wiehe, T. (2012). The chromatin insulator CTCF and the emergence of metazoan diversity. *Proceedings of the National Academy of Sciences of the United States of America*, *109*(43), 17507–17512. https://doi.org/10.1073/pnas.1111941109

Heidinger-Pauli, J. M., Mert, O., Davenport, C., Guacci, V., & Koshland, D. (2010). Systematic reduction of cohesin differentially affects chromosome segregation,

condensation, and DNA repair. *Current biology: CB*, *20*(10), 957–963. https://doi.org/10.1016/j.cub.2010.04.018

Herrera-Solorio, A. M., Vembar, S. S., MacPherson, C. R., Lozano-Amado, D., Meza, G. R., Xoconostle-Cazares, B., Martins, R. M., Chen, P., Vargas, M., Scherf, A., & Hernández-Rivas, R. (2019). Clipped histone H3 is integrated into nucleosomes of DNA replication genes in the human malaria parasite *Plasmodium falciparum*. *EMBO reports*, *20*(4), e46331. https://doi.org/10.15252/embr.201846331

Hillier, C., Pardo, M., Yu, L., Bushell, E., Sanderson, T., Metcalf, T., Herd, C., Anar, B., Rayner, J. C., Billker, O., & Choudhary, J. S. (2019). Landscape of the *Plasmodium* Interactome Reveals Both Conserved and Species-Specific Functionality. *Cell Reports*, *28*(6), 1635-1647.e5. https://doi.org/10.1016/j.celrep.2019.07.019

Hoeijmakers, W. A. M., Flueck, C., Françoijs, K. J., Smits, A. H., Wetzel, J., Volz, J. C., Cowman, A. F., Voss, T., Stunnenberg, H. G., & Bártfai, R. (2012). *Plasmodium falciparum* centromeres display a unique epigenetic makeup and cluster prior to and during schizogony. *Cellular Microbiology*, *14*(9), 1391–1401. https://doi.org/10.1111/j.1462-5822.2012.01803.x

Hoeijmakers, W. A. M., Salcedo-Amaya, A. M., Smits, A. H., Françoijs, K. J., Treeck, M., Gilberger, T. W., Stunnenberg, H. G., & Bártfai, R. (2013). H2A.Z/H2B.Z double-variant nucleosomes inhabit the AT-rich promoter regions of the *Plasmodium falciparum* genome. *Molecular Microbiology*, *87*(5), 1061–1073. https://doi.org/10.1111/mmi.12151

Holzmann, J., Politi, A. Z., Nagasaka, K., Hantsche-Grininger, M., Walther, N., Koch, B., Fuchs, J., Dürnberger, G., Tang, W., Ladurner, R., Stocsits, R. R., Busslinger, G. A., Novák, B., Mechtler, K., Davidson, I. F., Ellenberg, J., & Peters, J. M. (2019). Absolute quantification of Cohesin, CTCF and their regulators in human cells. *ELife*, *8*. https://doi.org/10.7554/eLife.46269.001

Horrocks, P., Wong, E., Russell, K., & Emes, R. D. (2009). Control of gene expression in *Plasmodium falciparum* - Ten years on. *Molecular and Biochemical Parasitology*, *164*(1), 9–25. https://doi.org/10.1016/j.molbiopara.2008.11.010

Horsfield, J. A. (2022). Horsfield J. A. (2022). Full circle: a brief history of cohesin and the regulation of gene expression. *The FEBS journal*, 10.1111/febs.16362. https://doi.org/10.1111/febs.16362

Hsieh, F. L., Turner, L., Bolla, J. R., Robinson, C. V., Lavstsen, T., & Higgins, M. K. (2016). The structural basis for CD36 binding by the malaria parasite. *Nature communications*, *7*, 12837. https://doi.org/10.1038/ncomms12837

Hsieh, T. H. S., Cattoglio, C., Slobodyanyuk, E., Hansen, A. S., Rando, O. J., Tjian, R., & Darzacq, X. (2020). Resolving the 3D Landscape of Transcription-Linked Mammalian Chromatin Folding. *Molecular Cell*, *78*(3), 539-553.e8. https://doi.org/10.1016/j.molcel.2020.03.002

Hu, B., Itoh, T., Mishra, A., Katoh, Y., Chan, K. L., Upcher, W., Godlee, C., Roig, M. B., Shirahige, K., & Nasmyth, K. (2011). ATP hydrolysis is required for relocating cohesin from sites occupied by its Scc2/4 loading complex. *Current Biology*, *21*(1), 12–24. https://doi.org/10.1016/j.cub.2010.12.004

Hu, G., Cabrera, A., Kono, M., Mok, S., Chaal, B. K., Haase, S., Engelberg, K., Cheemadan, S., Spielmann, T., Preiser, P. R., Gilberger, T. W., & Bozdech, Z. (2010). Transcriptional profiling of growth perturbations of the human malaria parasite *Plasmodium falciparum*. *Nature Biotechnology*, *28*(1), 91–98. https://doi.org/10.1038/nbt.1597

Huang, C. E., Milutinovich, M., & Koshland, D. (2005). Rings, bracelet or snaps: Fashionable alternatives for Smc complexes. *Philosophical Transactions of the Royal Society of London. Series B, Biological Sciences*, *360*(1455), 537–542. https://doi.org/10.1098/rstb.2004.1609

Huis in ’t Veld, P., Herzog, F., Ladurner, R., Davidson, I. F., Piric, S., Kreidl, E., Bhaskara, V., Aebersold, R., & Peters, J. M. (2014). Characterization of a DNA exit gate in the human cohesin ring. *Science*, *346*(6212), 968–972. https://doi.org/10.1126/science.1256904

Ivanov, D., & Nasmyth, K. (2005). A topological interaction between cohesin rings and a circular minichromosome. *Cell*, *122*(6), 849–860. https://doi.org/10.1016/j.cell.2005.07.018

Izumi, K., Nakato, R., Zhang, Z., Edmondson, A. C., Noon, S., Dulik, M. C., Rajagopalan, R., Venditti, C. P., Gripp, K., Samanich, J., Zackai, E. H., Deardorff, M. A., Clark, D., Allen, J. L., Dorsett, D., Misulovin, Z., Komata, M., Bando, M., Kaur, M., … Krantz, I. D. (2015). Germline gain-of-function mutations in AFF4 cause a developmental syndrome functionally linking the super elongation complex and cohesin. *Nature Genetics*, *47*(4), 338–344. https://doi.org/10.1038/ng.3229

Jack, J., & DeLotto, Y. (1995). Structure and regulation of a complex locus: the cut gene of *Drosophila*. *Genetics*, *139*(4), 1689–1700. https://doi.org/10.1093/genetics/139.4.1689

Jack, J., Dorsett, D., Delotto, Y., & Liu, S. (1991). Expression of the cut locus in the *Drosophila* wing margin is required for cell type specification and is regulated by a distant enhancer. *Development*, *113*(3), 735–747. https://doi.org/10.1242/dev.113.3.735

Jiang, L., Mu, J., Zhang, Q., Ni, T., Srinivasan, P., Rayavara, K., Yang, W., Turner, L., Lavstsen, T., Theander, T. G., Peng, W., Wei, G., Jing, Q., Wakabayashi, Y., Bansal, A., Luo, Y., Ribeiro, J. M., Scherf, A., Aravind, L., Zhu, J., … Miller, L. H. (2013). PfSETvs methylation of histone H3K36 represses virulence genes in *Plasmodium falciparum*. *Nature*, *499*(7457), 223–227. https://doi.org/10.1038/nature12361

Josling, G. A., & Llinás, M. (2015). Sexual development in *Plasmodium* parasites: Knowing when it's time to commit. *Nature Reviews Microbiology*, *13*(9), 573–587. https://doi.org/10.1038/nrmicro3519

Josling, G. A., Petter, M., Oehring, S. C., Gupta, A. P., Dietz, O., Wilson, D. W., Schubert, T., Längst, G., Gilson, P. R., Crabb, B. S., Moes, S., Jenoe, P., Lim, S. W., Brown, G. v., Bozdech, Z., Voss, T. S., & Duffy, M. F. (2015). A *Plasmodium falciparum* Bromodomain Protein Regulates Invasion Gene Expression. *Cell Host and Microbe*, *17*(6), 741–751. https://doi.org/10.1016/j.chom.2015.05.009

Kagey, M. H., Newman, J. J., Bilodeau, S., Zhan, Y., Orlando, D. A., van Berkum, N. L., Ebmeier, C. C., Goossens, J., Rahl, P. B., Levine, S. S., Taatjes, D. J., Dekker, J., & Young, R. A. (2010). Mediator and cohesin connect gene expression and chromatin architecture. *Nature*, *467*(7314), 430–435. https://doi.org/10.1038/nature09380

Kamakaka, R. T., & Biggins, S. (2005). Histone variants: deviants?. *Genes & development*, *19*(3), 295–310. https://doi.org/10.1101/gad.1272805

Kantele, A., & Jokiranta, T. S. (2011). Review of cases with the emerging fifth human malaria parasite, *Plasmodium knowlesi*. *Clinical Infectious Diseases*, *52*(11), 1356–1362. https://doi.org/10.1093/cid/cir180

Keeley, A., & Soldati, D. (2004). The glideosome: a molecular machine powering motility and host-cell invasion by Apicomplexa. *Trends in Cell Biology*, *14*(10), 528–532. https://doi.org/10.1016/j.tcb.2004.08.002

Kelly, J. M., McRobert, L., & Baker, D. A. (2006). Evidence on the chromosomal location of centromeric DNA in *Plasmodium falciparum* from etoposide-mediated topoisomerase-II cleavage. *Proceedings of the National Academy of Sciences of the United States of America*, *103*(17), 6706–6711. https://doi.org/10.1073/pnas.0510363103

Kempfer, R., & Pombo, A. (2020). Methods for mapping 3D chromosome architecture. *Nature reviews. Genetics*, *21*(4), 207–226. https://doi.org/10.1038/s41576-019-0195-2

Kensche, P. R., Hoeijmakers, W. A. M., Toenhake, C. G., Bras, M., Chappell, L., Berriman, M., & Bártfai, R. (2016). The nucleosome landscape of *Plasmodium falciparum* reveals chromatin architecture and dynamics of regulatory sequences. *Nucleic Acids Research*, *44*(5), 2110–2124. https://doi.org/10.1093/nar/gkv1214

Kim, S., Yu, N. K., & Kaang, B. K. (2015). CTCF as a multifunctional protein in genome regulation and gene expression. *Experimental & molecular medicine*, *47*(6), e166. https://doi.org/10.1038/emm.2015.33

Kim, Y., Shi, Z., Zhang, H., Finkelstein, I. J., & Yu, H. (2019). Human cohesin compacts DNA by loop extrusion. *Science*, *366*(6471), 1345–1349. https://doi.org/10.1126/science.aaz4475

Kitajima, T. S., Kawashima, S. A., & Watanabe, Y. (2004). The conserved kinetochore protein shugoshin protects centromeric cohesion during meiosis. *Nature*, *427*(6974), 510–517. https://doi.org/10.1038/nature02312

Klaus, S., Binder, P., Kim, J., Machado, M., Funaya, C., Schaaf, V., Klaschka, D., Kudulyte, A., Cyrklaff, M., Laketa, V., Höfer, T., Guizetti, J., Becker, N. B., Frischknecht, F., Schwarz, U. S., & Ganter, M. (2022). Asynchronous nuclear cycles in multinucleated *Plasmodium falciparum* facilitate rapid proliferation. *Science advances*, *8*(13), eabj5362. https://doi.org/10.1126/sciadv.abj5362

Kong, X., Ball, A. R., Pham, H. X., Zeng, W., Chen, H.-Y., Schmiesing, J. A., Kim, J.-S., Berns, M., & Yokomori, K. (2014). Distinct Functions of Human Cohesin-SA1 and Cohesin-SA2 in Double-Strand Break Repair. *Molecular and Cellular Biology*, *34*(4), 685–698. https://doi.org/10.1128/mcb.01503-13

Koreny, L., & Field, M. C. (2016). Ancient eukaryotic origin and evolutionary plasticity of nuclear lamina. *Genome Biology and Evolution*, *8*(9), 2663–2671. https://doi.org/10.1093/gbe/evw087

Kornberg, R. D. (2005). Mediator and the mechanism of transcriptional activation. *Trends in biochemical sciences*, *30*(5), 235–239. https://doi.org/10.1016/j.tibs.2005.03.011

Kubo, N., Ishii, H., Xiong, X., Bianco, S., Meitinger, F., Hu, R., Hocker, J. D., Conte, M., Gorkin, D., Yu, M., Li, B., Dixon, J. R., Hu, M., Nicodemi, M., Zhao, H., & Ren, B. (2021). Promoter-proximal CTCF binding promotes distal enhancer-dependent gene activation. *Nature Structural and Molecular Biology*, 28(2), 152–161. https://doi.org/10.1038/s41594-020-00539-5

Langsley, G., Hyde, J. E., Goman, M., & Scaife, J. G. (1983). Cloning and characterization of the rRNA genes from the human malaria parasite *Plasmodium falciparum*. *Nucleic acids research*, *11*(24), 8703–8717. https://doi.org/10.1093/nar/11.24.8703

Lanzer, M., de Bruin, D., & Ravetch, J. V. (1992). Transcription mapping of a 100 kb locus of *Plasmodium falciparum* identifies an intergenic region in which transcription terminates and reinitiates. *The EMBO journal*, *11*(5), 1949–1955. https://doi.org/10.1002/j.1460-2075.1992.tb05248.x

Laugsch, M., Seebach, J., Schnittler, H., & Jessberger, R. (2013). Imbalance of SMC1 and SMC3 Cohesins Causes Specific and Distinct Effects. *PLoS ONE*, *8*(6). https://doi.org/10.1371/journal.pone.0065149

Laveran, A. (1907, December 11). *Alphonse Laveran—Nobel Lecture: Protozoa as Causes of Diseases.* Alphonse Laveran—Nobel Lecture: Protozoa as Causes of Diseases. http://www.nobelprize.org/nobel_prizes/medicine/laureates/1907/laveran-lecture.html.

Lemieux, J. E., Gomez-Escobar, N., Feller, A., Carret, C., Amambua-Ngwa, A., Pinches, R., Day, F., Kyes, S. A., Conway, D. J., Holmes, C. C., & Newbold, C. I. (2009). Statistical estimation of cell-cycle progression and lineage commitment in *Plasmodium falciparum* reveals a homogeneous pattern of transcription in ex vivo culture. *Proceedings of the National Academy of Sciences*, *106*(18), 7559–7564. https://doi.org/10.1073/pnas.0811829106

Lemieux, J. E., Kyes, S. A., Otto, T. D., Feller, A. I., Eastman, R. T., Pinches, R. A., Berriman, M., Su, X. zhuan, & Newbold, C. I. (2013). Genome-wide profiling of chromosome interactions in *Plasmodium falciparum* characterizes nuclear architecture and reconfigurations associated with antigenic variation. *Molecular Microbiology*, *90*(3), 519–537. https://doi.org/10.1111/mmi.12381

Lengronne, A., Katou, Y., Mori, S., Yokabayashi, S., Kelly, G. P., Ito, T., Watanabe, Y., Shirahige, K., & Uhlmann, F. (2004). Cohesin relocation from sites of chromosomal loading to places of convergent transcription. *Nature*, *430*(6999), 573–578. https://doi.org/10.1038/nature02742

Li, H., & Durbin, R. (2009). Fast and accurate short read alignment with Burrows-Wheeler transform. *Bioinformatics*, *25*(14), 1754–1760. https://doi.org/10.1093/bioinformatics/btp324

Li, H., Handsaker, B., Wysoker, A., Fennell, T., Ruan, J., Homer, N., Marth, G., Abecasis, G., & Durbin, R. (2009). The Sequence Alignment/Map format and SAMtools. *Bioinformatics*, *25*(16), 2078–2079. https://doi.org/10.1093/bioinformatics/btp352

Lin, Z., Luo, X., & Yu, H. (2016). Structural basis of cohesin cleavage by separase. *Nature*, *532*(7597), 131–134. https://doi.org/10.1038/nature17402

Litwin, I., Pilarczyk, E., & Wysocki, R. (2018). The Emerging Role of Cohesin in the DNA Damage Response. *Genes*, *9*(12), 581. https://doi.org/10.3390/genes9120581

Llinás, M., Bozdech, Z., Wong, E. D., Adai, A. T., & DeRisi, J. L. (2006). Comparative whole genome transcriptome analysis of three *Plasmodium falciparum* strains. *Nucleic Acids Research*, *34*(4), 1166–1173. https://doi.org/10.1093/nar/gkj517

Lopez-Rubio, J. J., Mancio-Silva, L., & Scherf, A. (2009). Genome-wide Analysis of Heterochromatin Associates Clonally Variant Gene Regulation with Perinuclear Repressive Centers in Malaria Parasites. *Cell Host and Microbe*, *5*(2), 179–190. https://doi.org/10.1016/j.chom.2008.12.012

Losada, A., Hirano, M., & Hirano, T. (1998). Identification of Xenopus SMC protein complexes required for sister chromatid cohesion. *Genes & development*, *12*(13), 1986–1997. https://doi.org/10.1101/gad.12.13.1986

Losada, A., & Hirano, T. (2005). Dynamic molecular linkers of the genome: the first decade of SMC proteins. *Genes & development*, *19*(11), 1269–1287. https://doi.org/10.1101/gad.1320505

Love, M. I., Huber, W., & Anders, S. (2014). Moderated estimation of fold change and dispersion for RNA-seq data with DESeq2. *Genome Biology*, *15*(12). https://doi.org/10.1186/s13059-014-0550-8

Loy, D. E., Liu, W., Li, Y., Learn, G. H., Plenderleith, L. J., Sundararaman, S. A., Sharp, P. M., & Hahn, B. H. (2017). Out of Africa: origins and evolution of the human malaria parasites *Plasmodium falciparum* and *Plasmodium vivax*. *International journal for parasitology*, *47*(2-3), 87–97. https://doi.org/10.1016/j.ijpara.2016.05.008

Lu, B., Liu, M., Gu, L., Li, Y., Shen, S., Guo, G., Wang, F., He, X., Zhao, Y., Shang, X., Wang, L., Yang, G., Zhu, Q., Cao, J., Jiang, C., Culleton, R., Wei, G., & Zhang, Q. (2021). The Architectural Factor HMGB1 Is Involved in Genome Organization in the Human Malaria Parasite *Plasmodium falciparum*. *mBio*, *12*(2), e00148-21. https://doi.org/10.1128/mBio.00148-21

Lupiáñez, D. G., Kraft, K., Heinrich, V., Krawitz, P., Brancati, F., Klopocki, E., Horn, D., Kayserili, H., Opitz, J. M., Laxova, R., Santos-Simarro, F., Gilbert-Dussardier, B., Wittler, L., Borschiwer, M., Haas, S. A., Osterwalder, M., Franke, M., Timmermann, B., Hecht, J., … Mundlos, S. (2015). Disruptions of topological chromatin domains cause pathogenic rewiring of gene-enhancer interactions. *Cell*, *161*(5), 1012–1025. https://doi.org/10.1016/j.cell.2015.04.004

MacPherson, C. R., & Scherf, A. (2015). Flexible guide-RNA design for CRISPR applications using Protospacer Workbench. *Nature Biotechnology*, *33*(8), 805–806. https://doi.org/10.1038/nbt.3291

Mahajan, B., Selvapandiyan, A., Gerald, N. J., Majam, V., Zheng, H., Wickramarachchi, T., Tiwari, J., Fujioka, H., Moch, J. K., Kumar, N., Aravind, L., Nakhasi, H. L., & Kumar, S. (2008). Centrins, cell cycle regulation proteins in human malaria parasite *Plasmodium falciparum*. *Journal of Biological Chemistry*, *283*(46), 31871–31883. https://doi.org/10.1074/jbc.M800028200

Maier, A. G., Cooke, B. M., Cowman, A. F., & Tilley, L. (2009). Malaria parasite proteins that remodel the host erythrocyte. *Nature Reviews Microbiology*, *7*(5), 341–354. https://doi.org/10.1038/nrmicro2110

Mairet-Khedim, M., Leang, R., Marmai, C., Khim, N., Kim, S., Ke, S., Kauy, C., Kloeung, N., Eam, R., Chy, S., Izac, B., Mey Bouth, D., Dorina Bustos, M., Ringwald, P., Ariey, F., & Witkowski, B. (2021). Clinical and in Vitro Resistance of *Plasmodium falciparum* to Artesunate-Amodiaquine in Cambodia. *Clinical Infectious Diseases*, *73*(3), 406–413. https://doi.org/10.1093/cid/ciaa628

Maison, C., Bailly, D., Peters, A. H. F. M., Quivy, J. P., Roche, D., Taddei, A., Lachner, M., Jenuwein, T., & Almouzni, G. (2002). Higher-order structure in pericentric heterochromatin involves a distinct pattern of histone modification and an RNA component. *Nature Genetics*, *30*(3), 329–334. https://doi.org/10.1038/ng843

Mancio-Silva, L., Zhang, Q., Scheidig-Benatar, C., & Scherf, A. (2010). Clustering of dispersed ribosomal DNA and its role in gene regulation and chromosome-end associations in malaria parasites. *Proceedings of the National Academy of Sciences of the United States of America*, *107*(34), 15117–15122. https://doi.org/10.1073/pnas.1001045107

Mannini, L., C Lamaze, F., Cucco, F., Amato, C., Quarantotti, V., Rizzo, I. M., Krantz, I. D., Bilodeau, S., & Musio, A. (2015). Mutant cohesin affects RNA polymerase II regulation in Cornelia de Lange syndrome. *Scientific reports*, *5*, 16803. https://doi.org/10.1038/srep16803

Maston, G. A., Evans, S. K., & Green, M. R. (2006). Transcriptional regulatory elements in the human genome. *Annual review of genomics and human genetics*, *7*, 29–59. https://doi.org/10.1146/annurev.genom.7.080505.115623

Matthews, H., Duffy, C. W., & Merrick, C. J. (2018). Checks and balances? DNA replication and the cell cycle in *Plasmodium*. *Parasites & vectors*, *11*(1), 216. https://doi.org/10.1186/s13071-018-2800-1

Matthews, N. E., & White, R. (2019). Chromatin Architecture in the Fly: Living without CTCF/Cohesin Loop Extrusion?: Alternating Chromatin States Provide a Basis for Domain Architecture in Drosophila. *BioEssays: news and reviews in molecular, cellular and developmental biology*, *41*(9), e1900048. https://doi.org/10.1002/bies.201900048

Matthey-Doret, C., Baudry, L., Breuer, A., Montagne, R., Guiglielmoni, N., Scolari, V., Jean, E., Campeas, A., Chanut, P. H., Oriol, E., Méot, A., Politis, L., Vigouroux, A., Moreau, P., Koszul, R., & Cournac, A. (2020). Computer vision for pattern detection in chromosome contact maps. *Nature communications*, *11*(1), 5795. https://doi.org/10.1038/s41467-020-19562-7

Mattingly, M., Seidel, C., Muñoz, S., Hao, Y., Zhang, Y., Wen, Z., Florens, L., Uhlmann, F., & Gerton, J. L. (2022). Mediator recruits the cohesin loader Scc2 to RNA Pol II-transcribed genes and promotes sister chromatid cohesion. *Current Biology*, *32*(13), 2884-2896.e6. https://doi.org/10.1016/j.cub.2022.05.019

Matz, J. M., Beck, J. R., & Blackman, M. J. (2020). The parasitophorous vacuole of the blood-stage malaria parasite. *Nature reviews. Microbiology*, *18*(7), 379–391. https://doi.org/10.1038/s41579-019-0321-3

Mazumdar, C., Shen, Y., Xavy, S., Zhao, F., Reinisch, A., Li, R., Corces, M. R., Flynn, R. A., Buenrostro, J. D., Chan, S. M., Thomas, D., Koenig, J. L., Hong, W. J., Chang, H. Y., & Majeti, R. (2015). Leukemia-Associated Cohesin Mutants Dominantly Enforce Stem Cell Programs and Impair Human Hematopoietic Progenitor Differentiation. *Cell Stem Cell*, *17*(6), 675–688. https://doi.org/10.1016/j.stem.2015.09.017

McGuinness, B. E., Hirota, T., Kudo, N. R., Peters, J. M., & Nasmyth, K. (2005). Shugoshin prevents dissociation of cohesin from centromeres during mitosis in

vertebrate cells. *PLoS Biology*, *3*(3), 0433–0449. https://doi.org/10.1371/journal.pbio.0030086

McStay, B., & Grummt, I. (2008). The epigenetics of rRNA genes: from molecular to chromosome biology. *Annual review of cell and developmental biology*, *24*, 131–157. https://doi.org/10.1146/annurev.cellbio.24.110707.175259

Megee, P. C., Mistrot, C., Guacci, V., & Koshland, D. (1999). The centromeric sister chromatid cohesion site directs Mcd1p binding to adjacent sequences. *Molecular cell*, *4*(3), 445–450. https://doi.org/10.1016/s1097-2765(00)80347-0

Mehnert, A.-K., Simon, C. S., & Guizetti, J. (2019). Immunofluorescence staining protocol for STED nanoscopy of *Plasmodium*-infected red blood cells. *Molecular and Biochemical Parasitology*, *229*, 47–52. https://doi.org/10.1016/j.molbiopara.2019.02.007

Merrick, C. J., & Duraisingh, M. T. (2007). Plasmodium falciparum Sir2: An unusual sirtuin with dual histone deacetylase and ADP-ribosyltransferase activity. *Eukaryotic Cell*, *6*(11), 2081–2091. https://doi.org/10.1128/EC.00114-07

Mesén-Ramírez, P., Reinsch, F., Blancke Soares, A., Bergmann, B., Ullrich, A. K., Tenzer, S., & Spielmann, T. (2016). Stable Translocation Intermediates Jam Global Protein Export in *Plasmodium falciparum* Parasites and Link the PTEX Component EXP2 with Translocation Activity. *PLoS Pathogens*, *12*(5). https://doi.org/10.1371/journal.ppat.1005618

Miao, J., Fan, Q., Cui, L., Li, J., Li, J., & Cui, L. (2006). The malaria parasite *Plasmodium falciparum* histones: Organization, expression, and acetylation. *Gene*, *369*(1–2), 53–65. https://doi.org/10.1016/j.gene.2005.10.022

Michaelis, C., Ciosk, R., & Nasmyth, K. (1997). Cohesins: Chromosomal Proteins that Prevent Premature Separation of Sister Chromatids. *Cell*, *91*(1), 35–45. https://doi.org/10.1016/s0092-8674(01)80007-6

Miller, L. H., & Su, X. (2011). Artemisinin: discovery from the Chinese herbal garden. *Cell*, *146*(6), 855–858. https://doi.org/10.1016/j.cell.2011.08.024

Mirkovic, M., & Oliveira, R. A. (2017). Centromeric Cohesin: Molecular Glue and Much More. *Progress in Molecular and Subcellular Biology*, 485–513. https://doi.org/10.1007/978-3-319-58592-5_20

Misteli, T. (2020). The Self-Organizing Genome: Principles of Genome Architecture and Function. *Cell*, *183*(1), 28–45. https://doi.org/10.1016/j.cell.2020.09.014

Mistry, J., Chuguransky, S., Williams, L., Qureshi, M., Salazar, G. A., Sonnhammer, E. L. L., Tosatto, S. C. E., Paladin, L., Raj, S., Richardson, L. J., Finn, R. D., & Bateman, A. (2021). Pfam: The protein families database in 2021. *Nucleic Acids Research*, *49*(D1), D412–D419. https://doi.org/10.1093/nar/gkaa913

Modrzynska, K., Pfander, C., Chappell, L., Yu, L., Suarez, C., Dundas, K., Gomes, A. R., Goulding, D., Rayner, J. C., Choudhary, J., & Billker, O. (2017). A Knockout Screen of ApiAP2 Genes Reveals Networks of Interacting Transcriptional Regulators Controlling the *Plasmodium* Life Cycle. *Cell Host and Microbe*, *21*(1), 11–22. https://doi.org/10.1016/j.chom.2016.12.003

Mok, B. W., Ribacke, U., Sherwood, E., & Wahlgren, M. (2008). A highly conserved segmental duplication in the subtelomeres of *Plasmodium falciparum* chromosomes varies in copy number. *Malaria Journal*, *7*, 1–9. https://doi.org/10.1186/1475-2875-7-46

Mönnich, M., Banks, S., Eccles, M., Dickinson, E., & Horsfield, J. (2009). Expression of cohesin and condensin genes during zebrafish development supports a non-proliferative role for cohesin. *Gene Expression Patterns*, *9*(8), 586–594. https://doi.org/10.1016/j.gep.2009.08.004

Moraes, C. B., Dorval, T., Contreras-Dominguez, M., Dossin, F. de M., Hansen, M. A. E., Genovesio, A., & Freitas-Junior, L. H. (2013). Transcription Sites Are Developmentally Regulated during the Asexual Cycle of *Plasmodium falciparum*. *PLoS ONE*, *8*(2). https://doi.org/10.1371/journal.pone.0055539

Mullenders, J., Aranda-Orgilles, B., Lhoumaud, P., Keller, M., Pae, J., Wang, K., Kayembe, C., Rocha, P. P., Raviram, R., Gong, Y., Premsrirut, P. K., Tsirigos, A., Bonneau, R., Skok, J. A., Cimmino, L., Hoehn, D., & Aifantis, I. (2015). Cohesin loss alters adult hematopoietic stem cell homeostasis, leading to myeloproliferative

neoplasms. *Journal of Experimental Medicine*, *212*(11), 1833–1850. https://doi.org/10.1084/jem.20151323

Muller, H., Gil, J., & Drinnenberg, I. A. (2019). The Impact of Centromeres on Spatial Genome Architecture. *Trends in Genetics*, *35*(8), 565–578. https://doi.org/10.1016/j.tig.2019.05.003

Murayama, Y., & Uhlmann, F. (2014). Biochemical reconstitution of topological DNA binding by the cohesin ring. *Nature*, *505*(7483), 367–371. https://doi.org/10.1038/nature12867

Muto, A., Ikeda, S., Lopez-Burks, M. E., Kikuchi, Y., Calof, A. L., Lander, A. D., & Schilling, T. F. (2014). Nipbl and Mediator Cooperatively Regulate Gene Expression to Control Limb Development. *PLoS Genetics*, *10*(9). https://doi.org/10.1371/journal.pgen.1004671

Nativio, R., Wendt, K. S., Ito, Y., Huddleston, J. E., Uribe-Lewis, S., Woodfine, K., Krueger, C., Reik, W., Peters, J. M., & Murrell, A. (2009). Cohesin is required for higher-order chromatin conformation at the imprinted IGF2-H19 locus. *PLoS Genetics*, *5*(11). https://doi.org/10.1371/journal.pgen.1000739

Neiva, A. (1910). Formação de raça do hematozoario do impaludismo resistente a quinina. *Memórias do Instituto Oswaldo Cruz.*, *2*, 131–140.

Nishiyama, T. (2019). Cohesion and cohesin-dependent chromatin organization. *Current opinion in cell biology*, *58*, 8–14. https://doi.org/10.1016/j.ceb.2018.11.006

Nishiyama, T., Ladurner, R., Schmitz, J., Kreidl, E., Schleiffer, A., Bhaskara, V., Bando, M., Shirahige, K., Hyman, A. A., Mechtler, K., & Peters, J. M. (2010). Sororin mediates sister chromatid cohesion by antagonizing Wapl. *Cell*, *143*(5), 737–749. https://doi.org/10.1016/j.cell.2010.10.031

Nishiyama, T., Sykora, M. M., Huis, P. J., Mechtler, K., & Peters, J. M. (2013). Aurora B and Cdk1 mediate Wapl activation and release of acetylated cohesin from chromosomes by phosphorylating Sororin. *Proceedings of the National Academy of Sciences of the United States of America*, *110*(33), 13404–13409. https://doi.org/10.1073/pnas.1305020110

Nitzsche, A., Paszkowski-Rogacz, M., Matarese, F., Janssen-Megens, E. M., Hubner, N. C., Schulz, H., de Vries, I., Ding, L., Huebner, N., Mann, M., Stunnenberg, H. G., & Buchholz, F. (2011). RAD21 cooperates with pluripotency transcription factors in the maintenance of embryonic stem cell identity. *PLoS ONE*, *6*(5). https://doi.org/10.1371/journal.pone.0019470

Noor, A. M., & Alonso, P. L. (2022). The message on malaria is clear: progress has stalled. *Lancet*, *399*(10337), 1777. https://doi.org/10.1016/S0140-6736(22)00732-2

Nora, E. P., Lajoie, B. R., Schulz, E. G., Giorgetti, L., Okamoto, I., Servant, N., Piolot, T., van Berkum, N. L., Meisig, J., Sedat, J., Gribnau, J., Barillot, E., Blüthgen, N., Dekker, J., & Heard, E. (2012). Spatial partitioning of the regulatory landscape of the X-inactivation centre. *Nature*, *485*(7398), 381–385. https://doi.org/10.1038/nature11049

Nuebler, J., Fudenberg, G., Imakaev, M., Abdennur, N., & Mirny, L. A. (2018). Chromatin organization by an interplay of loop extrusion and compartmental segregation. *Proceedings of the National Academy of Sciences of the United States of America*, *115*(29), 6697–6706. https://doi.org/10.1073/pnas.1717730115

Oakley, M. S., Gerald, N., McCutchan, T. F., Aravind, L., & Kumar, S. (2011). Clinical and molecular aspects of malaria fever. *Trends in parasitology*, *27*(10), 442–449. https://doi.org/10.1016/j.pt.2011.06.004

O'Donnell, R. A., de Koning-Ward, T. F., Burt, R. A., Bockarie, M., Reeder, J. C., Cowman, A. F., & Crabb, B. S. (2001). Antibodies against Merozoite Surface Protein (Msp)-119 Are a Major Component of the Invasion-Inhibitory Response in Individuals Immune to Malaria. *Journal of Experimental Medicine*, *193*(12), 1403–1412. https://doi.org/10.1084/jem.193.12.1403

O'Donnell, R. A., Freitas-Junior, L. H., Preiser, P. R., Williamson, D. H., Duraisingh, M., McElwain, T. F., Scherf, A., Cowman, A. F., & Crabb, B. S. (2002). A genetic screen for improved plasmid segregation reveals a role for Rep20 in the interaction of *Plasmodium falciparum* chromosomes. *EMBO Journal*, *21*(5), 1231–1239. https://doi.org/10.1093/emboj/21.5.1231

O'Donnell, R. A., Saul, A., Cowman, A. F., & Crabb, B. S. (2000). Functional conservation of the malaria vaccine antigen MSP-119 across distantly related *Plasmodium* species. *Nature Medicine*, *6*(1), 91–95. https://doi.org/10.1038/71595

Oh, S., Shao, J., Mitra, J., Xiong, F., D'Antonio, M., Wang, R., Garcia-Bassets, I., Ma, Q., Zhu, X., Lee, J. H., Nair, S. J., Yang, F., Ohgi, K., Frazer, K. A., Zhang, Z. D., Li, W., & Rosenfeld, M. G. (2021). Enhancer release and retargeting activates disease-susceptibility genes. *Nature*, *595*(7869), 735–740. https://doi.org/10.1038/s41586-021-03577-1

Oliveira, R. A., Hamilton, R. S., Pauli, A., Davis, I., & Nasmyth, K. (2010). Cohesin cleavage and Cdk inhibition trigger formation of daughter nuclei. *Nature Cell Biology*, *12*(2), 185–192. https://doi.org/10.1038/ncb2018

Paddon, C. J., & Keasling, J. D. (2014). Semi-synthetic artemisinin: a model for the use of synthetic biology in pharmaceutical development. *Nature reviews. Microbiology*, *12*(5), 355–367. https://doi.org/10.1038/nrmicro3240

Paddon, C. J., Westfall, P. J., Pitera, D. J., Benjamin, K., Fisher, K., McPhee, D., Leavell, M. D., Tai, A., Main, A., Eng, D., Polichuk, D. R., Teoh, K. H., Reed, D. W., Treynor, T., Lenihan, J., Jiang, H., Fleck, M., Bajad, S., Dang, G., … Newman, J. D. (2013). High-level semi-synthetic production of the potent antimalarial artemisinin. *Nature*, *496*(7446), 528–532. https://doi.org/10.1038/nature12051

Painter, H. J., Campbell, T. L., & Llinás, M. (2011). The Apicomplexan AP2 family: Integral factors regulating *Plasmodium* development. *Molecular and Biochemical Parasitology*, *176*(1), 1–7. https://doi.org/10.1016/j.molbiopara.2010.11.014

Painter, H. J., Chung, N. C., Sebastian, A., Albert, I., Storey, J. D., & Llinás, M. (2018). Genome-wide real-time in vivo transcriptional dynamics during *Plasmodium falciparum* blood-stage development. *Nature Communications*, *9*(1), 2656. https://doi.org/10.1038/s41467-018-04966-3

Parelho, V., Hadjur, S., Spivakov, M., Leleu, M., Sauer, S., Gregson, H. C., Jarmuz, A., Canzonetta, C., Webster, Z., Nesterova, T., Cobb, B. S., Yokomori, K., Dillon, N., Aragon, L., Fisher, A. G., & Merkenschlager, M. (2008). Cohesins Functionally Associate with CTCF on Mammalian Chromosome Arms. *Cell*, *132*(3), 422–433. https://doi.org/10.1016/j.cell.2008.01.011

Peters, J. M., Tedeschi, A., & Schmitz, J. (2008). The cohesin complex and its roles in chromosome biology. *Genes & development*, *22*(22), 3089–3114. https://doi.org/10.1101/gad.1724308

Poinar, G. (2005). *Plasmodium dominicana* n. sp. (Plasmodiidae: Haemospororida) from Tertiary Dominican amber. *Systematic Parasitology*, *61*(1), 47–52. https://doi.org/10.1007/s11230-004-6354-6

Pombo, A., & Dillon, N. (2015). Three-dimensional genome architecture: players and mechanisms. *Nature reviews. Molecular cell biology*, *16*(4), 245–257. https://doi.org/10.1038/nrm3965

Ponts, N., Harris, E. Y., Prudhomme, J., Wick, I., Eckhardt-Ludka, C., Hicks, G. R., Hardiman, G., Lonardi, S., & le Roch, K. G. (2010). Nucleosome landscape and control of transcription in the human malaria parasite. *Genome Research*, *20*(2), 228–238. https://doi.org/10.1101/gr.101063.109

Prommana, P., Uthaipibull, C., Wongsombat, C., Kamchonwongpaisan, S., Yuthavong, Y., Knuepfer, E., Holder, A. A., & Shaw, P. J. (2013). Inducible Knockdown of *Plasmodium* Gene Expression Using the *glmS* Ribozyme. *PLoS One*, *8*(8). https://doi.org/10.1371/journal.pone.0073783

Quinlan, A. R., & Hall, I. M. (2010). BEDTools: A flexible suite of utilities for comparing genomic features. *Bioinformatics*, *26*(6), 841–842. https://doi.org/10.1093/bioinformatics/btq033

R Core Team. (2021). R: A language and environment for statistical computing. R Foundation for Statistical Computing, Vienna, Austria. https://www.R-project.org/

Ralph, S. A., Scheidig-Benatar, C., & Scherf, A. (2005). Antigenic variation in *Plasmodium falciparum* is associated with movement of *var* loci between subnuclear locations. *Proceedings of the National Academy of Sciences*, *102*(15), 5414–5419. https://doi.org/10.1073/pnas.0408883102

Ramírez, F., Ryan, D. P., Grüning, B., Bhardwaj, V., Kilpert, F., Richter, A. S., Heyne, S., Dündar, F., & Manke, T. (2016). deepTools2: a next generation web server for deep-sequencing data analysis. *Nucleic Acids Research*, *44*(1), 160–165. https://doi.org/10.1093/NAR/GKW257

Rao, S. S. P., Huang, S. C., Glenn St Hilaire, B., Engreitz, J. M., Perez, E. M., Kieffer-Kwon, K. R., Sanborn, A. L., Johnstone, S. E., Bascom, G. D., Bochkov, I. D., Huang, X., Shamim, M. S., Shin, J., Turner, D., Ye, Z., Omer, A. D., Robinson, J. T., Schlick,

T., Bernstein, B. E., … Aiden, E. L. (2017). Cohesin Loss Eliminates All Loop Domains. *Cell*, *171*(2), 305-320.e24. https://doi.org/10.1016/j.cell.2017.09.026

Rawat, M., Kanyal, A., Sahasrabudhe, A., Vembar, S. S., Lopez-Rubio, J. J., & Karmodiya, K. (2021). Histone acetyltransferase PfGCN5 regulates stress responsive and artemisinin resistance related genes in *Plasmodium falciparum*. *Scientific Reports*, *11*(1), 1–13. https://doi.org/10.1038/s41598-020-79539-w

Remeseiro, S., Cuadrado, A., Gómez-Lãpez, G., Pisano, D. G., & Losada, A. (2012). A unique role of cohesin-SA1 in gene regulation and development. *EMBO Journal*, *31*(9), 2090–2102. https://doi.org/10.1038/emboj.2012.60

Riglar, D. T., Richard, D., Wilson, D. W., Boyle, M. J., Dekiwadia, C., Turnbull, L., Angrisano, F., Marapana, D. S., Rogers, K. L., Whitchurch, C. B., Beeson, J. G., Cowman, A. F., Ralph, S. A., & Baum, J. (2011). Super-resolution dissection of coordinated events during malaria parasite invasion of the human erythrocyte. *Cell Host and Microbe*, *9*(1), 9–20. https://doi.org/10.1016/j.chom.2010.12.003

Robinson, J. T., Thorvaldsdóttir, H., Winckler, W., Guttman, M., Lander, E. S., Getz, G., & Mesirov, J. P. (2011). Integrative genomics viewer. *Nature Biotechnology*, *29*(1), 24–26. https://doi.org/10.1038/nbt0111-24

Roig, M. B., Löwe, J., Chan, K.-L., Beckouët, F., Metson, J., & Nasmyth, K. (2014). Structure and function of cohesin's Scc3/SA regulatory subunit. *FEBS Letters*, *588*(20), 3692–3702. https://doi.org/10.1016/j.febslet.2014.08.015

Rollins, R. A., Morcillo, P., & Dorsett, D. (1999). Nipped-B, a *Drosophila* homologue of chromosomal adherins, participates in activation by remote enhancers in the cut and Ultrabithorax genes. *Genetics*, *152*(2), 577–593. https://doi.org/10.1093/genetics/152.2.577

Ross, R. (1902, December 12). *Ronald Ross—Nobel Lecture: Researches on Malaria*. Ronald Ross—Nobel Lecture, Researches on Malaria. http://www.nobelprize.org/nobel_prizes/medicine/laureates/1902/ross-lecture.html.

Rothbart, S. B., & Strahl, B. D. (2014). Interpreting the language of histone and DNA modifications. *Biochimica et biophysica acta*, *1839*(8), 627–643. https://doi.org/10.1016/j.bbagrm.2014.03.001

Rowland, B. D., Roig, M. B., Nishino, T., Kurze, A., Uluocak, P., Mishra, A., Beckouët, F., Underwood, P., Metson, J., Imre, R., Mechtler, K., Katis, V. L., & Nasmyth, K. (2009). Building Sister Chromatid Cohesion: Smc3 Acetylation Counteracts an Antiestablishment Activity. *Molecular Cell*, *33*(6), 763–774. https://doi.org/10.1016/j.molcel.2009.02.028

Rowley, M. J., & Corces, V. G. (2016). The three-dimensional genome: principles and roles of long-distance interactions. *Current opinion in cell biology*, *40*, 8–14. https://doi.org/10.1016/j.ceb.2016.01.009

Rowley, M. J., & Corces, V. G. (2018). Organizational principles of 3D genome architecture. *Nature Reviews. Genetics*, *19*(12), 789–800. https://doi.org/10.1038/s41576-018-0060-8

Rowley, M. J., Nichols, M. H., Lyu, X., Ando-Kuri, M., Rivera, I. S. M., Hermetz, K., Wang, P., Ruan, Y., & Corces, V. G. (2017). Evolutionarily Conserved Principles Predict 3D Chromatin Organization. *Molecular Cell*, *67*(5), 837-852.e7. https://doi.org/10.1016/j.molcel.2017.07.022

RTSS SAGE/MPAG Working Group. (2021). Full Evidence Report on the RTS,S/AS01 Malaria Vaccine.

Rubio, E. D., Reiss, D. J., Welcsh, P. L., Disteche, C. M., Filippova, G. N., Baliga, N. S., Aebersold, R., Ranish, J. A., & Krumm, A. (2008). CTCF physically links cohesin to chromatin. *Proceedings of the National Academy of Sciences of the United States of America*, *105*(24), 8309–8314. https://doi.org/10.1073/pnas.0801273105

Rudlaff, R. M., Kraemer, S., Marshman, J., & Dvorin, J. D. (2020). Three-dimensional ultrastructure of *Plasmodium falciparum* throughout cytokinesis. *PLoS Pathogens*, *16*(6). https://doi.org/10.1371/journal.ppat.1008587

Ruiz, J. L., Tena, J. J., Bancells, C., Cortés, A., Gómez-Skarmeta, J. L., & Gomez-Díaz, E. (2018). Characterization of the accessible genome in the human malaria parasite *Plasmodium falciparum*. *Nucleic Acids Research*, *46*(18), 9414–9431. https://doi.org/10.1093/nar/gky643

Ryu, J.-K., Bouchoux, C., Liu, H. W., Kim, E., Minamino, M., de Groot, R., Katan, A. J., Bonato, A., Marenduzzo, D., Michieletto, D., Uhlmann, F., & Dekker, C. (2021).

Bridging-induced phase separation induced by cohesin SMC protein complexes. *Science advances*, *7*(7). https://doi.org/10.1126/sciadv.abe5905

Salcedo-Amaya, A. M., van Driel, M. A., Alako, B. T., Trelle, M. B., van den Elzen, A. M. G., Cohen, A. M., Janssen-Megens, E. M., van de Vegte-Bolmer, M., Selzer, R. R., Iniguez, A. L., Green, R. D., Sauerwein, R. W., Jensen, O. N., & Stunnenberg, H. G. (2009). Dynamic histone H3 epigenome marking during the intraerythrocytic cycle of *Plasmodium falciparum*. *Proceedings of the National Academy of Sciences of the United States of America*, *106*(24), 9655–9660. https://doi.org/10.1073/pnas.0902515106

Santos, J. M., Josling, G., Ross, P., Joshi, P., Campbell, T., Schieler, A., & Cristea, I. M. (2017). Red blood cell invasion by the malaria parasite is coordinated by the PfAP2-I transcription factor. *Cell Host Microbe*, *21*(6), 731–741. https://doi.org/10.1016/j.chom.2017.05.006

Saraf, A., Cervantes, S., Bunnik, E. M., Ponts, N., Sardiu, M. E., Chung, D. W. D., Prudhomme, J., Varberg, J. M., Wen, Z., Washburn, M. P., Florens, L., & le Roch, K. G. (2016). Dynamic and combinatorial landscape of histone modifications during the intraerythrocytic developmental cycle of the malaria parasite. *Journal of Proteome Research*, *15*(8), 2787–2801. https://doi.org/10.1021/acs.jproteome.6b00366

Sarma, K., & Reinberg, D. (2005). Histone variants meet their match. *Nature Reviews. Molecular Cell Biology*, *6*(2), 139–149. https://doi.org/10.1038/nrm1567

Schaaf, C. A., Kwak, H., Koenig, A., Misulovin, Z., Gohara, D. W., Watson, A., Zhou, Y., Lis, J. T., & Dorsett, D. (2013). Genome-Wide Control of RNA Polymerase II Activity by Cohesin. *PLoS Genetics*, *9*(3). https://doi.org/10.1371/journal.pgen.1003382

Scherf, A., Figueiredo, L. M., & Freitas-Junior, L. H. (2001). *Plasmodium* telomeres: A pathogen's perspective. *Current Opinion in Microbiology*, *4*(4), 409–414. https://doi.org/10.1016/S1369-5274(00)00227-7

Scherf, A., Lopez-Rubio, J. J., & Riviere, L. (2008). Antigenic Variation in *Plasmodium falciparum*. *Annual Review of Microbiology*, *62*(1), 445–470. https://doi.org/10.1146/annurev.micro.61.080706.093134

Schmidt, D., Schwalie, P. C., Ross-Innes, C. S., Hurtado, A., Brown, G. D., Carroll, J. S., Flicek, P., & Odom, D. T. (2010). A CTCF-independent role for cohesin in tissue-specific transcription. *Genome Research*, *20*(5), 578–588. https://doi.org/10.1101/gr.100479.109

Schuldiner, O., Berdnik, D., Levy, J. M., Wu, J. S., Luginbuhl, D., Gontang, A. C., & Luo, L. (2008). piggyBac-Based Mosaic Screen Identifies a Postmitotic Function for Cohesin in Regulating Developmental Axon Pruning. *Developmental Cell*, *14*(2), 227–238. https://doi.org/10.1016/j.devcel.2007.11.001

Schwarzer, W., Abdennur, N., Goloborodko, A., Pekowska, A., Fudenberg, G., Loe-Mie, Y., Fonseca, N. A., Huber, W., Haering, C. H., Mirny, L., & Spitz, F. (2017). Two independent modes of chromatin organization revealed by cohesin removal. *Nature*, *551*(7678), 51–56. https://doi.org/10.1038/nature24281

Seitan, V. C., Krangel, M. S., & Merkenschlager, M. (2012). Cohesin, CTCF and lymphocyte antigen receptor locus rearrangement. *Trends in immunology*, *33*(4), 153–159. https://doi.org/10.1016/j.it.2012.02.004

Sherling, E. S., Knuepfer, E., Brzostowski, J. A., Miller, L. H., Blackman, M. J., & van Ooij, C. (2017). The *Plasmodium falciparum* rhoptry protein RhopH3 plays essential roles in host cell invasion and nutrient uptake. *ELife*, *6*. https://doi.org/10.7554/eLife.23239.001

Shokri, L., Inukai, S., Hafner, A., Weinand, K., Hens, K., Vedenko, A., Gisselbrecht, S. S., Dainese, R., Bischof, J., Furger, E., Feuz, J. D., Basler, K., Deplancke, B., & Bulyk, M. L. (2019). A Comprehensive *Drosophila melanogaster* Transcription Factor Interactome. *Cell Reports*, *27*(3), 955-970. https://doi.org/10.1016/j.celrep.2019.03.071

Siegel, T. N., Hon, C. C., Zhang, Q., Lopez-Rubio, J. J., Scheidig-Benatar, C., Martins, R. M., Sismeiro, O., Coppée, J. Y., & Scherf, A. (2014). Strand-specific RNA-Seq reveals widespread and developmentally regulated transcription of natural antisense transcripts in *Plasmodium falciparum*. *BMC Genomics*, *15*(1). https://doi.org/10.1186/1471-2164-15-150

Sierra-Miranda, M., Vembar, S. S., Delgadillo, D. M., Ávila-López, P. A., Herrera-Solorio, A. M., Lozano Amado, D., Vargas, M., & Hernandez-Rivas, R. (2017). *Pf*AP2Tel,

harbouring a non-canonical DNA-binding AP2 domain, binds to *Plasmodium falciparum* telomeres. *Cellular microbiology*, *19*(9), 10.1111/cmi.12742. https://doi.org/10.1111/cmi.12742

Sikorska, N., & Sexton, T. (2020). Defining Functionally Relevant Spatial Chromatin Domains: It is a TAD Complicated. *Journal of molecular biology*, *432*(3), 653–664. https://doi.org/10.1016/j.jmb.2019.12.006

Smith, J. D., Rowe, J. A., Higgins, M. K., & Lavstsen, T. (2013). Malaria's deadly grip: cytoadhesion of *Plasmodium falciparum*-infected erythrocytes. *Cellular microbiology*, *15*(12), 1976–1983. https://doi.org/10.1111/cmi.12183

Srinivasan, M., Scheinost, J. C., Petela, N. J., Gligoris, T. G., Wissler, M., Ogushi, S., Collier, J. E., Voulgaris, M., Kurze, A., Chan, K. L., Hu, B., Costanzo, V., & Nasmyth, K. A. (2018). The Cohesin Ring Uses Its Hinge to Organize DNA Using Non-topological as well as Topological Mechanisms. *Cell*, *173*(6), 1508-1519.e18. https://doi.org/10.1016/j.cell.2018.04.015

Stanojcic, S., Kuk, N., Ullah, I., Sterkers, Y., & Merrick, C. J. (2017). Single-molecule analysis reveals that DNA replication dynamics vary across the course of schizogony in the malaria parasite *Plasmodium falciparum*. *Scientific Reports*, *7*(1). https://doi.org/10.1038/s41598-017-04407-z

Stedman, W., Kang, H., Lin, S., Kissil, J. L., Bartolomei, M. S., & Lieberman, P. M. (2008). Cohesins localize with CTCF at the KSHV latency control region and at cellular c-myc and H19/Igf2 insulators. *EMBO Journal*, *27*(4), 654–666. https://doi.org/10.1038/emboj.2008.1

Straimer, J., Gnädig, N. F., Witkowski, B., Amaratunga, C., Duru, V., Ramadani, A. P., Dacheux, M., Khim, N., Zhang, L., Lam, S., Gregory, P. D., Urnov, F. D., Mercereau-Puijalon, O., Benoit-Vical, F., Fairhurst, R. M., Ménard, D., & Fidock, D. A. (2015). K13-propeller mutations confer artemisinin resistance in *Plasmodium falciparum* clinical isolates. *Science*, *347*(6220), 428–431. https://doi.org/10.1126/science.1260867

Sullivan, W. J., Naguleswaran, A., & Angel, S. O. (2006). Histones and histone modifications in protozoan parasites. *Cellular microbiology*, *8*(12), 1850–1861. https://doi.org/10.1111/j.1462-5822.2006.00818.x

Sun, F., Chronis, C., Kronenberg, M., Chen, X. F., Su, T., Lay, F. D., Plath, K., Kurdistani, S. K., & Carey, M. F. (2019). Promoter-Enhancer Communication Occurs Primarily within Insulated Neighborhoods. *Molecular Cell*, *73*(2), 250-263.e5. https://doi.org/10.1016/j.molcel.2018.10.039

Sutherland, C. J., Tanomsing, N., Nolder, D., Oguike, M., Jennison, C., Pukrittayakamee, S., Dolecek, C., Hien, T. T., do Rosário, V. E., Arez, A. P., Pinto, J., Michon, P., Escalante, A. A., Nosten, F., Burke, M., Lee, R., Blaze, M., Otto, T. D., Barnwell, J. W., … Polley, S. D. (2010). Two Nonrecombining Sympatric Forms of the Human Malaria Parasite Plasmodium ovale Occur Globally . *The Journal of Infectious Diseases*, *201*(10), 1544–1550. https://doi.org/10.1086/652240

Symmons, O., Uslu, V. V., Tsujimura, T., Ruf, S., Nassari, S., Schwarzer, W., Ettwiller, L., & Spitz, F. (2014). Functional and topological characteristics of mammalian regulatory domains. *Genome Research*, *24*(3), 390–400. https://doi.org/10.1101/gr.163519.113

Szabo, Q., Bantignies, F., & Cavalli, G. (2019). Principles of genome folding into topologically associating domains. *Science Advances*, *5*(4). https://doi.org/10.1126/sciadv.aaw1668

Tanaka, T., Cosma, M. P., Wirth, K., & Nasmyth, K. (1999). Identification of Cohesin Association Sites at Centromeres and along Chromosome Arms. *Cell*, *98*, 847–858. https://doi.org/10.1016/S0092-8674(00)81518-4

Tanaka, T., Fuchs, J., Loidl, J., & Nasmyth, K. (2000). Tanaka, T., Fuchs, J., Loidl, J., & Nasmyth, K. (2000). Cohesin ensures bipolar attachment of microtubules to sister centromeres and resists their precocious separation. *Nature cell biology*, *2*(8), 492–499. https://doi.org/10.1038/35019529

Tang, J., Chisholm, S. A., Yeoh, L. M., Gilson, P. R., Papenfuss, A. T., Day, K. P., Petter, M., & Duffy, M. F. (2020). Histone modifications associated with gene expression and genome accessibility are dynamically enriched at Plasmodium falciparum regulatory sequences. *Epigenetics & chromatin*, *13*(1), 50. https://doi.org/10.1186/s13072-020-00365-5

Templeton, T. J., Iyer, L. M., Anantharaman, V., Enomoto, S., Abrahante, J. E., Subramanian, G. M., Hoffman, S. L., Abrahamsen, M. S., & Aravind, L. (2004).

Comparative analysis of apicomplexa and genomic diversity in eukaryotes. *Genome Research*, *14*(9), 1686–1695. https://doi.org/10.1101/gr.2615304

Thanh, N. V., Thuy-Nhien, N., Tuyen, N. T. K., Tong, N. T., Nha-Ca, N. T., Dong, L. T., Quang, H. H., Farrar, J., Thwaites, G., White, N. J., Wolbers, M., & Hien, T. T. (2017). Rapid decline in the susceptibility of *Plasmodium falciparum* to dihydroartemisinin-piperaquine in the south of Vietnam. *Malaria Journal*, *16*(1), 1–10. https://doi.org/10.1186/s12936-017-1680-8

Tintó-Font, E., Michel-Todó, L., Russell, T. J., Casas-Vila, N., Conway, D. J., Bozdech, Z., Llinás, M., & Cortés, A. (2021). A heat-shock response regulated by the *Pf*AP2-HS transcription factor protects human malaria parasites from febrile temperatures. *Nature microbiology*, *6*(9), 1163–1174. https://doi.org/10.1038/s41564-021-00940-w

Toenhake, C. G., & Bártfai, R. (2019). What functional genomics has taught us about transcriptional regulation in malaria parasites. *Briefings in Functional Genomics*, *18*(5), 290–301. https://doi.org/10.1093/bfgp/elz004

Toenhake, C. G., Fraschka, S. A. K., Vijayabaskar, M. S., Westhead, D. R., van Heeringen, S. J., & Bártfai, R. (2018). Chromatin Accessibility-Based Characterization of the Gene Regulatory Network Underlying *Plasmodium falciparum* Blood-Stage Development. *Cell Host and Microbe*, *23*(4), 557-569.e9. https://doi.org/10.1016/j.chom.2018.03.007

Tolhuis, B., Blom, M., Kerkhoven, R. M., Pagie, L., Teunissen, H., Nieuwland, M., Simonis, M., de Laat, W., van Lohuizen, M., & van Steensel, B. (2011). Interactions among polycomb domains are guided by chromosome architecture. *PLoS Genetics*, *7*(3). https://doi.org/10.1371/journal.pgen.1001343

Tomonaga, T., Nagao, K., Kawasaki, Y., Furuya, K., Murakaini, A., Morishita, J., Yuasa, T., Sutani, T., Kearsey, S. E., Uhlmann, F., Nasmyth, K., & Yanagida, M. (2000). Characterization of fission yeast cohesin: Essential anaphase proteolysis of Rad21 phosphorylated in the S phase. *Genes and Development*, *14*(21), 2757–2770. https://doi.org/10.1101/gad.832000

Tonkin, C. J., Carret, C. K., Duraisingh, M. T., Voss, T. S., Ralph, S. A., Hommel, M., Duffy, M. F., da Silva, L. M., Scherf, A., Ivens, A., Speed, T. P., Beeson, J. G., &

Cowman, A. F. (2009). Sir2 paralogues cooperate to regulate virulence genes and antigenic variation in *Plasmodium falciparum*. *PLoS Biology*, *7*(4), 771–788. https://doi.org/10.1371/journal.pbio.1000084

Tonkin, C. J., van Dooren, G. G., Spurck, T. P., Struck, N. S., Good, R. T., Handman, E., Cowman, A. F., & McFadden, G. I. (2004). Localization of organellar proteins in *Plasmodium falciparum* using a novel set of transfection vectors and a new immunofluorescence fixation method. *Molecular and Biochemical Parasitology*, *137*(1), 13–21. https://doi.org/10.1016/j.molbiopara.2004.05.009

Trape, J.-F., Pison, G., Spiegel, A., Enel, C., & Rogier, C. (2002). Combating malaria in Africa. *Trends in Parasitology*, *18*(5), 224–230. https://doi.org/10.1016/S1471-4922(02)02249-3

Trelle, M. B., Salcedo-Amaya, A. M., Cohen, A. M., Stunnenberg, H. G., & Jensen, O. N. (2009). Global histone analysis by mass spectrometry reveals a high content of acetylated lysine residues in the malaria parasite Plasmodium falciparum. *Journal of Proteome Research*, *8*(7), 3439–3450. https://doi.org/10.1021/pr9000898

Tu, Y. (2011). The discovery of artemisinin (qinghaosu) and gifts from Chinese medicine. *Nature medicine*, *17*(10), 1217–1220. https://doi.org/10.1038/nm.2471

Tu Youyou. (2015, December 7). *Tu Youyou -Nobel Lecture: Artemisinin—A Gift from Traditional Chinese Medicine to the World*. Tu Youyou -Nobel Lecture: Artemisinin—A Gift from Traditional Chinese Medicine to the World. https://www.nobelprize.org/uploads/2018/06/tu-lecture.pdf

Turner, L., Lavstsen, T., Berger, S. S., Wang, C. W., Jens, E. v, Avril, M., Brazier, A. J., Freeth, J., Jespersen, J. S., Morten, A., Magistrado, P., Lusingu, J., Smith, J. D., Higgins, M. K., & Theander, T. G. (2013). Severe malaria is associated with parasite binding to endothelial protein C receptor. *Nature*, *498*(7455), 502–505. https://doi.org/10.1038/nature12216

Uhlmann, F. (2016). SMC complexes: From DNA to chromosomes. *Nature Reviews. Molecular Cell Biology*, *17*(7), 399–412. https://doi.org/10.1038/nrm.2016.30

Uhlmann, F., Lottspeich, F., & Nasmyth, K. (1999). Sister-chromatid separation at anaphase onset is promoted by cleavage of the cohesin subunit Scc1. *Nature*, *400*(6739), 37–42. https://doi.org/10.1038/21831

Ukaegbu, U. E., Kishore, S. P., Kwiatkowski, D. L., Pandarinath, C., Dahan-Pasternak, N., Dzikowski, R., & Deitsch, K. W. (2014). Recruitment of *Pf*SET2 by RNA Polymerase II to Variant Antigen Encoding Loci Contributes to Antigenic Variation in *P. falciparum*. *PLoS Pathogens*, *10*(1). https://doi.org/10.1371/journal.ppat.1003854

Uwimana, A., Legrand, E., Stokes, B. H., Ndikumana, J. L. M., Warsame, M., Umulisa, N., Ngamije, D., Munyaneza, T., Mazarati, J. B., Munguti, K., Campagne, P., Criscuolo, A., Ariey, F., Murindahabi, M., Ringwald, P., Fidock, D. A., Mbituyumuremyi, A., & Menard, D. (2020). Emergence and clonal expansion of in vitro artemisinin-resistant *Plasmodium falciparum* kelch13 R561H mutant parasites in Rwanda. *Nature Medicine*, *26*(10), 1602–1608. https://doi.org/10.1038/s41591-020-1005-2

van Dooren, G. G., & Striepen, B. (2013). The algal past and parasite present of the apicoplast. *Annual Review of Microbiology*, *67*, 271–289. https://doi.org/10.1146/annurev-micro-092412-155741

van Steensel, B., & Belmont, A. S. (2017). Lamina-Associated Domains: Links with Chromosome Architecture, Heterochromatin, and Gene Repression. *Cell*, *169*(5), 780–791. https://doi.org/10.1016/j.cell.2017.04.022

Vaquerizas, J. M., Kummerfeld, S. K., Teichmann, S. A., & Luscombe, N. M. (2009). A census of human transcription factors: Function, expression and evolution. *Nature. Reviews Genetics*, *10*(4), 252–263. https://doi.org/10.1038/nrg2538

Vembar, S. S., Macpherson, C. R., Sismeiro, O., Coppée, J. Y., & Scherf, A. (2015). The *Pf*Alba1 RNA-binding protein is an important regulator of translational timing in *Plasmodium falciparum* blood stages. *Genome Biology*, *16*(1). https://doi.org/10.1186/s13059-015-0771-5

Venugopal, K., Hentzschel, F., Valkiūnas, G., & Marti, M. (2020). Plasmodium asexual growth and sexual development in the haematopoietic niche of the host. *Nature Reviews. Microbiology*, *18*(3), 177–189. https://doi.org/10.1038/s41579-019-0306-2

Viebig, N. K., Gamain, B., Scheidig, C., Lépolard, C., Przyborski, J., Lanzer, M., Gysin, J., & Scherf, A. (2005). A single member of the Plasmodium falciparum var multigene family determines cytoadhesion to the placental receptor chondroitin sulphate A. EMBO Reports, 6(8), 775–781. https://doi.org/10.1038/sj.embor.7400466

Voinson, M., Nunn, C. L., & Goldberg, A. (2022). Primate malarias as a model for cross-species parasite transmission. *eLife*, *11*, e69628. https://doi.org/10.7554/eLife.69628

Voss, T. S., Healer, J., Marty, A. J., Duffy, M. F., Thompson, J. K., Beeson, J. G., Reeder, J. C., Crabb, B. S., & Cowman, A. F. (2006). A *var* gene promoter controls allelic exclusion of virulence genes in *Plasmodium falciparum* malaria. *Nature*, *439*(7079), 1004–1008. https://doi.org/10.1038/nature04407

Waddington, C. H. (1957). *The Strategy of the Genes; a Discussion of Some Aspects of Theoretical Biology*. George Allen & Unwin.

Waizenegger, I. C., Hauf, S., Meinke, A., & Peters, J.-M. (2000). Two distinct pathways remove mammalian cohesin from chromosome arms in prophase and from centromeres in anaphase. *Cell*, *103*(3), 399–410. https://doi.org/10.1016/s0092-8674(00)00132-x

Weatherall, D. J., Miller, L. H., Baruch, D. I., Marsh, K., Doumbo, O. K., Casals-Pascual, C., & Roberts, D. J. (2002). Malaria and the red cell. *Hematology. American Society of Hematology. Education Program*, 35–57. https://doi.org/10.1182/asheducation-2002.1.35

Weiner, A., Dahan-Pasternak, N., Shimoni, E., Shinder, V., von Huth, P., Elbaum, M., & Dzikowski, R. (2011). 3D nuclear architecture reveals coupled cell cycle dynamics of chromatin and nuclear pores in the malaria parasite *Plasmodium falciparum. Cellular Microbiology*, *13*(7), 967–977. https://doi.org/10.1111/j.1462-5822.2011.01592.x

Weiss, G. E., Crabb, B. S., & Gilson, P. R. (2016). Overlaying Molecular and Temporal Aspects of Malaria Parasite Invasion. *Trends in Parasitology*, *32*(4), 284–295. https://doi.org/10.1016/J.PT.2015.12.007

Wellems, T. E., Hayton, K., & Fairhurst, R. M. (2009). The impact of malaria parasitism: from corpuscles to communities. *The Journal of clinical investigation*, *119*(9), 2496–2505. https://doi.org/10.1172/JCI38307

Wendt, K. S., Yoshida, K., Itoh, T., Bando, M., Koch, B., Schirghuber, E., Tsutsumi, S., Nagae, G., Ishihara, K., Mishiro, T., Yahata, K., Imamoto, F., Aburatani, H., Nakao, M., Imamoto, N., Maeshima, K., Shirahige, K., & Peters, J. M. (2008). Cohesin mediates transcriptional insulation by CCCTC-binding factor. *Nature*, *451*(7180), 796–801. https://doi.org/10.1038/nature06634

Westenberger, S. J., Cui, L., Dharia, N., Winzeler, E., & Cui, L. (2009). Genome-wide nucleosome mapping of *Plasmodium falciparum* reveals histone-rich coding and histone-poor intergenic regions and chromatin remodeling of core and subtelomeric genes. *BMC Genomics*, *10*, 1–17. https://doi.org/10.1186/1471-2164-10-610

White, M. W., & Suvorova, E. S. (2018). Apicomplexa Cell Cycles: Something Old, Borrowed, Lost, and New. *Trends in Parasitology*, *34*(9), 759–771. https://doi.org/10.1016/j.pt.2018.07.006

WHO. (2020). *Report on antimalarial drug efficacy, resistance and response: 10 years of surveillance (2010–2019)*. Geneva: World Health Organization

WHO. (2021). *WHO recommends groundbreaking malaria vaccine for children at risk*. https://www.who.int/news/item/06-10-2021-who-recommends-groundbreaking-malaria-vaccine-for-children-at-risk

World Health Organization. (2015). *Global technical strategy for malaria, 2016-2030*. Geneva : World Health Organization

World Health Organization. (2021). *World malaria report 2021*. Geneva: World Health Organization

Yan, J., Enge, M., Whitington, T., Dave, K., Liu, J., Sur, I., Schmierer, B., Jolma, A., Kivioja, T., Taipale, M., & Taipale, J. (2013b). Transcription factor binding in human cells occurs in dense clusters formed around cohesin anchor sites. *Cell*, *154*(4). https://doi.org/10.1016/j.cell.2013.07.034

Yeoh, S., O'Donnell, R. A., Koussis, K., Dluzewski, A. R., Ansell, K. H., Osborne, S. A., Hackett, F., Withers-Martinez, C., Mitchell, G. H., Bannister, L. H., Bryans, J. S., Kettleborough, C. A., & Blackman, M. J. (2007). Subcellular Discharge of a Serine Protease Mediates Release of Invasive Malaria Parasites from Host Erythrocytes. *Cell*, *131*(6), 1072–1083. https://doi.org/10.1016/j.cell.2007.10.049

Young, J. A., Johnson, J. R., Benner, C., Yan, S. F., Chen, K., le Roch, K. G., Zhou, Y., & Winzeler, E. A. (2008). In silico discovery of transcription regulatory elements in Plasmodium falciparum. *BMC Genomics*, *9*. https://doi.org/10.1186/1471-2164-9-70

Yun, J., Song, S., Kim, H., Han, S., Yi, E. C., & Kim, T. (2016). Dynamic cohesin-mediated chromatin architecture controls epithelial–mesenchymal plasticity in cancer. *EMBO Reports*, *17*(9), 1343–1359. https://doi.org/10.15252/embr.201541852

Zhang, M., Wang, C., Otto, T. D., Oberstaller, J., Liao, X., Adapa, S. R., Udenze, K., Bronner, I. F., Casandra, D., Mayho, M., Brown, J., Li, S., Swanson, J., Rayner, J. C., Jiang, R. H. Y., & Adams, J. H. (2018). Uncovering the essential genes of the human malaria parasite *Plasmodium falciparum* by saturation mutagenesis. *Science*, *360*(6388). https://doi.org/10.1126/science.aap7847

Zhang, N., Kuznetsov, S. G., Sharan, S. K., Li, K., Rao, P. H., & Pati, D. (2008). A handcuff model for the cohesin complex. *Journal of Cell Biology*, *183*(6), 1019–1031. https://doi.org/10.1083/jcb.200801157

Zhang, Q., Huang, Y., Zhang, Y., Fang, X., Claes, A., Duchateau, M., Namane, A., Lopez-Rubio, J. J., Pan, W., & Scherf, A. (2011). A Critical role of perinuclear filamentous Actin in spatial repositioning and mutually exclusive expression of virulence genes in malaria parasites. *Cell Host and Microbe*, *10*(5), 451–463. https://doi.org/10.1016/j.chom.2011.09.013

Zhang, Q., & Liu, H. (2020). Functioning mechanisms of Shugoshin-1 in centromeric cohesion during mitosis. *Essays in biochemistry*, *64*(2), 289–297. https://doi.org/10.1042/EBC20190077

Zhang, Y., Liu, T., Meyer, C. A., Eeckhoute, J., Johnson, D. S., Bernstein, B. E., Nussbaum, C., Myers, R. M., Brown, M., Li, W., & Shirley, X. S. (2008). Model-based analysis of ChIP-Seq (MACS). *Genome Biology*, *9*(9). https://doi.org/10.1186/gb-2008-9-9-r137

Zheng, X., Hu, J., Yue, S., Kristiani, L., Kim, M., Sauria, M., Taylor, J., Kim, Y., & Zheng, Y. (2018). Lamins Organize the Global Three-Dimensional Genome from the Nuclear Periphery. *Molecular Cell*, *71*(5), 802-815.e7. https://doi.org/10.1016/j.molcel.2018.05.017